Draft version December 2, 2019
Typeset using LaTeX **twocolumn** style in AASTeX62

Expanding the Y Dwarf Census with *Spitzer* Follow-up of the Coldest CatWISE Solar Neighborhood Discoveries

Aaron M. Meisner,[1] Dan Caselden,[2] J. Davy Kirkpatrick,[3] Federico Marocco,[4,3,*] Christopher R. Gelino,[3] Michael C. Cushing,[5] Peter R. M. Eisenhardt,[4] Edward L. Wright,[6] Jacqueline K. Faherty,[7] Renata Koontz,[8] Elijah J. Marchese,[8] Mohammed Khalil,[9,3,10] John W. Fowler,[11] and Edward F. Schlafly[12]

[1] *NSF's National Optical-Infrared Astronomy Research Laboratory, 950 N. Cherry Ave., Tucson, AZ 85719, USA*
[2] *Gigamon Applied Threat Research, 619 Western Avenue, Suite 200, Seattle, WA 98104, USA*
[3] *IPAC, Mail Code 100-22, California Institute of Technology, 1200 E. California Blvd., Pasadena, CA 91125, USA*
[4] *Jet Propulsion Laboratory, California Institute of Technology, 4800 Oak Grove Drive, M/S 169-327, Pasadena, CA 91109, USA*
[5] *Department of Physics and Astronomy, University of Toledo, 2801 West Bancroft St., Toledo, OH 43606, USA*
[6] *Department of Physics and Astronomy, UCLA, 430 Portola Plaza, Box 951547, Los Angeles, CA 90095-1547, USA*
[7] *Department of Astrophysics, American Museum of Natural History, Central Park West at 79th Street, NY 10024, USA*
[8] *University of California, Riverside, 900 University Ave, Riverside, CA 92521, USA*
[9] *International College, PO Box 113-5373 Hamra, Bliss Street, Beirut, Lebanon*
[10] *Stanford University, 450 Serra Mall, Stanford, CA 94305, USA*
[11] *230 Pacific St., Apt. 205, Santa Monica, CA 90405, USA*
[12] *Lawrence Berkeley National Laboratory, Berkeley, CA, 94720, USA*

ABSTRACT

We present *Spitzer* 3.6μm and 4.5μm follow-up of 170 candidate extremely cool brown dwarfs newly discovered via the combination of WISE and NEOWISE imaging at 3−5μm. CatWISE, a joint analysis of archival WISE and NEOWISE data, has improved upon the motion measurements of AllWISE by leveraging a >10× time baseline enhancement, from 0.5 years (AllWISE) to 6.5 years (CatWISE). As a result, CatWISE motion selection has yielded a large sample of previously unrecognized brown dwarf candidates, many of which have archival detections exclusively in the WISE 4.6μm (W2) channel, suggesting that they could be both exceptionally cold and nearby. Where these objects go undetected in WISE W1 (3.4μm), *Spitzer* can provide critically informative detections at 3.6μm. Of our motion-confirmed discoveries, seventeen have a best-fit *Spitzer* [3.6]−[4.5] color most consistent with spectral type Y. CWISEP J144606.62−231717.8 ($\mu \approx 1.3''$/yr) is likely the reddest, and therefore potentially coldest, member of our sample with a very uncertain [3.6]−[4.5] color of 3.71 ± 0.44 magnitudes. We also highlight our highest proper motion discovery, WISEA J153429.75−104303.3, with $\mu \approx 2.7''$/yr. Given that the prior list of confirmed and presumed Y dwarfs consists of just 27 objects, the *Spitzer* follow-up presented in this work has substantially expanded the sample of identified Y dwarfs. Our new discoveries thus represent significant progress toward understanding the bottom of the substellar mass function, investigating the diversity of the Y dwarf population, and selecting optimal brown dwarf targets for JWST spectroscopy.

Keywords: brown dwarfs — infrared: stars — proper motions — solar neighborhood

1. INTRODUCTION

How complete is our census of the Sun's closest neighbors? How far does the population of substellar objects born like stars extend into the planetary-mass regime? The Wide-field Infrared Survey Explorer (WISE; Wright et al. 2010), with its unique full-sky sensitivity at 4.6μm, has unrivaled potential to answer these open questions by identifying the coldest brown dwarfs down to planetary masses. WISE-based discoveries already include the three nearest known brown dwarfs, among which is the coldest known brown dwarf (WISE 0855−0714), a ∼250 K planetary-mass object (Luhman 2014a,b, 2013). Wright et al. (2014) esti-

Corresponding author: Aaron M. Meisner
ameisner@noao.edu

* NASA Postdoctoral Program Fellow

mate that between 3 and 34 WISE 0855−0714 analogs should be detectable with WISE, yet only perhaps one such candidate has thus far been found (Marocco et al. 2019).

The coolest brown dwarfs revealed by WISE will be key *James Webb Space Telescope* (JWST; Gardner et al. 2006) targets, overlapping in mass and temperature with extrasolar giant planets and providing simplified laboratories for modeling planetary atmospheres, free of the irradiation and contaminating glare from a primary star. Indeed, WISE has already established the existence of a new brown dwarf spectral class with $T_{\rm eff} \lesssim 500$ K (Y dwarfs; Cushing et al. 2011; Kirkpatrick et al. 2011). Although prior WISE brown dwarf searches have been highly successful (e.g., Cushing et al. 2011; Kirkpatrick et al. 2011, 2012; Griffith et al. 2012; Mace et al. 2013a; Luhman 2014a; Kirkpatrick et al. 2014, 2016; Pinfield et al. 2014a; Schneider et al. 2016; Kuchner et al. 2017; Tinney et al. 2018; Burningham 2018), the Y dwarf census has stagnated in recent years at a sample size of just ∼25-30 objects.

The discoveries of nearly all known Y dwarfs can be traced back to WISE. The WISE 3.4μm (W1) and 4.6μm (W2) bands were designed for optimal sensitivity to the coldest brown dwarfs (Mainzer et al. 2011a), such that selecting for large W1−W2 color is a highly effective search strategy (e.g., Griffith et al. 2012; Kirkpatrick et al. 2011, 2012). Even more powerful is the combination of WISE-based color and motion criteria, eliminating stationary extragalactic contaminants (e.g., Luhman 2014a,b). Pinfield et al. (2014b) illustrated that faint, unrecognized Y dwarfs remain to be found in the WISE imaging, identifiable with novel search criteria using WISE data alone. Follow-up techniques such as methane on/off imaging (Tinney et al. 2012, 2018) and adaptive optics imaging (Liu et al. 2012; Dupuy et al. 2015) have also proven effective at pinpointing Y dwarfs among the numerous WISE solar neighborhood discoveries.

Our "CatWISE" analysis (Eisenhardt et al. 2019) represents a major step toward realizing the entire WISE data set's full sensitivity for brown dwarf discovery. Mining the vast WISE imaging archive to its faintest depths is a formidable challenge, and prior WISE motion searches have generally been limited by restricting to bright single-exposure detections and/or the short half-year time baseline of 2010-2011 observations. CatWISE pushes several magnitudes deeper than foregoing WISE-based motion surveys by jointly analyzing four years of WISE and NEOWISE (Mainzer et al. 2011b, 2014) data spanning the 2010-2016 time period. CatWISE thereby provides long time baseline WISE proper motions for roughly a billion mid-infrared sources over the full sky.

Using the CatWISE Preliminary catalog[1] and drawing upon well-established faint moving object selection/confirmation techniques (e.g., Lépine et al. 2002), we have performed an extensive motion-based search for previously undiscovered solar neighborhood constituents. As part of our ground and space based follow-up program, we have obtained *Spitzer* IRAC (Werner et al. 2004; Fazio et al. 2004) photometry of ∼170 newly discovered brown dwarf candidates suspected of being extremely cold and/or nearby. At CatWISE depths, the hallmark of such targets is the presence of a moving 4.6μm (W2) source with no firmly detected 3.4μm (W1) counterpart.

Detectable motion and a W2 magnitude alone are insufficient to estimate the basic parameters of most immediate interest for these brown dwarf candidates: spectral type, temperature, luminosity, distance, and near-infrared flux. The mid-infrared color, whether W1−W2 from WISE or [3.6]−[4.5] from *Spitzer*, represents a critical diagnostic in obtaining estimates for all of these quantities, as both colors tend to increase monotonically toward later spectral types beyond mid-T (e.g., Patten et al. 2006; Kirkpatrick et al. 2011). For our targets with W1 non-detections, *Spitzer* provides the only opportunity to measure a mid-infrared color. With spectral type estimates based on IRAC colors in hand, luminosity, distance and near-infrared flux estimates also follow.

Based on the *Spitzer* follow-up we present in this work, many of our discoveries have photometric spectral type estimates placing them within the 20 pc volume and/or very red [3.6]−[4.5] colors most consistent with spectral type Y. Among these, CWISEP J144606.62−231717.8 (hereafter CWISEP 1446−2317) stands out with an exceptionally large but highly uncertain [3.6]−[4.5] color of 3.71 ± 0.44 magnitudes.

In §2 we briefly summarize relevant characteristics of the WISE and NEOWISE missions. In §3 we provide a concise overview of CatWISE. In §4 we describe our selection of brown dwarf candidate targets for follow-up *Spitzer* photometry. In §5 we present the basic properties of our *Spitzer* photometry target sample. In §6 we explain our *Spitzer* observing strategy. In §7 we present our *Spitzer* color measurements. In §8 we combine WISE and *Spitzer* astrometry to confirm the motions of our brown dwarf candidates. In §9 we present complementary near-infrared photometry drawn from our

[1] https://catwise.github.io

ground-based follow-up observations and archival data sets. We discuss the combined implications of our photometric and astrometric analyses in §10. We conclude in §11.

2. WISE/NEOWISE OVERVIEW

Launched into low-Earth orbit in late 2009, WISE is a satellite-borne 40 cm aperture telescope. During early and mid 2010, WISE mapped the entire sky in four broad infrared bandpasses centered at 3.4μm (W1), 4.6μm (W2), 12μm (W3) and 22μm (W4). Although observations in the two longest wavelength channels were discontinued by late 2010 due to cryogen depletion, WISE kept observing in W1 and W2 until 2011 February as part of the NEOWISE mission (Mainzer et al. 2011b). WISE was placed into hibernation from 2011 February until 2013 December, at which point it recommenced surveying in W1 and W2 thanks to the NEOWISE-Reactivation (NEOWISE-R; Mainzer et al. 2014) mission extension. WISE has continued observations since reactivation to this writing (October 2019). A typical sky location is observed during a ∼1 day time period once every six months, and WISE has now performed a total of more than 13 complete sky passes in W1 and W2. The high quality of W1 and W2 imaging has remained essentially unchanged throughout the entire WISE lifetime (Mainzer et al. 2014; Cutri et al. 2015).

3. CATWISE

Although NEOWISE-R has now supplied the vast majority of W1/W2 observations, the mission itself does not provide any coadded data products optimized for science beyond the inner solar system. As a result, AllWISE (Cutri et al. 2013) has remained the definitive coadded WISE catalog for many years despite incorporating only the ∼13 months of pre-hibernation WISE imaging.

Our CatWISE archival data analysis program (Eisenhardt et al. 2019) has combined ∼4 years of 2010-2016 WISE/NEOWISE data to build a deeper, longer time baseline successor to AllWISE at 3−5μm. Whereas the AllWISE Source Catalog directly modeled WISE single-exposure images, CatWISE instead applies the AllWISE cataloging software to "unWISE" coadds (Lang 2014) as a computational convenience. By detecting W1/W2 sources in four-year depth unWISE stacks (Meisner et al. 2018a), CatWISE extracts 5σ sources to Vega magnitudes of W1 = 17.67 and W2 = 16.47, ∼0.6 mag deeper than AllWISE[2]. CatWISE fits apparent linear motions for every source using a set of "time-resolved" unWISE coadds (Meisner et al. 2018b,c). Each time-resolved coadd stacks the ∼1 day of WISE frames together at a given sky location during a single sky pass, sampling the motion at 6 month intervals. Such coaddition results in effectively no loss of motion information for objects in the solar neighborhood[3] ($\mu \lesssim 10''$/yr). By virtue of its >10× extended time baseline and 4× input imaging increase, CatWISE derives motions an order of magnitude more accurate than those of AllWISE for ∼900 million sources over the full sky[4]. We should therefore expect CatWISE motion and/or color selections to reveal many nearby brown dwarfs not previously identified with AllWISE. This includes objects below the AllWISE detection limit and also those with AllWISE motion measurements too noisy to be statistically significant.

Artifact flagging is a key ingredient in WISE-based rare object searches, where anomalies due to bright stars and blending dramatically outnumber the astrophysical sources of interest. Our brown dwarf searches take advantage of two complementary artifact flagging capabilities provided by CatWISE: (1) CC flags inherited from AllWISE via cross-match and (2) unWISE ab_flags similar to the CC flags, but available even in cases when a CatWISE source has no AllWISE counterpart[5].

4. *SPITZER* TARGET SELECTION

Our *Spitzer* follow-up observations presented throughout this work were acquired as part of program 14034 (hereafter p14034; PI Meisner). At the time of our Cycle 14 proposal submission (2018 March), *Spitzer*'s final observations were expected to take place on 2019 November 30. Given *Spitzer*'s impending retirement, we sought to fill our target list with the most exceptional WISE-based cold brown dwarf candidates selected by any/all means necessary, and as a result virtually no emphasis was placed on sample uniformity/homogeneity.

Additionally, our search for *Spitzer* targets was performed as part of a larger effort to fully mine CatWISE (and unWISE/AllWISE) for moving object discoveries, including earlier type candidates accessible via our ground-based photometric/spectroscopic observing programs. Only a subset of our brown dwarf searches were

[2] Magnitudes and colors quoted throughout this paper are in the Vega system unless otherwise noted.

[3] The time-resolved unWISE coaddition would only begin to incur significant smearing of fast-moving sources at linear motions of order 100″/yr. For comparison, the largest proper motion of any known star or brown dwarf is 10.4″/yr (Barnard's Star).

[4] CatWISE can be queried via IRSA at https://irsa.ipac.caltech.edu/applications/Gator/.

[5] unWISE artifact flagging is described in detail in the appendix of Meisner et al. (2019).

specifically tailored to supply targets for our p14034 *Spitzer* campaign. Through the combination of multiple searches described in §4.1-4.3, we discovered (and visually confirmed) a total of ∼2,500 previously unpublished moving objects. Most of these ∼2,500 discoveries are not appropriate *Spitzer* targets because they can be sensibly followed up from ground-based facilities. Discussion of additional CatWISE motion discoveries beyond those followed up via *Spitzer* p14034 is deferred to future papers.

We obtained p14034 observations for only the subset of our moving object discoveries which would be extremely difficult to follow up from any platform other than *Spitzer* and/or for which *Spitzer* 3.6μm (hereafter ch1) and 4.5μm (hereafter ch2) photometry provides a critically informative diagnostic. We therefore selected only discoveries falling into one or more of the following categories when constructing our p14034 target list:

1. **Non-stationary objects detected exclusively in W2**. Detectable motion ($\mu \gtrsim 200$ mas/yr at the typical W2 magnitude of our targets; Eisenhardt et al. 2019) suggests such objects must be relatively nearby. For a moving source, non-detections in W1 and all other shorter wavelengths indicate an extremely cold temperature, low luminosity and hence small distance. Moving objects detected solely in W2 are thus prime close-by Y dwarf candidates, and they were considered the highest priority target class for our *Spitzer* p14034 campaign.

2. **Moving objects detected in W1 but still potentially within 20 pc**. In some cases the presence of a faint W1 counterpart indicated that a moving object was insufficiently red to plausibly be a Y dwarf. We nevertheless retained such objects for p14034 consideration if the photometric distance estimate implied by W2 and W1−W2 indicated that the object could potentially be a new member of the 20 pc sample. Completing the census of objects within this volume is crucial for space density and mass function analyses (Kirkpatrick et al. 2019a). Furthermore, *Spitzer* ch1/ch2 photometry can provide significantly refined photometric distance and spectral type estimates relative to those dependent upon low-significance W1 detections. For these reasons, we deemed $d \lesssim 20$ pc candidates worthy p14034 *Spitzer* targets despite detection in W1.

3. **Candidate very late type ($\gtrsim$ T0) common proper motion (CPM) companion objects potentially in wide-separation visual binary systems**. Possible CPM status was usually noted serendipitously via our standard visual inspection motion vetting process (§4.4), and subsequently checked using the similarity between CatWISE motion of the candidate secondary versus that of the putative primary. *Spitzer* ch1/ch2 observations for CPM candidates can provide a relatively accurate photometric distance and astrometry for an improved motion estimate. These can then be compared against the distance/motion of the primary to better test the comoving pair hypothesis. Late-type wide CPM companions are rare, so it is also highly valuable to obtain *Spitzer* ch1/ch2 photometric data points for these critical benchmarks. Presentation of late-type CatWISE CPM discoveries followed up via *Spitzer* p14034 is deferred to a forthcoming paper (Marocco et al., in prep.).

4. **Objects with exceptionally large proper motion ($\mu \gtrsim 1''$/yr) and/or reduced proper motion**[6] **($H_{W2} \gtrsim 19.5$)**. Very high (reduced) proper motion of a source first recognized in the mid-infrared may be indicative of several interesting phenomena, including: a late type subdwarf, a very cold nearby neighbor to the Sun and/or large tangential space velocity.

A given object can sometimes fall under more than one of the above target categories. But no moving object discovery was placed on the p14034 program without meeting at least one of the above four selection criteria. All of our targets were, at the time of Astronomical Observation Request (AOR) submission to the p14034 program, never-before-published discoveries; our *Spitzer* campaign was not intended to provide supplementary follow-up of known objects drawn from the literature. Additionally, we vetoed candidates based on checking the *Spitzer* Heritage Archive (SHA) for existing unpublished observations by other teams targeting recent brown dwarf discoveries (e.g., Backyard Worlds; Kuchner et al. 2017) so as not to wastefully duplicate *Spitzer* pointings.

In our target selection decision-making, we sought to pursue a "high-risk, high-reward" strategy. We declined to place many of our unmistakable late-type moving object discoveries on p14034 because secure W1 detections made clear that they were simply T dwarfs at $\gtrsim$ 30 pc.

[6] W2 reduced proper motion is defined as $H_{W2} = m_{W2} + 5 + 5\log_{10}(\mu)$, where μ is the total proper motion in units of arcseconds per year.

Instead of such "safe" objects, we opted to prioritize very faint W2-only candidates with Y dwarf potential, even those so marginal in WISE that they might ultimately turn out to be entirely spurious. The rationale is that mid-T dwarfs don't necessitate *Spitzer*'s unique capabilities in the same way that Y dwarfs do, so we ought to observe as many Y dwarfs as possible before *Spitzer*'s retirement, even at the expense of false positives. Similarly, to find the most superlative targets before *Spitzer*'s retirement, we chose not to limit ourselves to searches based strictly on CatWISE, but instead leveraged additional data products at hand (the AllWISE Catalog and unWISE coadds; see §4.2 and §4.3, respectively).

The following subsections provide a detailed list of our many (14) distinct searches that contributed at least one target to the p14034 photometry presented in Table 1. For convenience, we refer to each search by a shorthand that consists of one capital letter followed by one digit. Table 1 lists which specific search(es) discovered each target in the "search method" column. Our searches generally rely on motion selection, color selection of objects that are very red in W1−W2, or some combination of the two. Each search's candidate identification yielded far more false positives than genuine newly discovered moving objects, so extensive visual inspection campaigns were performed to assess each candidate's possible motion by eye (§4.4). The dominant sources of false positives are bright star artifacts, blends and statistical measurement fluctuations that lead to the impression of potentially large motion and/or red W1−W2 color.

4.1. *CatWISE-based Selections*

Most of our p14034 targets were discovered by directly mining the CatWISE Preliminary Catalog. We ran a total of 11 distinct moving objects searches on this catalog. Note that our searches were performed on early, unfinished versions of CatWISE, rather than the published CatWISE Preliminary Catalog described in Eisenhardt et al. (2019). In many cases, limited or no artifact flagging existed in these early CatWISE databases; this often shaped/constrained our tailoring of search criteria. Also, all CatWISE-based selections were run at a time when there was no distinction between sources now separated into the CatWISE "catalog" and "reject" tables[7]. Appendix A of Eisenhardt et al. (2019) provides column descriptions for the CatWISE quantities involved in our selection criteria.

Our 11 CatWISE-based searches fall under two broad categories: (1) traditional catalog queries each implementing a set of hard cuts (§4.1.1) and (2) supervised machine learning methods trained on human-verified late-type moving objects (§4.1.2).

4.1.1. *CatWISE Catalog Cuts*

Prior WISE motion surveys such as the AllWISE and AllWISE2 motion searches (Kirkpatrick et al. 2014, 2016) were performed via selections cutting on motion, color and artifact flagging catalog columns. Motivated by the success of these previous WISE-based motion surveys, we modeled eight of our search methods after this same general approach, but now applied to the newly available CatWISE data set.

Selection method C1 combines CatWISE color and motion information to isolate objects that are both red in W1−W2 and have large W2 reduced proper motion (H_{W2}). The usage of H_{W2} rather than simply proper motion itself is a way of prioritizing fast-moving objects of low luminosity, such as Y dwarfs and late type subdwarfs. C1 candidates are obtained from a full-sky CatWISE query requiring (w2snr > 20), (w2snr_pm > 20), ($H_{W2} > 15$), (rchi2/rchi2_pm > 1.03), (w2rchi2_pm < 2), (W1−W2 ≥ 1.5) and ($Q < 10^{-5}$). Q is a significance of motion metric defined in §3.4.1 of Kirkpatrick et al. (2014) as $Q = e^{-\chi^2_{motion}/2}$, where χ^2_{motion} = (pmra/sigpmra)^2 + (pmdec/sigpmdec)^2. Note that typical WISE sources such as main sequence stars have a color of W1−W2 ≈ 0 (Vega). The relatively high W2 SNR requirements stipulated as part of this query were necessary to keep the candidate sample size manageable, as this search was performed at a time when no CatWISE artifact flagging was available.

Search C2 is a variant of search C1, but replacing the (W1−W2 ≥ 1.5) color cut with a proper motion cut of $\mu > 0.5''$/yr. Again, search C2 was executed without the benefit of any artifact flagging information.

Search C3 implements a combination of the cuts from C1 and C2, and was performed after artifact flagging columns had been added to our working CatWISE database. By leveraging the artifact flagging to remove many spurious candidates, C3 extended to lower W2 SNR than C1/C2, specifically restricting to the range $10 <$ w2snr_pm ≤ 20. C3 also included an additional requirement of (w2snr_pm $>$ w1snr_pm). The significance of motion criterion was made more stringent than in C1 and C2, requiring $Q < 10^{-6}$. Both the proper motion cut $\mu > 0.5''$/yr from C2 and the $H_{W2} > 15$ reduced proper motion cut from C1/C2 were applied.

[7] Only two of our p14034 targets are found in the CatWISE Preliminary reject table rather than in the main CatWISE Preliminary catalog: CWISEPR J062436.84−071147.2 and CWISEPR J065144.62−115106.1.

Lastly, search C3 sought to eliminate artifacts by requiring (ab_flags = '00').

Search C4 is a variant of C1 run after artifact flagging had been put in place. The CatWISE catalog cuts in C4 are the same as those in C1, aside from the following updates: C4 requires (ab_flags = '00'), flips the rchi2/rchi2_pm cut to (rchi2/rchi2_pm ≤ 1.03), and adds a new (w1snr_pm = `null`) W1 non-detection requirement.

Although based on CatWISE catalog cuts, searches C5-C8 are not immediate descendants of the C1-C4 approaches. Search C5 consists of an all-sky CatWISE query requiring $Q < 10^{-5}$, (w2mpro > 13), (w2snr > 10), (k1 = 0) and (k2 = 3). k1 (k2) is a CatWISE column indicating, for each object, which scan direction(s) provided a successful photometric measurement in W1 (W2). k1 = 0 means that neither ascending nor descending WISE scans provided good W1 photometry, while k2 = 3 means that good W2 photometry was obtained for both WISE scan directions. This query is thus, in effect, implementing an alternative means of identifying W2-only moving objects within the CatWISE catalog. Search C5 was also conducted prior to the existence of any CatWISE artifact flagging capabilities.

Search C6 is a full-sky CatWISE query requiring (w2snr > 10), w1flux < (w2flux·$10^{-1.5/2.5}$−2·w1sigflux), (rchi2/rchi2_pm > 1.03), (w2rchi2_pm < 2), $Q < 10^{-6}$, and AllWISE CC flags = '0000' when available. The AllWISE CC flags were gathered via a CatWISE-AllWISE positional cross-match. One notable aspect of this search is that a color cut of effectively (W1−W2 > 1.5) is implemented in terms of fluxes rather than magnitudes, to avoid the complications associated with e.g., quoting magnitudes in cases of zero or negative W1 flux (as can happen for a very red W1 non-detection). In the CatWISE catalog, both w1flux and w2flux have units of Vega nanomaggies[8].

Search C7 is a variant of search C6, but lowering the W2 SNR threshold to (w2snr > 5) in attempt to push fainter. To balance out the large influx of sources at relatively low SNR, the color criterion was made more stringent at effectively (W1−W2 > 2.5), with the actual flux-based cut being w1flux < (0.1·w2flux−2·w1sigflux). The significance of motion criterion was loosened to ($Q < 10^{-5}$) for search C7. We additionally required that AllWISE CC flags not contain a capital letter (when an AllWISE cross-match was available) and (ab_flags = '00').

[8] A source with total flux of 1 Vega nanomaggie has a magnitude of 22.5 in the Vega system.

Search C8 is a pure color selection. We required that candidates not be significantly detected at W1 (w1snr < 3) and be well-detected in W2 (w2snr > 10) in CatWISE. A negative cross-match (2.5″ radius) against AllWISE sources with (w3mpro < 13) was used to remove extragalactic contaminants that tend to be red in W2−W3 color. C8 made use of CatWISE ab_flags to require that candidates not be flagged as W2 ghosts, W2 latents, or W2 diffraction spikes.

4.1.2. *CatWISE Machine Learning*

Search method M1 is described fully in §3 of Marocco et al. (2019). In brief, M1 uses the *XGBoost* software package (Chen & Guestrin 2016) to perform supervised machine learning on the CatWISE catalog. A training set was constructed from the CatWISE sources corresponding to known high proper motion late T and Y dwarfs, with the goal of finding other CatWISE entries displaying similar properties. Search M1 is restricted to CatWISE objects that are faint and red by only classifying the subset of CatWISE rows with (w2mpro > 14) and also satisfying:

$$(w1mpro - (3 \times w1sigmpro)) - (w2mpro + (3 \times w2sigmpro)) \geq 1.0 \quad (1)$$

This enforces a requirement that each retained source would have a color of (W1−W2 ≥ 1) even if the CatWISE-reported magnitudes turned out to be 3σ bright in W2 and 3σ faint in W1.

Search M2 is a variant of search M1, with the classifier trained on a sample including hitherto identified p14034 targets rather than a sample consisting exclusively of previously published late-type brown dwarfs.

Search M3 is also a modified version of search M1, but removing the W1−W2 color criterion in Equation 1. The motivation for this variant is the possibility of recovering overlooked late-type moving objects with WISE color measurements corrupted due to blending with background sources, plus the potential to find additional fast-moving sources irrespective of W1−W2 color.

4.2. *AllWISE-based Selections*

From our prior experiences searching the AllWISE database, we considered it likely that more late T and Y dwarfs remained to be found in that data set, particularly with the aid of our recently upgraded suite of visualization tools used to scrutinize candidates (§4.4). Two AllWISE-based moving object searches contributed to the p14034 target list, both utilizing only simple catalog cuts.

In search A1, our candidates are drawn from a full-sky query of the AllWISE catalog, requiring very red

W1−W2 color (w1mpro−w2mpro > 3), relatively little W3 flux (w2mpro−w3mpro < 3.5) to weed out extragalactic contaminants, w2sigmpro not `null`, and W2 CC flags not containing `H`, `O`, `P` or `D` to avoid bright star artifacts. Because of the very extreme W1−W2 color cut imposed, this yielded a relatively small sample of candidates, ∼500 in total, which were then subjected to visual inspection.

Search A2 likewise identifies candidates using a pure color selection method based on the AllWISE catalog. We retain only those AllWISE rows that are effectively W1 non-detections (w1snr < 3), have very red W1−W2 colors (w1mpro−w2mpro > 2), have ($|b_{gal}| > 10°$) to avoid the crowded Galactic plane, (`nb` = 1) to remove blends, and none of `H`, `O`, `P` or `D` in either the W1 or W2 CC flags to discard bright star artifacts. This yielded a sample of ∼2,000 candidates spread across the entire $|b_{gal}| > 10°$ sky.

4.3. *unWISE-based Selection*

One of our selection techniques (search U1) proceeded directly from image-level analysis of the unWISE coadds themselves, rather than the CatWISE or AllWISE catalog. From the time-resolved unWISE coadds (Meisner et al. 2018c), we created two full-sky sets of meta-coadds in each band: one built by stacking together all pre-hibernation epochs, and a second built by stacking together all post-reactivation epochs. We subtracted the pre-hibernation W2 meta-coadds from the post-reactivation W2 meta-coadds and ran Source Extractor (Bertin & Arnouts 1996) on the difference images. The goal was to find sources that moved sufficiently during the ∼3 year WISE hibernation period so as to avoid self-subtraction. Source Extractor forced photometry on each of our four sets of meta-coadds (W1 and W2, pre and post hibernation) was performed at the positions of W2 post-reactivation difference image detections.

The catalog of W2 difference detections, augmented with forced photometry, was then analyzed to select moving object candidates. Specifically, we cross-matched the difference detection catalog with a sample of known late type brown dwarfs to form a training set. An *XGBoost* classifier similar to those described in §4.1.2 was then used to identify difference detection catalog entries with properties similar to those of the training sample.

Search U1 was employed because we expected it to perform well for very fast moving sources ($\mu_{tot} \gtrsim 2''$/yr), whereas CatWISE source detection might reasonably fail for extremely faint objects with exceptionally large proper motions. The fact that both of our discoveries presented in this work which lack CatWISE counterparts — WISEA J153429.75−104303.3 ($\mu_{tot} \approx 2.7''$/yr) and WISENF J193656.08+040801.2 ($\mu_{tot} \approx 1.3''$/yr) — were identified via search U1 attests to the capability of this method to find moving objects that the CatWISE pipeline was not optimized to handle properly.

4.4. *Visualization Tools*

Extensive visual inspection of moving object candidates delivered by the searches described in §4.1-4.3 played a vital role in providing a high-purity sample of brown dwarf targets for our *Spitzer* p14034 campaign. In total, we visually inspected ∼130,000 candidates in the course of the searches described in §4.1-4.3. A major factor enabling our discoveries based on CatWISE, AllWISE and unWISE was our usage of visualization tools/aids that leveraged the full W1/W2 time baseline afforded by the combination of pre-hibernation and post-reactivation WISE/NEOWISE imaging.

4.4.1. *Finder Charts*

We created a new, customized version of the multi-panel, multi-wavelength finder chart program used by prior WISE motion searches such as Kirkpatrick et al. (2016) and Kirkpatrick et al. (2016); for an example see Figure 1 of Schneider et al. (2016). We added two sets of W1/W2 time-resolved unWISE coadd cutouts for each candidate, with one set at the beginning of the pre-hibernation WISE mission and one at the end of the third year of the post-reactivation NEOWISE mission. Taking advantage of the ∼6.5 year WISE-NEOWISE time baseline in this way allowed us to perceive the source motion (or lack thereof) using only W1/W2 data at widely spaced epochs, rather than needing to obtain an appreciable time baseline by comparison of WISE images to shorter wavelength data sets.

4.4.2. *WiseView Interactive Blinker*

Our visual inspection workflow relied heavily on a new visualization tool called WiseView (Caselden et al. 2018) not previously available for WISE moving object searches such as the AllWISE and AllWISE2 motion surveys. In contrast to static multi-wavelength finder charts, WiseView is an interactive browser-based interface for creating customized animated blinks of time-resolved unWISE coadds. Numerous blink parameters are tunable in real time, including the band(s) shown (W1, W2, or both), the central sky position, the frame rate, the stretch and the field of view size. Figure 1 illustrates an example of the WiseView interface as employed when vetting one of our W2-only brown dwarf discoveries.

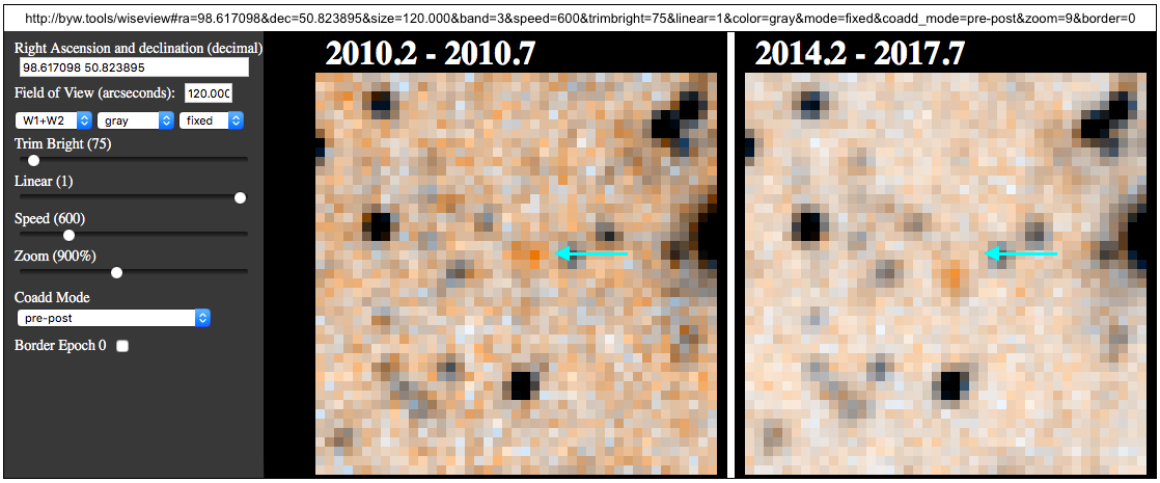

Figure 1. Depiction of the WiseView interactive image blinking tool (§4.4.2) used for visual inspection of potential p14034 targets. At left of the vertical white space is a screen shot of the WiseView interface, including blink tuning widgets and the first of two color composite images created based on the user-specified blink parameters. This blink sequence is centered on CWISEP J063428.10+504925.9, the orange source indicated by the cyan arrow. The cyan arrow remains at the same sky position in both panels; it is not present in WiseView, but rather has been edited in to highlight the large southeasterly motion of this object. The "pre-post" Coadd Mode selected generates two meta-coadds per band, with the first spanning the full pre-hibernation time period (2010.2-2010.7 in this case) and the second spanning the available post-reactivation time period (2014.2-2017.7 in this case). A screenshot of the post-reactivation WiseView color composite is included at right of the vertical white space, with the WiseView widget panel omitted. Although these two images are shown side-by-side here, WiseView presents a single animated blink alternating between these two images, with both images aligned in the same position on the screen. The parameters of this blink are encoded in a WiseView URL provided at top — one can experience this WiseView animation in action by visiting that URL.

4.4.3. *DESI Imaging Viewer*

To select moving objects detected in W2 but not at any shorter wavelengths, we made extensive use of the DESI pre-imaging "Legacy Surveys" sky viewer[9] to inspect red-optical survey images. This viewer allows for interactive exploration of wide-area survey data sets with deep z and Y band imaging, in particular DECaLS/MzLS ($z \approx 23.0$ AB at 5σ over $\sim$1/3 of the sky; Dey et al. 2019) and Dark Energy Survey DR1 ($z \approx 23.4$ AB and $Y \approx 22.2$ AB at 5σ over $\sim$1/8 of the sky; Abbott et al. 2018). Visible z and/or Y counterparts were generally treated as evidence that a moving object candidate was either insufficiently red to be a Y dwarf or else extragalactic if the red-optical counterpart appeared extended.

4.4.4. *IRSA Finder Chart*

In some cases where conclusively confirming/denying motion by eye proved difficult, we consulted AllWISE W3 and W4 images via the IRSA Finder Chart application[10]. Because our motion candidates are so faint (median W2 $\sim$ 15.9; see §5), a strong counterpart at W3 and/or W4 would only be expected in the case of a stationary extragalactic source but not for a late-type brown dwarf. We therefore avoided selecting sources seen to have coincident W3/W4 emission as p14034 targets.

4.4.5. *PanSTARRS-1 Cutouts*

Before placing candidates on the p14034 target list, we inspected PanSTARRS-1 image cutouts[11] for objects north of $\delta \approx -30°$ (Chambers et al. 2016). Visible detections in PanSTARRS-1 were in general used to veto potential Y dwarf candidates — given the faintness of our sample in W2, detection in any PanSTARRS-1 filter would be inconsistent with a Y dwarf spectral type.

5. GENERAL P14034 SAMPLE PROPERTIES

We filled our allocated 40.5 hours of Cycle 14 *Spitzer* time with 174 unique brown dwarf candidate targets, each of which received a single corresponding AOR as detailed in §6. As discussed in §4, these 174 targets represent only a small subset of the visually vetted moving object discoveries yielded by our searches. Figure 2 shows that our targets are much fainter than those of previous WISE motion surveys, including the AllWISE and AllWISE2 searches (Kirkpatrick et al. 2014, 2016).

[9] http://legacysurvey.org/viewer
[10] https://irsa.ipac.caltech.edu/applications/finderchart/
[11] http://ps1images.stsci.edu/cgi-bin/ps1cutouts

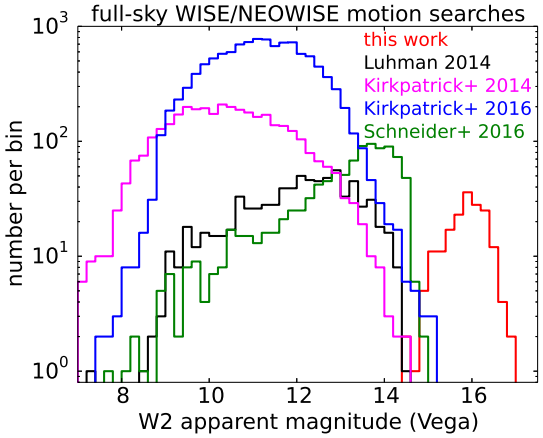

Figure 2. Comparison of W2 magnitude distributions for moving object discoveries from published full-sky WISE/NEOWISE motion surveys. Each histogram shows the number of new discoveries per 0.2 mag W2 bin for a given sample. Note the logarithmic scale. Red is our entire 174-object *Spitzer* p14034 target list (including 4 CPM targets and 6 spurious candidates from §7.1) plus our 3 brown dwarf candidates with ch1/ch2 photometry based on archival *Spitzer* imaging. Our discoveries are much fainter than those of previous full-sky WISE/NEOWISE motion searches.

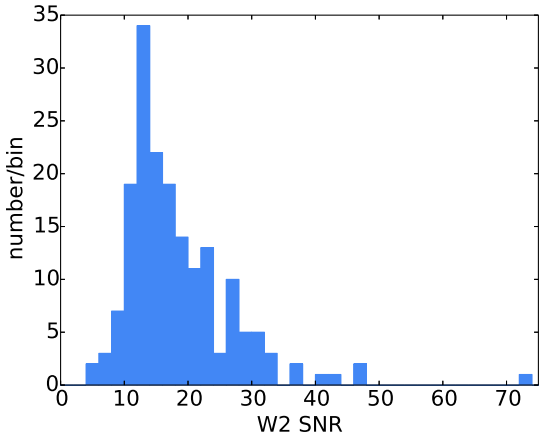

Figure 3. W2 signal-to-noise distribution for our moving object discoveries characterized with *Spitzer*. The histogram shows our entire 174-object *Spitzer* p14034 target list (including 4 CPM and 6 spurious candidates from §7.1) plus our 3 brown dwarf candidates with ch1/ch2 photometry based on archival *Spitzer* imaging. The median (mean) W2 SNR is 16.2 (18.4), with a dispersion of 8.6.

The median W2 magnitude of our targets is 15.93, with a dispersion of 0.47 mags. For comparison, the W2 single-exposure depth is W2 ≈ 14.5, which has represented the faint limit of prior WISE-based motion searches (e.g., Luhman 2014a; Schneider et al. 2016). Figure 3 shows the W2 SNR distribution of our *Spitzer* photometry sample. The median (mean) W2 SNR is just 16.2 (18.4), with a dispersion of 8.6. Note that these values indicate the total W2 SNR when combining 4 years of WISE/NEOWISE imaging; detections in any time slice of the available W2 imaging will generally be of even lower significance.

Figure 4 shows the spatial distribution of our p14034 targets, which, as expected, are scattered fairly uniformly across the entire sky while preferentially avoiding the confused Galactic plane.

5.1. *Candidates with Archival ch1/ch2 Data*

Three of our discoveries not previously recognized as brown dwarf candidates happened to have sufficient serendipitous archival ch1/ch2 imaging in SHA to enable robust phototyping without the need for additional p14034 observations. We performed our usual *Spitzer* photometry (§7) and astrometry (§8.4) on these archival observations to obtain ch1−ch2 colors. These three objects (CWISEP 0229+7246, CWISEP 1721+5950 and CWISEP 2247−0041) are denoted by blue squares in Figure 4.

5.2. *Targets as yet Unobserved by Spitzer*

Three of our p14034 brown dwarf targets are scheduled for *Spitzer* photometry in the near future but remain unobserved by *Spitzer* as of this writing (2019 October; CWISEP 1353−0037, CWISEP 1515−2157 and CWISEP 0601−5922). In all three such cases, the motion is conclusively confirmed with WISE astrometry alone, so we have chosen to present these three discoveries in this paper despite the current lack of available *Spitzer* photometry/astrometry. These three targets are therefore listed in Table 1, but with *Spitzer* photometry columns left empty.

6. *SPITZER* OBSERVING STRATEGY

We based our observing strategy on those of prior *Spitzer* campaigns designed to measure the colors of WISE-selected late T and Y dwarf candidates (e.g., programs 70062 and 80109; PI Kirkpatrick). These foregoing *Spitzer* programs generally observed substantially brighter objects than those comprising our p14034 target list, and showed that coaddition of five 30 second ch1 dithers typically achieves signal-to-noise of 10 (5) at a Vega magnitude of ch1 = 18.0 (18.75).

The boundary between the ch1−ch2 colors of late T and Y dwarfs occurs at ch1−ch2 ≈ 2.4 (e.g., Kirkpatrick et al. 2019a), and our primary goal was to obtain ch1 imaging deep enough to distinguish between late T and Y dwarfs. We therefore attempted to engineer our number of ch1 dithers such that a 5σ ch1 detection would always establish a color of at least ch1−ch2 = 2.75 magnitudes.

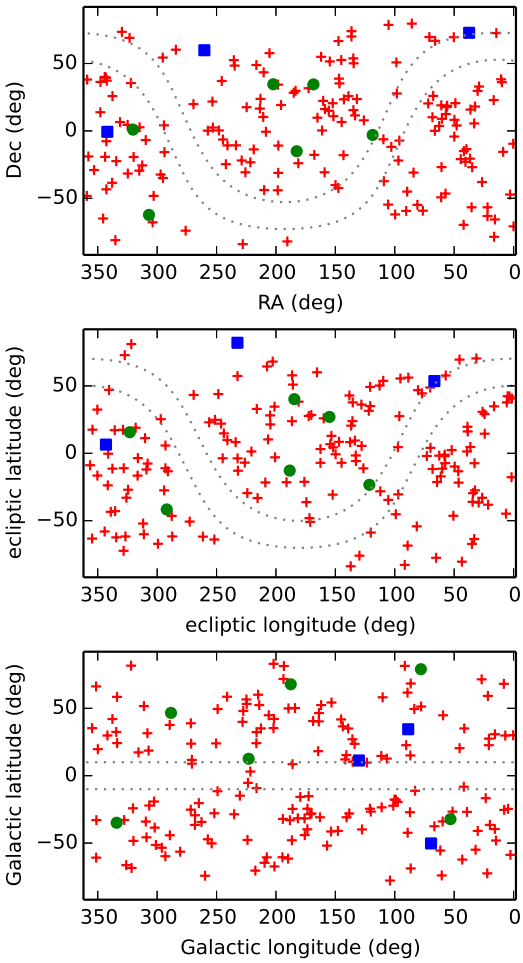

Figure 4. Spatial distribution of late-type brown dwarf candidates on p14034 or for which archival *Spitzer* data yielded a ch1−ch2 color. CPM candidates have been removed, since those are presented separately in a forthcoming paper. Red plus marks are p14034 targets. Green circles are spurious p14034 candidates (see Table 2). Blue squares are brown dwarf candidates for which our ch1−ch2 colors are based on serendipitously available archival *Spitzer* imaging. Top: equatorial coordinates. Middle: ecliptic coordinates. Bottom: Galactic coordinates. In all cases the dotted grey lines denote Galactic latitude of ±10°

For each target, we chose either 5, 7, 9, 11, or 13 ch1 dithers (at 30 seconds per dither) so that we would achieve ch1 SNR of at least 5 for ch1−ch2 = 2.75, under the assumption that the ch2 mag would be equal to the W2 mag. According to this strategy, W2 ≤ 16 candidates receive five ch1 dithers, and the break point between 5 and 7 dithers is W2 = 16.0. Then the break point between 7 and 9 dithers occurs at W2 = 16.18, and so forth. We exercised some case-by-case discretion in bumping up the exact number of dithers chosen, but always used ch1 SNR of 5 at ch1−ch2 = 2.75 to enforce a minimum number of ch1 dithers.

For each target, both ch1 and ch2 were obtained as part of the same AOR. This minimizes slew overheads and ensures that our color measurements cannot be corrupted by any long timescale variability aliasing into images of the same target taken at large time separation. We always acquired the same number of 30 second dithers in both ch1 and ch2 for each target. This effectively maintains a fixed ch2 SNR of ∼75 for the high-significance ch2 detection across all members of our sample, which ensures the high value of each target's ch2 detection for astrometry (§8.4). We dithered with a 'cycling' pattern of medium scale[12].

The *Spitzer* p14034 imaging analyzed in this work was acquired between 2018 October 21 and 2019 August 16.

7. *SPITZER* PHOTOMETRY

All of our *Spitzer* photometry/astrometry analyses presented in this work are based on custom mosaics built from the single-dither BCD images with MOPEX (Makovoz & Khan 2005; Makovoz & Marleau 2005). We created one such custom mosaic per band (ch1, ch2) per AOR. Relative to using the default "PBCD" mosaics supplied for each AOR via SHA, creating our own custom mosaics provided us extra freedom, for example to reject occasional problematic single-frame IRAC images with e.g., a cosmic ray contaminating the targeted brown dwarf candidate. The algorithmic rejection of single-frame outliers such as cosmic rays also appears to be much better overall in our custom mosaics than in the PBCD stacks. In a handful of cases, we excised one or two BCD frames from our custom mosaics due to the presence of a cosmic ray contaminating the faint ch1 counterpart (CWISEP 0035−1532, CWISEP 0403−4916, CWISEP 1434−1344, CWISEP 2251−0740 and CWISEP 2355+3804).

Extraction and photometry of sources within our custom *Spitzer* mosaics proceeded as described in §4 of Marocco et al. (2019). In brief we use the MOPEX/APEX software to detect sources in our custom mosaics and perform both PRF-fit and aperture photometry (including the application of an aperture correction) in each of ch1 and ch2. Note that our photometry was always run independently in ch1 and ch2 — we did not employ a forced photometry approach. By default we used an SNR = 5 source detection threshold. In the case of two very red objects (CWISEP 1434−1344 and CWISEP 1446−2317), obtaining a ch1 counterpart

[12] https://irsa.ipac.caltech.edu/data/SPITZER/docs/irac/calibrationfiles/di

extraction required lowering the ch1 detection threshold to SNR = 2.

Table 1 lists our ch1 and ch2 photometry results. The quoted magnitude values and their uncertainties are derived by averaging the aperture-based and PRF-fit quantities for each target in each *Spitzer* band. Table 1 also reports the W1 and W2 photometry for each target. With only a small number of exceptions, such as our two discoveries not detected by CatWISE, this WISE magnitude information is drawn from the CatWISE columns w1mpro_pm, w1sigmpro_pm, w2mpro_pm, and w2sigmpro_pm.

7.1. *Spurious Candidates*

A small number of our p14034 targets turned out to be entirely absent in the deeper, higher-resolution *Spitzer* imaging we obtained (i.e., a *Spitzer* counterpart could neither be extracted nor visually identified). Table 2 lists such cases (6/174 = 3.4% of our targets). Throughout this paper, these 6 completely spurious targets are omitted from various tabulations and analyses, particularly those such as the ch1/ch2 photometry listed in Table 1 that would require a *Spitzer* detection.

We note that Eisenhardt et al. (2019) quotes a CatWISE reliability of just under 98% at W2 = 16. Given that our sample's median magnitude is W2 = 15.93, a 3.4% rate of spurious sources is within reason.

7.2. *Candidates with Two Spitzer Counterparts*

In two cases, our WISE-based brown dwarf candidate turned out to have two distinct, closely spaced *Spitzer* ch2 counterparts. CWISEP 1541+5230 has two *Spitzer* counterparts in both ch1 and ch2, whereas CWISEP 0229+7246 has two *Spitzer* counterparts in ch2 but only one blended/elongated *Spitzer* counterpart in ch1. In these cases we label the two components by adding a suffix of either "N" (northern) or "S" (southern) to their designations, based on their relative *Spitzer* ch2 (RA, Dec) positions. In both of these cases, it remains plausible that there are simply two static *Spitzer* counterparts corresponding to our single WISE target, so we vetoed these candidates from being formally considered motion-confirmed in downstream analyses.

8. ASTROMETRY

We seek to use motion as a proxy for confirming an object is a nearby brown dwarf. High-significance motion establishes solar neighborhood membership, whereas objects consistent with remaining stationary may be of e.g., extragalactic origin. Because we lack spectroscopic confirmations and our most interesting p14034 targets are detected only in WISE and *Spitzer*, detailed astrometric analysis is needed to best determine whether each source is indeed moving. In this section we explain how we have combined astrometry from both WISE and *Spitzer* to best identify the subset of our brown dwarf candidates that have statistically significant proper motions. The inclusion of *Spitzer* astrometry is a critical component of this analysis, since our *Spitzer* data point provides a completely independent cross-check on the perceived WISE-based motion used to select our candidates; if the *Spitzer* detection "lines up" along the WISE astrometric trajectory, then this gives us strong reassurance that the candidate was selected due to true motion rather than a rare fluke in the WISE data.

Using the methodology described here, we limit our astrometric analysis to fits of apparent linear motion; we do not seek to obtain/constrain the parallaxes of our targets. In general, fitting parallaxes for brown dwarfs as faint as our targets will require multiple epochs of *Spitzer* (or similarly precise) observations sampling both sides of the parallactic ellipse (e.g., Kirkpatrick et al. 2019a), whereas our p14034 imaging provides just a single *Spitzer* astrometric epoch. Additionally, as discussed in §8.3, we typically must coadd data acquired from both sides of WISE's orbit in order to obtain W2 detections of our exceedingly faint targets, meaning that our WISE astrometry is generally unsuitable for parallax fitting.

Our astrometric analysis incorporates ch2 and W2, but never ch1 or W1. This is because our targets are very red in both ch1−ch2 and W1−W2. For our p14034 *Spitzer* imaging, where both bands received the same total exposure time, the SNR of each target's ch2 detection will be much higher than that of its ch1 detection. Further, because the ch1 and ch2 images of a given target are nearly contemporaneous, folding in ch1 does not offer the possibility of an appreciably extended time baseline, and in combination with ch2 astrometry would merely lead to a negligible improvement in the p14034 *Spitzer* positional precision. The same considerations apply with regard to W1: data acquisition in W1 and W2 is simultaneous, so W1 astrometry would provide only a set of much less precise positions at the same epochs as our W2 astrometric data points.

All *Gaia*-recalibrated W2 and ch2 (RA, Dec) coordinates quoted throughout this paper are in ICRS. The *Spitzer* and WISE positions reported in Tables 3 and 4 are relative rather than absolute — we did not attempt to correct for the typically very small parallaxes of our astrometric calibration sources.

8.1. *Gauging Significance of Motion*

There are various ways one could imagine quantifying significance of motion. In this work, we opt for a simple,

intuitive metric that has been applied in the course of past WISE-based moving object analyses:

$$\chi^2_{motion} = (\mu_\alpha/\sigma_{\mu_\alpha})^2 + (\mu_\delta/\sigma_{\mu_\delta})^2 \quad (2)$$

This χ^2_{motion} statistic has previously been used during e.g., the AllWISE and AllWISE2 motion surveys (Kirkpatrick et al. 2014, 2016). χ^2_{motion} tends to increase with larger (absolute) linear motion components and also with decreasing uncertainties on the linear motion measurements. It can also be thought of as corresponding to a false alarm rate, $Q = e^{-\chi^2_{motion}/2}$, where Q is the probability of a statistical fluke causing χ^2_{motion} to be exceeded.

In this work, we set the threshold for WISE+*Spitzer* 'motion confirmation' at $Q = 10^{-5}$, which corresponds to $\chi^2_{motion} = 23.03$. Ignoring the relatively high-precision *Spitzer* astrometric data points available from p14034 follow-up, a substantial fraction of our sample's targets (46% = 79/173) have CatWISE χ^2_{motion} less than this threshold, illustrating the critical need to combine ch2 and W2 astrometry toward better confirming/refuting source motions.

8.2. *Strategy for Combining WISE & Spitzer Astrometry*

Given that CatWISE linear motion estimates are almost always available for our targets, one might imagine concocting a scheme to combine these with our *Spitzer* astrometric data points and thereby derive high-quality WISE+*Spitzer* linear motions. There are many reasons why we find this approach undesirable, for instance:

- It isn't entirely clear how to properly combine a CatWISE motion estimate and a *Spitzer* position in order to obtain a χ^2_{motion} value.
- Two of our most exciting discoveries are absent from the CatWISE catalog (WISEA 1534−1043, WISENF 1936+0408). Another two targets have 'null' motion uncertainties in CatWISE (CWISEP 0402−2651, CWISEP 0430+2556). So in any event, we need to develop an alternative motion-fitting methodology not reliant on CatWISE to address this subset of our targets.
- In cases when CatWISE linear motions are corrupted by blending at some subset of WISE epochs, this can be circumvented by careful subselection of epochal W2 detections.
- CatWISE used an ad hoc scaling of unWISE pixel-level uncertainties, which could lead to non-optimal CatWISE motion uncertainty estimates.
- CatWISE only incorporated NEOWISE data through 2016, whereas additional NEOWISE data are now available.
- CatWISE fits W1 and W2 simultaneously — any nonzero weighting of W1 data in CatWISE motion fits will essentially have added noise to its motion measurements for our W2-only sources.

The alternative approach we prefer is to extract our own epochal WISE source catalogs and use these to assemble a vetted list of high-quality W2 astrometric detections for each brown dwarf candidate. For each target, its set of W2 detections can then be straightforwardly combined with our *Spitzer* astrometric data point via simple least squares fitting of apparent linear motions in each of RA and Dec. Moreover, the carefully assembled lists of W2 positions derived during this process may be of substantial interest in their own right, as they can be combined with any future astrometric follow-up acquired. §8.3 (§8.4) explains in detail how we obtain the WISE W2 (*Spitzer* ch2) astrometric detections for our targets.

8.3. *WISE Astrometry*

It is challenging to obtain a time series of WISE astrometric detections for moving sources as faint as our targets. By selection, our brown dwarf candidates tend to be completely undetected in W1. In W2, they typically have SNR of just ∼15 even when combining four years of WISE/NEOWISE data (see Figure 3). As a result, it is almost never possible to extract single-exposure W2 astrometry for any target in our sample, and we do not attempt to do so. Furthermore, in most cases it is not possible to obtain W2 detections of our targets even in time-resolved unWISE coadds that stack together the $\gtrsim$12 W2 exposures at each sky location during each single six-monthly WISE sky pass. Therefore, we often must perform source extraction on W2 stacks that combine multiple WISE sky passes.

The latest full-sky unWISE data release (Meisner et al. 2019) provides time-resolved coadds that bin W2 exposures into a series of single WISE sky passes, incorporating both the pre-hibernation time period (2010-2011) and the first four years of NEOWISE-R observations (2013-2017). These time-resolved unWISE coadds form the starting point for our W2 astrometry analysis. Ideally, we would also have access to such unWISE coadds for the calendar 2018 time period, but these have not yet been generated. However, since the 2018 NEOWISE-R data is only slightly earlier in time than our *Spitzer* p14034 imaging, there would be relatively little marginal benefit attained by including 2018 W2 data — this ad-

ditional W2 imaging would not increase our overall WISE+*Spitzer* time baseline and would only contribute a relatively weak astrometric constraint adjacent in time to our much higher precision p14034 *Spitzer* data point. With the Meisner et al. (2019) unWISE data set, we typically have five years of W2 imaging available at each sky location, corresponding to 10 time-resolved W2 coadds, which are labeled with names e000, e001, ..., e009. For concreteness, one representative cadence of such time-resolved unWISE coadds at fixed sky location is e000 $\sim$ 2010.4, e001 $\sim$ 2010.9, e002 $\sim$ 2014.4, ..., e009 $\sim$ 2017.9.

In gathering astrometric detections for our brown dwarf candidates, we always attempt extractions from all available e??? W2 unWISE coadds. Because this still leaves many of our faint targets undetected, we also generate and perform source extraction on a set of W2 'meta-coadd' time slices. This set of meta-coadd 'slices' is listed in Table 5. The 'pre' slice stacks all pre-hibernation e??? W2 unWISE coadds together to form a deeper 2010-2011 meta-coadd. Analogously, the 'post' slice stacks all post-hibernation e??? W2 unWISE coadds together, resulting in a deep 2013-2017 coadd. The 'post?_1yr' meta-coadd slices stack the post-hibernation e??? W2 unWISE coadds within a series of four non-overlapping 1-year time intervals. Lastly, the 'post?_2yr' meta-coadd slices stack the post-reactivation e??? W2 unWISE coadds within a series of two non-overlapping 2-year time intervals.

We generate our W2 meta-coadds for the full 1.56° $\times$ 1.56° unWISE coadd tile footprint containing each target. This has multiple advantages relative to considering only small postage stamps about our targets. First, it allows us to obtain a large number of *Gaia* DR2 (Gaia Collaboration et al. 2018) calibrator sources with which to produce refined WCS solutions for each W2 time slice (§8.3.1). Second, it provides sufficient numbers of bright point sources to accurately model the W2 PSF within each time slice.

We create W2 meta-coadds by performing an inverse variance weighted sum of the contributing e??? unWISE coadds, making use of the unWISE `-invvar-m` inverse variance maps. Using these same inverse variance weights, we also create a corresponding map of the mean MJD for each meta-coadd, enabling us to quote MJD values corresponding to our W2 astrometric detections.

Our modeling of the time-resolved unWISE coadds and meta-coadds, including source detection and centroiding, was performed using the `crowdsource` crowded field photometry pipeline (Schlafly et al. 2019). `crowdsource` has proven adept at modeling unWISE W1 and W2 images during creation of the full-sky unWISE Catalog (Schlafly et al. 2019). `crowdsource` derives a PSF model for each unWISE image it processes, and reports profile-fit astrometry that is equivalent to flux-weighted centroiding because the nominal PSF center is defined to coincide with the PSF model's flux-weighted centroid.

For the unWISE tile footprint containing each target, we ran `crowdsource` on all W2 time-resolved coadds (e??? time slices) and all meta-coadds (Table 5 time slices). Next, we proceeded to select the subset of these `crowdsource` detections that are counterparts to each brown dwarf candidate and will ultimately be combined with *Spitzer* astrometry during our final linear motion fits. We began by identifying a visually vetted set of pre-hibernation W2 `crowdsource` counterparts, one for each target. In combination with our *Spitzer* positions (§8.4), this allowed us to bracket each target's $\sim$2010-2019 trajectory and derive a crude linear motion estimate. Using this preliminary motion estimate, we then identified all `crowdsource` detections near the moving object's trajectory in all time slices. We visually inspected all such potential counterparts, removing severe blends and static contaminants.

The last step in selecting `crowdsource` detections for our final WISE+*Spitzer* motion fits is to pare down the full set of available detections for each target into a list that incorporates information from each WISE sky pass exactly once[13]. In this context, our faintest targets are the simplest. These objects will only have W2 detections in the deepest meta-coadds on each side of the WISE hibernation boundary: the 'pre' and 'post' time slices. Indeed, the simple combination of 'pre' and 'post' `crowdsource` astrometry was adopted for 104 of our 167 targets[14], as can be seen in Table 3. For brighter targets, we have the freedom to choose the specific set of time slices adopted. For instance, bright targets will have e000, e001 and 'pre' time slice detections available. We cannot use all of these in our joint WISE+*Spitzer* fits, since this would effectively double-count W2 imaging during the 2010-2011 time period. In these situations, we carefully constructed lists of `crowdsource` detections for each target that omitted as few W2 sky passes as

[13] In some rare cases, such as moving objects severely blended with static contaminants at certain WISE epochs, it was not possible (or desirable) to achieve this idealized goal.

[14] In the course of this work, we consider a total of 177 moving object candidates: 174 from our p14034 campaign and 3 with archival *Spitzer* imaging. Table 3 omits 4 of these discoveries that will be presented in an upcoming paper on CatWISE CPM systems (Marocco et al., in prep.) and another 6 targets which turned out to be spurious (§7.1), leaving 167 objects in Table 3.

possible while never double-counting. In doing so, we enforced a preference for shorter time slices, with the rationale being that longer time slices incur more smearing of the moving object, which is non-optimal for centroid measurements. Table 3 lists the W2 time slices employed for each target in our production WISE+*Spitzer* linear motion fits. On average, ∼3 W2 detections per target are used.

8.3.1. *W2 Astrometric Recalibration*

The time-resolved unWISE coadds inherit low-level (up to a few hundred mas) astrometric systematics by virtue of propagating the single-exposure WISE astrometry without modification (Meisner et al. 2018b, 2019). We therefore sought to improve the accuracy of our `crowdsource` W2 astrometry by recalibrating it to *Gaia* DR2.

For the `crowdsource` catalog corresponding to each time slice of each unWISE tile footprint, we seek to compute a scalar astrometric offset along each sky direction so as to bring our W2 centroids into best agreement with *Gaia* DR2. In practice, this is accomplished by adding a small offset to each of the two CRPIX components in the native W2 unWISE coadd WCS.

Each coadd from which we draw a brown dwarf candidate W2 detection covers a ∼2.4 square degree sky area, resulting in an abundance of available *Gaia* DR2 calibrators. To assemble a set of *Gaia*-`crowdsource` calibration sources, we crossmatch the full list of `crowdsource` detections against a subset of *Gaia* DR2 rows using a 2″ radius. We require that our *Gaia* DR2 astrometric calibrators have *Gaia* proper motions available, and we use these to propagate each calibrator's position to the mean epoch of the W2 coadd under consideration. We do not attempt to correct for the *Gaia* calibrator parallaxes, which have a mean amplitude of only ∼1-2 mas. The median number of *Gaia* DR2 calibrators employed per W2 coadd is 6,880.

With *Gaia* positions at the relevant epoch in hand, we calculate the two-element shift that needs to be applied to the native CRPIX to zero out the median offsets between the *Gaia* calibrators and their `crowdsource` matches along the coadd x and y pixel directions. We then apply this offset to create a slightly modified CRPIX value that, in combination with the other native W2 WCS parameters, provides a recalibrated astrometric solution most consistent with *Gaia* at zeroth order.

The mean amplitude of the per-coordinate offsets applied to the native CRPIX values is ∼50 mas. Using the recalibrated WCS for each coadd, the typical bright end scatter (assessed with $10 < \mathrm{W2} < 11.6$ unsaturated sources) relative to *Gaia* 'truth' is just 44 mas (41 mas) in RA (Dec). This is a very small fraction of the ∼6.5″ W2 PSF FWHM (∼1/150 FWHM), providing confidence in the astrometric fidelity of our W2 (meta-)coadds.

The systematics floor of our W2 astrometry as characterized by the bright end scatter is very small compared to the typical per-coordinate statistical uncertainties on our W2 `crowdsource` centroids, which have a median value of 515 mas. The W2 centroid statistical uncertainties are large because of the broad W2 PSF and low SNR of our `crowdsource` W2 detections (median SNR = 9.8). Figure 5 provides a visual illustration of the large statistical noise inevitably present in our W2 centroids.

Table 3 provides the positions and associated metadata of all W2 detections that feed into our final WISE+*Spitzer* linear motion fits. The σ_{RA} and σ_{Dec} values quoted each result from summing the statistical centroid uncertainty and bright end scatter systematics floor in quadrature (even though the former strongly dominates over the latter). σ_{RA} is in angular rather than coordinate units.

8.4. *Spitzer Astrometry*

Whereas our typical per-coordinate W2 centroid precision is larger than 500 mas, we should expect the ch2 per-coordinate centroid precision to be characteristically an order of magnitude smaller. This is simply due to the much higher SNR of our target detections in ch2 (median SNR ≈ 77) than in W2 (median SNR ≈ 10) and ∼3× narrower ch2 PSF. Because our centroid uncertainties are so much smaller in ch2 than in W2, the uncertainties on our eventual WISE+*Spitzer* linear motion measurements will be almost entirely dictated by the W2 positional uncertainties. Thus, we need not become fixated on obtaining *Spitzer* astrometry that achieves the ch2 imaging's theoretically optimal precision floor.

Kirkpatrick et al. (2019a) described a procedure for measuring *Spitzer* ch2 astrometry while achieving a systematics floor of just 10 mas per coordinate. This entailed a rather involved analysis which proceeds directly from the set of individual *Spitzer* BCD frames contributing to each AOR. On the other hand, Martin et al. (2018) demonstrated that a systematics floor of ∼20 mas per coordinate could be achieved via a substantially more convenient procedure based on astrometric measurements performed on MOPEX mosaics. Because reducing our ch2 systematics floor from ∼20 mas to ∼10 mas would negligibly decrease the uncertainties on our WISE+*Spitzer* linear motions and we already have MOPEX mosaics/extractions in hand for each target's field (§7), we opt to perform a mosaic-based *Spitzer* astrometric analysis.

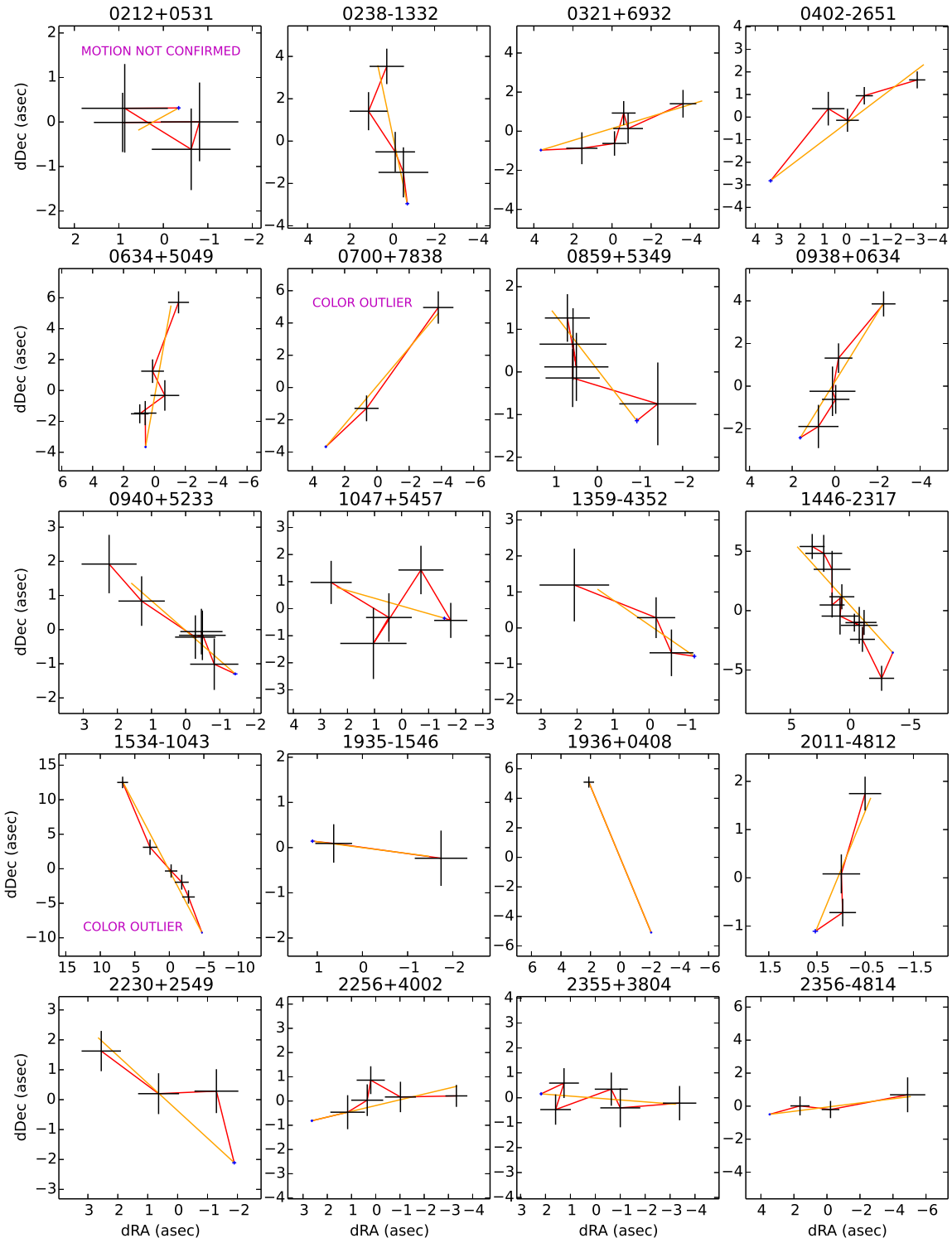

Figure 5. Combined WISE+*Spitzer* astrometric trajectories for all 18 of our discoveries with best-fit ch1−ch2 color most consistent with type ≥Y0. Except for CWISEP 0212+0531, all of these brown dwarf candidates are motion-confirmed according to our χ^2_{motion} criterion. Also included are two fast-moving ($\mu_{tot} > 1''$/yr) targets with unusually large J−ch2 colors relative to their ch1−ch2 colors: WISEA 1534−1043 and CWISEP 0700+7838 (see Figure 7). The black plus marks are centered on the WISE detections, with line segments extending $\pm 1\sigma$. The much smaller blue plus marks provide the same information for each target's *Spitzer* p14034 astrometric data point. Red lines connect positions adjacent to one another in time. Orange lines show the best-fit linear motion trajectory (Table 7) over the same time period spanned by the combination of WISE and *Spitzer* data points.

Our approach for deriving recalibrated *Spitzer* ch2 astrometric measurements from the p14034 imaging is largely modeled after the procedure laid out in Martin et al. (2018). Our starting point is the list of ch2 MOPEX/APEX pixel coordinate centroids and (RA, Dec) world coordinate values for all sources in each of our AORs. These are the same MOPEX/APEX catalogs used previously to obtain our ch2 magnitudes for each target in §7. The world coordinates natively provided by MOPEX/APEX rely on a WCS solution calibrated to 2MASS, and typically show offsets of several tenths of a mosaic pixel (0.6″/pixel) relative to *Gaia*. The systematics inherent in the initial 2MASS WCS solutions are thus much larger than the systematics floor attainable through astrometric recalibration to *Gaia*.

8.4.1. *ch2 Astrometric Recalibration*

The primary challenge in recalibrating each ch2 mosaic's astrometry is identifying a sufficient number of *Gaia* DR2 calibration sources (N_{calib}) with high-SNR ch2 counterparts. In selecting astrometric calibrators, we always restrict to the 'non-flanking' region of each p14034 ch2 mosaic (the portion of the mosaic built from single-frame BCD images which contain the brown dwarf candidate's location). Given our dither strategy, this results in a full frame coverage sky area from which to select *Gaia* calibrators of only 13-15 square arcminutes, depending on the number of dithers.

Ideally, we would be able to obtain at least 10 *Gaia* DR2 calibrators in each ch2 mosaic's non-flanking, full-coverage sky region with very high SNR ch2 counterparts (SNR $\geq$ 100) and *Gaia* proper motions available. However, this was possible for just 67 of our 164 ch2 mosaics (see the first row of Table 6). In cases where this ideal set of calibrator selection criteria (which we refer to as method #1) yielded fewer than 10 calibrators, we tried a sequence of somewhat loosened cuts in order to always obtain at least 5 *Gaia* calibrators[15]. We sequentially tried each set of selection criteria listed in Table 6, in order of ascending "method number" (leftmost column in Table 6) until a set of selection cuts yielded $N_{calib} \geq N_{calib,min}$. Method #2 is the same as our ideal set of cuts, but reduces the ch2 counterpart SNR threshold to 50. Method #3 further reduces the ch2 SNR threshold to 30 and additionally reduces the minimum required number of *Gaia* calibrators from 10 to 5 (as specified in the $N_{calib,min}$ column of Table 6).

[15] 5 is the minimum number of calibrators used for any field in the *Spitzer* ch2 parallax-fitting astrometric analysis of Kirkpatrick et al. (2019a).

Methods #4, #5, #6 are the same as methods #1, #2, #3 respectively, but with the requirement of *Gaia* DR2 proper motion availability dropped (see boolean '*Gaia* PM required' column of Table 6). Our inability to correct for calibrator motion between the *Gaia* 2015.5 epoch and our *Spitzer* ch2 epoch a few years later is regrettable but a necessary compromise when resorting to methods #4-#6. The typical motions of our *Gaia* DR2 calibrators are very small, so this should have a negligible impact on our final WISE+*Spitzer* linear motion results, and only 7 of 164 AORs end up using *Gaia* calibrators lacking proper motions.

Methods #7, #8, #9 are the same as methods #1, #2, #3 respectively, but reduce the minimum mosaic BCD frame coverage requirement from full coverage to at least 50% coverage. While this is not ideal, only 5 of 164 AORs needed to employ this lowered frame coverage requirement.

The 'method number' column of Table 4 specifies which set of *Gaia* DR2 calibrator selection criteria was used in determining each row's recalibrated *Spitzer* ch2 position. The N_{calib} column of Table 4 lists the number of *Gaia* DR2 calibrators employed for each recalibrated ch2 position measurement. The minimum (maximum) number of astrometric calibrators per AOR is 5 (92). The median (mean) number of astrometric calibrators per AOR is 12 (16). In all cases where our selection criteria demand that *Gaia* DR2 calibrators have proper motions available, we use these proper motions to propagate the *Gaia* calibrator positions to the *Spitzer* ch2 epoch.

Having selected a set of *Gaia* DR2 calibrators for each AOR, we proceed to re-fit 6 parameters of each ch2 mosaic's WCS: all four elements of the CD matrix and the two CRPIX components. The bright end systematics floor achieved via our recalibrated ch2 mosaic WCS solutions is very similar to that of Martin et al. (2018). The median per-mosaic bright end scatter is 25 (23) mas in RA (Dec). The 16th-84th percentile ranges are 15-44 mas in RA and 14-39 mas in Dec. For comparison, Martin et al. (2018) cites a typical systematics floor of ∼15-40 mas for their ch2 mosaic WCS recalibration.

Table 4 lists the recalibrated ch2 (RA, Dec) position obtained for each target, including metadata such as the AOR used and the MJD. The uncertainties σ_{RA} and σ_{Dec} are computed by summing the per-AOR bright end scatter in quadrature with the statistical uncertainty on each target's ch2 centroid measurement.

8.5. *WISE+Spitzer Linear Motion Fits*

For each brown dwarf candidate, we gather its combined list of WISE and *Spitzer* positions, corresponding

MJD values, and positional uncertainties from Tables 3 and 4. The typical combined WISE+*Spitzer* time baseline for targets with p14034 imaging available is ∼8.6 years. Along each coordinate direction (RA and Dec) we fit a linear model to the combined list of WISE and *Spitzer* positions as a function of MJD in order to measure μ_α and μ_δ. Throughout this paper the quoted μ_α values are in angular rather than coordinate units i.e., they already have the cos(δ) factor multiplied into them. Through these same per-coordinate linear fits we also obtain parameters α_0 and δ_0, the object's (RA, Dec) coordinates at a fiducial time MJD_0. MJD_0 is the inverse variance weighted mean MJD of the contributing astrometric data points. MJD_0 ends up typically being similar to the MJD of the *Spitzer* observation, since the ch2 positional uncertainties are much smaller than those in W2. Our linear fits are performed using weighted linear least squares and so naturally produce uncertainties on the fiducial location and best-fit linear motion components via simple matrix algebra. The measurement uncertainties fed to the weighted linear least squared routine are the σ_{RA} and σ_{Dec} values provided in Tables 3 and 4. No rescaling of the σ_{RA}, σ_{Dec} positional uncertainties is performed.

We do not allow for any outlier rejection in our per-coordinate linear motion fits. All detections used in our WISE+*Spitzer* motion fits were visually vetted, so there should be no need for outlier rejection.

For our targets which turned out to have two *Spitzer* counterparts (§7.2), we performed separate linear motion fits for each *Spitzer* counterpart, where the two motion fits both use the same set of WISE detections (since in such cases the brown dwarf candidate appears as just a single object in WISE).

Table 7 lists our linear motion fit results for all targets. The μ_α, σ_{α_0} and σ_{μ_α} values are all in angular rather than coordinate units. The total motion μ_{tot} values are calculated by summing the RA and Dec linear motion components in quadrature, and the quoted μ_{tot} uncertainties are based on first order propagation of the σ_{μ_α}, σ_{μ_δ} errors.

Figure 6 shows a histogram that vertically stacks the number of non motion-confirmed targets (black) on top of the number of motion-confirmed targets (blue). Targets with $\mu_{tot} > 380$ mas/yr are always motion confirmed. The motion-confirmed fraction decreases to 50% at $\mu_{tot} \approx 265$ mas/yr. The minimum best-fit μ_{tot} of any motion-confirmed member of our sample is 139 mas/yr. The minimum value of $\mu_{tot}/\sigma_{\mu_{tot}}$ for any motion-confirmed target is 4.85, which suggests that, roughly speaking, our $\chi^2_{motion} = 23.03$ threshold is akin to a requirement of 5σ significant motion. 114 of our discoveries are motion confirmed via the astrometric analysis presented in this work, as indicated in the boolean 'motion confirmed' column of Table 1.

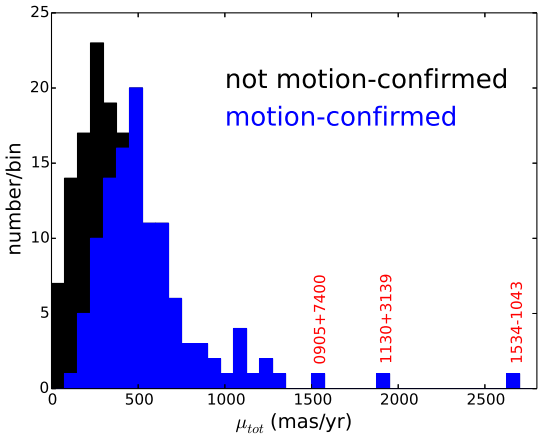

Figure 6. Histogram of total motion measurements resulting from our sample's linear motion fits (§8.5). The number of targets per bin which we could not motion confirm is shown in black, stacked on top of the number of motion-confirmed targets per bin (blue). We exclude the 6 spurious candidates (Table 2), 4 CPM objects, and the two targets which each have two *Spitzer* counterparts (§7.2). Three of our motion-confirmed discoveries have best-fit $\mu_{tot} > 1500$ mas/yr, and twelve have $\mu_{tot} > 1000$ mas/yr.

9. GROUND-BASED PHOTOMETRY

Although *Spitzer* ch1−ch2 color provides the most efficient means for constraining the spectral types of our brown dwarf candidates, J band photometry can further inform spectral type estimates and represents a crucial step toward ultimately obtaining NIR spectroscopic confirmations. Beyond T5, $J-$W2 color increases rapidly toward later spectral types, with the T/Y boundary at $J-\mathrm{W2} \sim 5$ mag (Kirkpatrick et al. 2011). For candidates thought to be potential very late T or Y dwarfs, we therefore sought to obtain ground-based J band follow up to a depth of at least $J \sim 21$ (given that W2 ≈ 16 is typical for our sample as discussed in §5). Our NIR imaging was not intended to be used for high-fidelity astrometry, and we do not attempt to incorporate ground-based NIR data into our astrometric analyses for several reasons. Among these, the NIR observations generally do not extend our overall time baseline appreciably beyond our *Spitzer* p14034 epoch.

9.1. *Gemini/FLAMINGOS-2 Follow-up*

For southern targets, we acquired follow-up J band imaging at Gemini South. Through program GS-2019A-Q-316 (PI Gelino) we obtained FLAMINGOS-2 (Eikenberry et al. 2006) J band photometry for 16 of

the discoveries presented in this paper. The J band photometry from Gemini that we provide is in the MKO photometric system. To calibrate the photometry in each target's field using 2MASS, we applied the color transformation equation from Hodgkin et al. (2009):

$$J_{MKO} = J_{2MASS} - 0.065 \times (J_{2MASS} - H_{2MASS}) \quad (3)$$

For each target, we requested a 60 second exposure time per dither with a 9-position dither pattern.

9.2. *Palomar Hale/WIRC Follow-up*

For northern targets, we obtained follow-up J band imaging with the Wide Field Infrared Camera (WIRC; Wilson et al. 2003) at the Palomar Hale 200 inch telescope (PI Marocco). This WIRC photometry is also in the MKO system, and we again used Equation 3 to photometrically calibrate each field. We obtained WIRC J band photometry for 32 of the discoveries presented in this paper. The total exposure time varied depending on environmental conditions and the anticipated J band magnitude of each target, but 15 dithers at 2 minutes per dither represents a typical observing sequence for one object.

9.3. *Archival Near-infrared Photometry*

9.3.1. *2MASS*

By selection, we expect very few of our targets to have 2MASS counterparts. Nevertheless, we checked our entire sample for 2MASS counterparts. We used our best-fit WISE+*Spitzer* proper motions from Table 7 to predict each target's (RA, Dec) at a fiducial 2MASS epoch of year = 1999.5, then visually inspected 2MASS images to look for a counterpart at that location. In all, we only found 2MASS counterparts[16] to two discoveries in our sample: CWISEP 1402+1021 and CWISEP 2015−6750. Both of these are relatively bright/blue members of our sample, selected specifically because we expected they may be mid-T brown dwarfs potentially within a distance of 20 pc. Both 2MASS counterparts are detected only in J_{2MASS}, and in both cases the J_{2MASS} magnitude is in good agreement with that predicted based on ch2 magnitude and *Spitzer* phototype. Table 8 lists the two 2MASS counterparts recovered. The magnitude limits in Table 8 are based on 95% confidence flux upper limits.

9.3.2. *UKIRT/WFCAM and VISTA/VIRCAM*

We searched the entire WFCAM Science Archive (WSA) and VISTA Science Archive (VSA) for JHK/K_S counterparts to our brown dwarf candidates. Specifically, we searched all "pawprint" exposure sets[17] through 2017 January 1 in VSA and 2014 March 7 in WSA[18]. We queried for counterparts within a 5″ radius of a nominal epoch ∼2014 position for each target, based on our linear motion solutions. We retrieved all matched VSA/WSA detections within this relatively large 5″ radius, allowing us to perform more detailed disambiguation downstream. Further, when possible, we retrieved available 5σ magnitude limits in cases where no matches were found within a 5″ radius yet archival VSA/WSA imaging at the target location exists.

In total we retrieved ∼1,100 VSA/WSA matched detections or magnitude limits in JHK/K_S. These were drawn predominantly from the UKIRT Hemisphere Survey (UHS; Dye et al. 2018) and VISTA Hemisphere Survey (VHS; McMahon et al. 2013), but also incorporate contributions from a variety of other smaller-area surveys including ULAS (Lawrence et al. 2007), VIKING (Edge et al. 2013), and a few PI programs. In many cases a single brown dwarf candidate has multiple VSA/WSA detections/limits in one NIR band.

We therefore sought to condense/vet our raw VSA/WSA query results and thereby compose a summary consisting of at most one VSA or WSA magnitude or magnitude limit per NIR band per target. To do so, we used the linear motion solutions from Table 7 to predict the moving target's position at each VSA/WSA pawprint MJD. We then retained only matches within 1.5″ of each predicted position. In cases where a single target has multiple matched detections within 1.5″ in a single band, we adopt the magnitude of the closest match. When a target has no counterparts in a given band within 1.5″, we quote a magnitude limit in that band if one is available. In cases where there is no counterpart but multiple limits, we adopt the deepest limit. We also enforced a veto list containing a small handful of VSA/WSA detections which were noted to be static contaminants (wrong cross-matches) based on visual inspection of the VIRCAM/WFCAM imaging. We additionally discarded all VSA/WSA detections with nonzero PPERRBITS data quality flags[19] and/or with an extended morphological classification (CLASS = 1), so as to avoid artifacts and incorrectly matched galaxies.

[16] In both cases the 2MASS counterpart is drawn from the Point Source Reject Table.

[17] http://www.vista.ac.uk/glossary.htm#pawprint

[18] Public availability of data in VSA/WSA becomes a relatively complex issue at later dates.

[19] http://wsa.roe.ac.uk/ppErrBits.html

Photometry from WFCAM JHK and VIRCAM JH is in the MKO system, whereas VIRCAM employs a K_S filter.

9.3.3. *Merging Archival & Follow-up NIR Photometry*

In order to produce color-color diagrams such as those of Figure 7 and Figure 8, we sought to merge our Palomar, Gemini, WFCAM, VIRCAM and 2MASS NIR photometry into a single compilation with at most one magnitude or magnitude limit per NIR band per target. In doing so, we always give precedence to our dedicated CatWISE follow-up over archival information in J band when both options are available. In one isolated instance, we have archival photometry available from both VISTA and 2MASS while lacking CatWISE follow-up: J band for CWISEP 2015−6750. In this case we adopt the much higher SNR measurement from VISTA. Table 9 provides the merged compilation of VSA/WSA and follow-up JHK/K_S magnitudes and limits for motion-confirmed discoveries with at least one such NIR magnitude or limit available. 2MASS photometry is listed separately in Table 8. All limits quoted in Table 9 are 5σ. Finally, Table 10 lists our Palomar and Gemini J band follow-up for sources that were not motion-confirmed by our astrometric analysis.

10. DISCUSSION

10.1. *Photometric Spectral Type Estimates*

Obtaining photometric spectral type estimates was the primary motivation for conducting our *Spitzer* p14034 follow-up campaign. We use the ch1−ch2 colors from Table 1 to estimate spectral types. We do not attempt to fold NIR magnitudes/limits into our phototyping in this work. For our spectral type estimates, we use a type versus ch1−ch2 color grid constructed from the Kirkpatrick et al. (2019a) relation for T5.5-Y1 and Kirkpatrick et al. (2011) for T0-T5. These grids are quantized at the level of 0.5 type. Quoted spectral type estimates result from evaluating these type versus ch1−ch2 grids at the best fit (i.e., central) ch1−ch2 color from Table 1. Our photometric type estimates do not extend colder than Y1 due to the scarcity of empirical data in this regime, and as a result objects with best-fit phototypes of Y1 are listed as ≥Y1 in Tables 11 and 12. Table 11 presents a number of derived properties for each of our motion-confirmed discoveries, including our spectral type estimates in a column labeled SpT for short.

Figure 9 shows a histogram of our measured ch1−ch2 colors for motion-confirmed brown dwarf candidates. The median ch1−ch2 color within our motion-confirmed sample is 1.75 mag, corresponding to a spectral type of approximately T8. CWISEP 0959−4010 has the bluest ch1−ch2 color of any motion-confirmed target in our sample, ch1−ch2 = 0.50 ± 0.12 mag, for which we obtain a spectral type estimate of T3.5. The reddest best-fit ch1−ch2 color of any motion-confirmed target in our sample is 3.71 ± 0.44 mag for CWISEP 1446−2317, which has its reported spectral type estimate listed as ≥Y1.

We caution against overinterpretation of our spectral type estimates on an object-by-object basis, since we regard these as considerably uncertain for a number of reasons. The Kirkpatrick et al. (2019a) tabulation of ch1−ch2 versus spectral type does not provide a direct formula for spectral type as a function of ch1−ch2 color, nor a prescription for quoting uncertainties on spectral type estimates inferred from *Spitzer* color. Additionally, spectral typing becomes relatively poorly defined at types ≳Y1, due to a number of factors including small sample size, lack of NIR spectroscopic data (e.g., WISE 0855−0714, WD 0806−661 B; Luhman et al. 2011), and difficulty fitting all examples into a common sequence of spectral morphology (see WISE 1828+2650; Beichman et al. 2013; Leggett et al. 2013).

Although these considerations lead us not to quote per-target spectral type errors, we can still use the Kirkpatrick et al. (2019a) compilation of spectral types and ch1−ch2 colors to provide an overall sense for the level of uncertainty on our type estimates. We fit a second order polynomial to the (ch1−ch2, spectral type) pairs with $0.9 \leq$ ch1−ch2 ≤ 3.0 in the bottom center panel of Kirkpatrick et al. (2019a) Figure 4, using ch1−ch2 as the independent variable. The residuals relative to the best fit show an RMS scatter of ±0.56 in spectral type. As a result of the p14034 observing strategy, our ch1−ch2 color uncertainties ramp up from ∼0.06 mag for ch1−ch2 < 1.2 to ∼0.2 mag at type ∼Y1. Propagating this color uncertainty through our best-fit polynomial relation for spectral type, this translates into a scatter of ∼0.15 (∼0.65) in type at mid-T (Y1). Adding the worst-case 0.65 type scatter in quadrature with that of the type versus ch1−ch2 polynomial residuals and that from our 0.5 type quantization yields an overall errorbar of roughly 1.0 in spectral type for our reported estimates.

We emphasize that it is not actually possible to measure a spectral type with the data at hand — our ch1−ch2 colors are measured in a totally different wavelength regime than that in which the spectral type is defined (at J and H bands), so we can only provide our best estimate as to near-IR type based on its known correlation with *Spitzer* color. True spectral types can

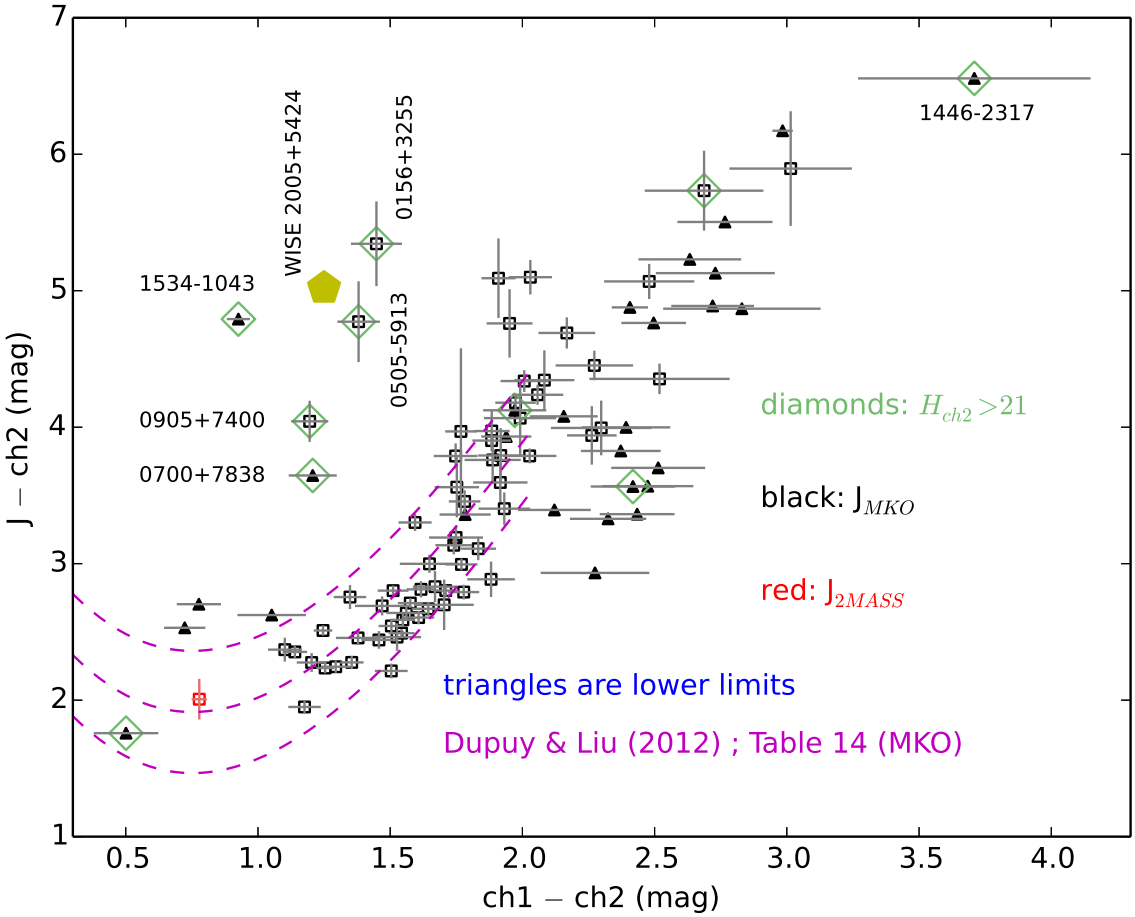

Figure 7. $J-$ch2 versus ch1$-$ch2 for motion-confirmed discoveries with *Spitzer* photometry available. The J band photometry is drawn from our Gemini/FLAMINGOS-2 and Palomar/WIRC follow-up, the WFCAM and VISTA archives, and 2MASS. The purple dashed lines trace the expected trend for late-type brown dwarfs from Dupuy & Liu (2012), plus/minus the scatter in the relevant relations from their Table 14. Our motion-confirmed brown dwarf candidates largely follow this trend while continuing (as expected) to become even redder in $J-$ch2 beyond T9, where the Dupuy & Liu (2012) relations are not intended to be applicable. Light green diamonds indicate targets with exceptionally large reduced proper motion, $H_{ch2} > 21$ mag. Five targets (each specially labeled with its short name) are anomalously red in $J-$ch2 relative to their ch1$-$ch2 colors, inhabiting a region of parameter space with $J-$ch2 > 3.5 and ch1$-$ch2 < 1.5. All five of these major color outliers have $H_{ch2} > 21$, suggesting that they may represent a low metallicity subpopulation. Color limits are based on 5σ J band flux limits. The yellow pentagon denotes the location of the benchmark T8 subdwarf WISE 2005+5424 within this color-color space.

only be measured using spectra in the wavelength range of interest. In the absence of observationally prohibitive spectroscopic confirmations, spectral type estimation for our coldest motion-confirmed discoveries would greatly benefit from further astrometric follow-up in the future, with trigonometric distances yielding critical ch2 absolute magnitude estimates.

10.2. *Photometric Absolute Magnitude and Distance Estimates*

We use the Kirkpatrick et al. (2019a, Table 8) ch1$-$ch2 to M_{ch2} relation to obtain photometric absolute magnitude estimates, which in turn yield corresponding photometric distance estimates. These derived properties for our motion-confirmed targets are presented in Table 11. When calculating uncertainties on these absolute magnitude estimates, we take into account both our 1σ ch1$-$ch2 color uncertainties and the 0.3 mag residual scatter of the M_{ch2}(ch1$-$ch2) polynomial fit relative to its training data.

The Kirkpatrick et al. (2019a) M_{ch2}(ch1$-$ch2) relation is only valid for $0.9 \leq$ch1$-$ch2≤ 3.7. However, a handful of our motion-confirmed discoveries have ch1$-$ch2 < 0.9 mag, and in these cases we obtain M_{ch2} estimates by plugging our spectral type estimates from Table 11 into the Dupuy & Liu (2012, Table 14) M_{ch2}(SpT) relation, which is applicable in the relevant early-mid T regime.

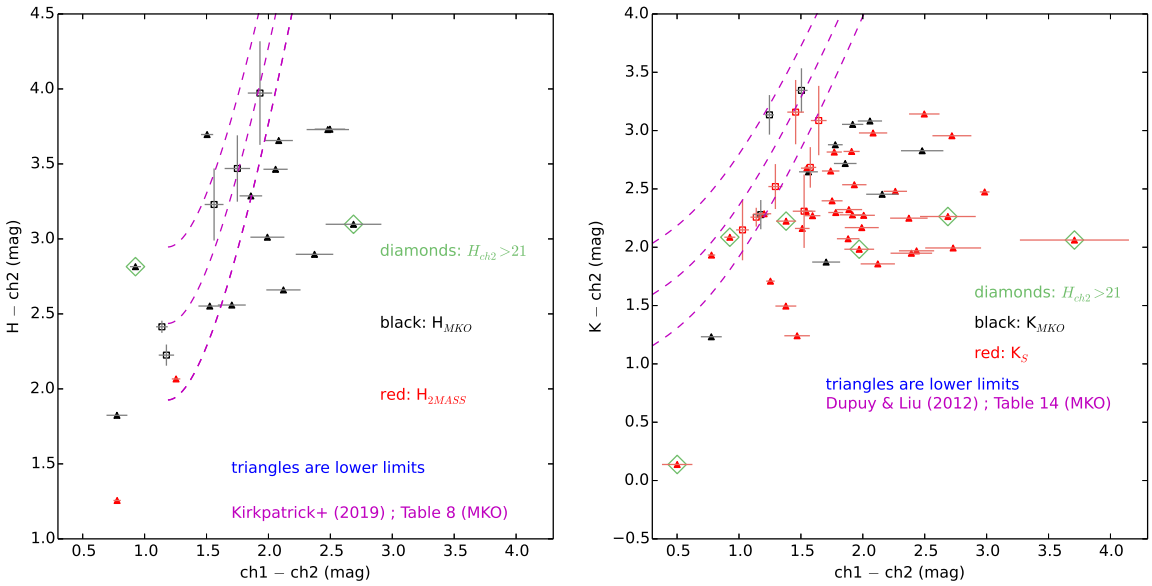

Figure 8. Same as Figure 7, but for $H-$ch2 (left) and $K-$ch2 (right). Relative to J, there are far fewer targets with available data at H and K, in part reflecting the availability of VISTA/UKIRT archival observations, but also because our NIR imaging follow-up campaigns at Gemini and Palomar only employ J band. The limited number of detections follow the literature trends reasonably well. In each panel, the CWISEP 1402+1021 and CWISEP 2015−6750 color lower limits are based on 95% confidence flux upper limits from 2MASS. All other color lower limits are based on 5σ flux upper limits.

CWISEP 1446−2317 is our only discovery with best-fit ch1−ch2 color too red for the Kirkpatrick et al. (2019a) M_{ch2}(ch1−ch2) relation. In this case, we quote only a lower limit of $M_{ch2} > 16.23$. This limit is derived by applying the Kirkpatrick et al. (2019a) M_{ch2}(ch1−ch2) relation to the ch1−ch2 color obtained by subtracting this object's 1σ *Spitzer* color uncertainty from its central ch1−ch2 color. Correspondingly, we quote only a distance upper limit of 8.3 pc for CWISEP 1446−2317 based on its M_{ch2} lower limit. Such limits should be treated with caution given our poor constraint on this object's *Spitzer* color.

The middle panel of Figure 9 shows a histogram of our motion-confirmed sample's photometric distance estimates. As discussed in §10.9, we suspect that many of the objects with unusually large distance estimates ($\gtrsim$50 pc) may be subdwarfs. The median distance estimate for motion-confirmed targets is 26 pc. Propagating our M_{ch2} estimates and their errorbars into distance estimates, the 1σ fractional uncertainty on our photometric distances is typically ∼15%.

10.3. *Photometric Effective Temperature Estimates*

Table 11 also provides T_{eff} estimates based on the Kirkpatrick et al. (2019a, Table 8) T_{eff}(ch1−ch2) polynomial relation. When calculating uncertainties on these T_{eff} estimates, we take into account both our 1σ ch1−ch2 color uncertainties and the 81 Kelvin residual scatter of the T_{eff}(ch1−ch2) polynomial fit relative to its training data. This floors our quoted T_{eff} uncertainties at 81 Kelvin.

The Kirkpatrick et al. (2019a) T_{eff}(ch1−ch2) relation is only valid for $0.9 \leq$ch1−ch2≤ 3.7. We omit T_{eff} estimates for the handful of our motion-confirmed discoveries with ch1−ch2 < 0.9 mag. There is currently no T_{eff}(ch1−ch2) relation available in this early-mid T regime, and within this range of spectral types T_{eff} maintains a roughly uniform value of ∼1400-1500 Kelvin anyway (e.g., Kirkpatrick 2005, Figure 7).

The best-fit CWISEP 1446−2317 *Spitzer* color is too red for the Kirkpatrick et al. (2019a) T_{eff}(ch1−ch2) relation. We therefore quote only an upper limit of $T_{eff} < 381$ K for CWISEP 1446−2317. This value arises from evaluating the T_{eff}(ch1−ch2) formula at a color 1σ bluer than the central value and further adding the aforementioned 81 K systematics floor of the T_{eff} relation in attempt to be conservative.

10.4. *Reduced Proper Motions and Tangential Velocities*

Reduced proper motions (H_{ch2}) can be calculated entirely on the basis of directly measured quantities: μ_{tot} (Table 7) and apparent ch2 magnitude (Table 1). In calculating uncertainties on H_{ch2} we account for the uncertainties on both μ_{tot} and ch2 magnitude. Table 11 lists H_{ch2} for all motion-confirmed targets with *Spitzer* imaging available. Figure 10 shows a scatter plot of H_{ch2} versus ch1−ch2 color for the same set of our dis-

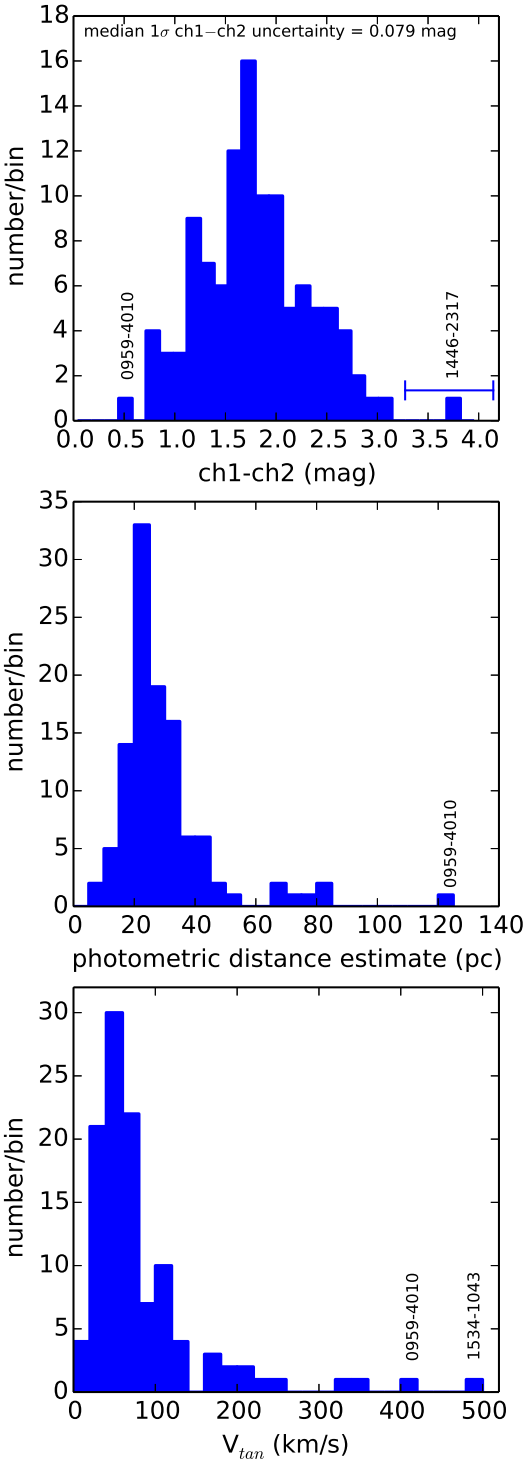

Figure 9. Histograms of measured *Spitzer* colors (top) and selected derived parameters (middle: photometric distance estimates, bottom: V_{tan} estimates) from Table 11 for motion-confirmed discoveries with *Spitzer* photometry available. Short names of outliers are added as annotations. As discussed in §10.9, we hypothesize that several objects with unusually large V_{tan} and/or distance estimates may be late-type subdwarfs.

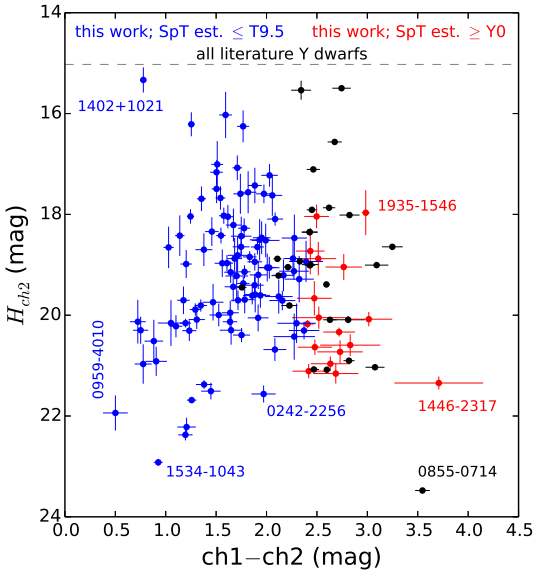

Figure 10. Reduced proper motion diagram showing all Y dwarfs from the prior literature (black) and all motion-confirmed discoveries from this study with *Spitzer* photometry available. Our targets with best-fit ch1−ch2 color most consistent with spectral type Y are shown in red, while all of our discoveries with earlier spectral type estimates are shown in blue.

coveries, plus all Y dwarfs from the prior literature to provide context. Interestingly, all three of our motion-confirmed discoveries with $H_{ch2} > 22$ mag are rather blue in ch1−ch2 color relative to the bulk of our sample. These three objects (CWISEP 0700+7838, CWISEP 0905+7400, WISEA 1534−1043) have ch1−ch2 <1.25 mag, making all of them bluer in *Spitzer* color than at least 85% of our motion-confirmed sample.

Computing V_{tan} values requires making use of our photometric distance estimates from §10.2. In computing uncertainties on V_{tan} we account for the uncertainties on both μ_{tot} and our distance estimates. Table 11 provides our V_{tan} estimates for motion-confirmed targets with *Spitzer* imaging available. The bottom panel of Figure 9 displays a histogram of the central V_{tan} values for this sample. As discussed in §10.9, a number of our highest V_{tan} motion-confirmed discoveries are also color outliers.

For CWISEP 1446−2317, our distance upper limit from Table 11 translates into a V_{tan} upper limit, $V_{tan} <$ 53 km/s.

10.5. *Y Dwarf Candidates*

Seventeen of our motion-confirmed discoveries have best-fit phototypes ≥Y0. In practice, within the spectral type estimation framework described in §10.1, this is to say that seventeen of our motion-confirmed targets

have central ch1−ch2 colors of at least 2.40 mag. Plots of our astrometric measurements and linear motion fits for all 17 of these Y dwarf candidates are shown in Figure 5. An eighteenth target, CWISEP 0212+0531, has ch1−ch2 > 2.40 mag, but its motion appears to be disconfirmed (or else very small) in light of our combined WISE and *Spitzer* astrometry.

Given our §10.1 appraisal that SpT estimates for our reddest objects carry an uncertainty of roughly 1 type, we cannot yet specify an exact list of our targets that will ultimately turn out to fall on the late-type side of the T/Y boundary. Nevertheless, we can perform some cross-checks on the hypothesis that our 17 reddest motion-confirmed discoveries are indeed Y dwarfs, and rate the relative likelihood that particular objects in this sample are/aren't in fact 'merely' T dwarfs.

We find that the archival and follow-up JHK/K_S NIR photometry assembled in §9 is consistent with the proposition that most motion-confirmed objects with ch1−ch2 ≥ 2.4 mag are Y dwarfs. All 17 targets with phototypes ≥Y0 have J band imaging available. Four of these targets have J band detections: CWISEP 0938+0634, CWISEP 2256+4002, CWISEP 2355+3804 and CWISEP 2356−4814. Their respective J−ch2 colors are 5.07±0.12, 5.90±0.41, 4.35±0.10 and 5.73±0.28 magnitudes. Three of these J−ch2 colors are consistent with Y spectral types. The fourth J−ch2 color, for CWISEP 2355+3804, seems to provide an indication that this target may actually be a late T dwarf.

The remaining 13 targets with type estimates ≥Y0 have J−ch2 limits available. Among these, five objects have 5σ J limits establishing that J−ch2 > 5 mag, bolstering the case (though still not guaranteeing) that they are Y dwarfs: CWISEP 0238−1332 (J−ch2 > 5.13), CWISEP 0321+6932 (J−ch2 > 5.23), CWISEP 0940+5233 (J−ch2 > 5.50), CWISEP 1446−2317 (J−ch2 > 6.56) and CWISEP 1935−1546 (J−ch2 > 6.17). Another 4 motion-confirmed candidates with ch1−ch2 ≥ 2.40 mag have J−ch2 limits corresponding to minimum colors that would be extremely red among the latest T dwarfs: CWISEP 0402−2651 (J− ch2> 4.89), WISENF 1936+0408 (J− ch2> 4.88), CWISEP 2011−4812 (J− ch2> 4.76) and CWISEP 2230+2549 (J− ch2 > 4.87). Lastly, four targets with type estimates ≥Y0 have J nondetections establishing relatively weak J−ch2 limits in the 3.35-3.70 mag range (CWISEP 0634+5049, CWISEP 0859+5349, CWISEP 1047+5457 and CWISEP 1359−4352). Clearly, deeper J band imaging follow-up would be highly valuable in pinning down which side of the T/Y boundary each of our ≥Y0 phototype discoveries falls on.

None of our ≥Y0 phototype targets have detections at H band. Three of our ≥Y0 phototype targets have H nondetections establishing H−ch2 limits in the range of 3.1-3.75 mags (CWISEP 0938+0634, CWISEP 2011−4812 and CWISEP 2356−4814). While these color limits are consistent with spectral type Y, they are essentially uninformative — an H−ch2 limit would need to reach ≳5 mag in order to begin disfavoring late T spectral types (e.g., Kirkpatrick et al. 2019a, Figure 4).

None of our ≥Y0 phototype targets have detections at K or K_S. Eight such objects have K/K_S nondetections establishing weak K−ch2 (or K_S−ch2) limits in the range of 1.97 to 3.14 magnitudes. A lack of bright K/K_S counterparts is consistent with these eight ≥Y0 phototype targets being very late T or Y dwarfs.

Table 12 lists 24 of our motion-confirmed discoveries which we believe merit further follow-up to better refute or confirm their status as Y dwarf candidates. There are three subclasses of objects listed in Table 12. Within each of the three subclasses, our discoveries are listed from reddest (top) to bluest (bottom) in terms of ch1−ch2 color. The first 17 targets are those with *Spitzer*-based phototypes ≥Y0. We include CWISEP 2355+3804 in this list even though its J−ch2 color suggests a more likely spectral type of late T. The second class of Y dwarf candidates listed are those sufficiently red to have ch1−ch2 colors within 1σ of our phototyping grid's T/Y boundary at ch1−ch2 = 2.4 mag, excluding candidates with J detections establishing J−ch2 < 5 mag. There are four such discoveries. The final class of possible Y dwarf candidates listed are those not within 1σ of the T/Y color boundary, but nevertheless having measured ch1−ch2 redder than that of the bluest known Y dwarf in terms of this color[20] and lacking a J detection establishing J−ch2 < 5 mag. Three of our discoveries fall in this category. We emphasize that Table 12 targets in the latter two groups of Y dwarf candidates are likely to be late T dwarfs, but they nevertheless stand out as our most plausible Y dwarf candidates in the 2.1 ≲ ch1−ch2 ≲ 2.4 regime where T and Y dwarfs overlap considerably.

The Table 12 column labeled $[(\text{ch1}-\text{ch2})-2.4]/\sigma_{ch1-ch2}$ measures how much redder/bluer each candidate is than the adopted T/Y boundary at ch1−ch2 = 2.4, in units

[20] For the bluest ch1−ch2 color of any known Y dwarf, we adopt a value of ch1−ch2 = 2.11, corresponding to the Y0 dwarf WISE 2056+1459. WISE 1141−3326 (type Y0) has a bluer reported color of ch1−ch2 = 1.76±0.04 (Kirkpatrick et al. 2019a), but this anomaly is thought to result from blending with a background source (Tinney et al. 2018).

of each target's *Spitzer* color uncertainty $\sigma_{ch1-ch2}$. This metric helps provide a sense for how certain we can be about whether each object is a T dwarf versus a Y dwarf. Five of our targets with phototype $\geq$Y0 are redder than our grid's T/Y boundary by more than 2σ. Much more follow-up is warranted in order to better measure/constrain the spectral types of the Y dwarf candidates presented in this section.

10.6. *Fastest-moving Discoveries*

The median μ_{tot} of our motion-confirmed targets is 490 mas/yr. At the high motion tail of this distribution, three of our discoveries have best-fit $\mu_{tot} > 1.5''$/yr (CWISEP 0905−7400, CWISEP 1130+3139, and WISEA 1534−1043). An additional nine of our motion confirmed discoveries have $1.0''$/yr $< \mu_{tot} < 1.5''$/yr. WISEA 1534−1043 has the highest total motion ($\mu_{tot} = 2697 \pm 68$ mas/yr) and reduced proper motion ($H_{ch2} = 22.92 \pm 0.06$ mag) of our motion-confirmed discoveries. The five largest H_{ch2} values among our sample all belong to objects with ch1−ch2 ≤ 1.26 mag, meaning that these targets occupy the bluest 20% of our sample in terms of ch1−ch2 color. Figure 10 shows a ch2 reduced proper motion diagram for all of our motion-confirmed targets with *Spitzer* imaging available, plus the entire sample of Y dwarfs from the prior literature for context. While our targets with phototypes $\geq$Y0 generally inhabit the $18 \lesssim H_{ch2} \lesssim 21.5$ regime broadly consistent with that of literature Y dwarfs, none of our very red (ch1−ch2 > 2.4 mag) Y dwarf candidates comes within 2 mags of WISE 0855−0714 in terms of H_{ch2}.

Using the §10.2 distance estimates, we obtain many V_{tan} values well exceeding the typical 'high kinematics' threshold of 100 km/s (e.g., Faherty et al. 2009). 27 (13, 8, 4, 2) of our motion-confirmed discoveries have central V_{tan} estimates in excess of 100 (150, 200, 300, 400) km/s. As discussed in §10.9, we suspect that many of our highest V_{tan} discoveries may be low-metallicity, subluminous objects, in which case their true tangential velocities would be lower than we have derived using the Kirkpatrick et al. (2019a) M_{ch2}(ch1−ch2) relation.

10.7. *Nearest Discoveries*

CWISEP 1935−1546 is our sample's only object with a central distance estimate placing it within 10 pc (Table 11). However, with $d = 9.8^{+1.5}_{-1.3}$ pc, CWISEP 1935−1546 may well reside outside of the 10 pc volume. Meanwhile, the poorly constrained color of CWISEP 1446−2317 translates to a distance upper limit of $d < 8.3$ pc. Three additional discoveries have central distance estimates falling outside of 10 pc, but are within their 1σ lower distance uncertainties of being closer than 10 pc (CWISEP 0402−2651, WISENF 1936+0408, CWISEP 2256+4002)

10.8. *The 20 pc Sample*

Completing the 20 pc census at types $\gtrsim$T5 represents a crucial step toward constraining late-type space densities, and ultimately the low-mass cutoff of the substellar mass function (e.g., Kirkpatrick et al. 2019a). According to Table 11, 21 of our motion-confirmed discoveries have central distance estimates (or a distance upper limit in the case of CWISEP 1446−2317) within 20 pc. These 21 targets have phototypes ranging from T7.5 to $\geq$Y1. An additional 24 of our motion-confirmed discoveries have central distance estimates larger than 20 pc, but are within their 1σ lower distance uncertainties of being closer than 20 pc. 7 of our discoveries have 1σ high distances still contained within 20 pc. Trigonometric distances will be needed to conclusively determine which of our discoveries indeed reside within 20 pc and take these new objects into account when computing space densities. In the absence of trigonometric distances, spectroscopic types could help refine absolute magnitude and hence distance estimates for our discoveries.

10.9. *NIR/Mid-IR Color-Color Plots*

Our §9 compilation of follow-up and archival JHK/K_S photometry allows us to make a set of NIR/mid-IR color-color plots and thereby identify objects/populations with unusual spectral energy distributions. Figure 7 provides a J−ch2 versus ch1−ch2 color-color diagram for motion-confirmed targets with *Spitzer* photometry and J band detections or limits available. By and large, our discoveries are in reasonable agreement with the literature trend for mid-late T dwarfs shown in magenta (Dupuy & Liu 2012). Our sample continues to display a rising J−ch2 trend toward the highest ch1−ch2 colors (latest spectral types), as anticipated.

However, we note a distinct subpopulation with anomalously large J−ch2 colors (J−ch2 >3.5 mag) given their relatively blue *Spitzer* colors (ch1−ch2 < 1.5 mag) among our sample. Five of our discoveries are clearcut members of this color outlier population: CWISEP 0156+3255, CWISEP 0505−5913, CWISEP 0700+7838, CWISEP 0905+7400 and WISEA 1534−1043. In all such cases, the measured J−ch2 colors/limits are at least 1.4 magnitudes redder than the Dupuy & Liu (2012) T dwarf trend (middle dashed magenta line in Figure 7).

There are several potential physical explanations for brown dwarf color outliers including metallicity, low/high gravity and binarity. Binarity is difficult to

judge given our complete lack of trigonometric distances, spectroscopy and high-resolution imaging follow-up. On the other hand, kinematics can be helpful in assessing whether our color outliers may be unusually old (low metallicity, high gravity) or young (high metallicity, low gravity). Indeed, all five of our color outliers have unusually large reduced proper motions, $H_{ch2} > 21$ mag (see Figure 10). Only 10 of the 93 discoveries in Figure 7 have $H_{ch2} > 21$ mag, and five of these are our color outliers, with another three much redder in ch1−ch2 phototyped as Y dwarfs. Additionally, all five color outliers have estimated $V_{tan} > 200$ km/s, suggesting they may be members of a halo population. In contrast, binarity would lead our V_{tan} estimates to be biased low, and would also tend to favor relatively low H_{ch2}. Young objects would also preferentially have low kinematics. Thus, the high kinematics of our color outliers provide strong indications that this subsample is old, with relatively low metallicity and high gravity.

Our color outliers bear a striking resemblance to the benchmark T8 subdwarf WISE J200520.38+542433.9 (Mace et al. 2013b), one of the best characterized mid-late T subdwarfs. Similar to our color outliers, WISE 2005+5424 is unusually red in $J-$ch2 ($J-$ch2 = 5.02 ± 0.09 mag) relative to its modest ch1−ch2 color of ch1−ch2 = 1.25 ± 0.03 mag. WISE 2005+5424 is shown in Figure 7 as a yellow pentagon, and falls squarely amidst our five color outliers. As noted by Mace et al. (2013b), the models of Burrows et al. (2006) do indeed predict that low metallicity objects with temperatures from 700-2200 K will have relatively red $J-$ch2 colors. We therefore believe that our color outliers are best considered mid-late T subdwarf candidates. If subdwarfs, their lower luminosities would correspond to smaller distances and hence help rein in their exceptionally large V_{tan} values we have derived assuming an M_{ch2}(ch1−ch2) relation applicable to typical T dwarfs.

Mace et al. (2013b) consider the ensemble of T dwarf color outliers, suggesting that $J-H$ color is useful in differentiating between old and young objects (see especially their Table 3 and Figure 8). Unfortunately, none of our five subdwarf candidates has an archival H band detection available. Only WISEA 1534−1043 has an H magnitude lower limit, and this corresponds to an uninformative color limit of $J-H < 1.98$ mag. It would be interesting to obtain deeper H band follow-up of our five late-type subdwarf candidates, to determine whether they match the $J-H > -0.2$ mag trend noted by Mace et al. (2013b) for old, low-metallicity T dwarfs.

Figure 8 shows color-color diagrams analogous to Figure 7, but for $H-$ch2 (left) and $K-$ch2 (right) rather than $J-$ch2. These plots provide at best a sanity check showing that the few targets with $H/K/K_S$ detections line up roughly along the expected trends for late type brown dwarfs. For the most part, our targets either have no archival $H/K/K_S$ imaging available or else obtain weak magnitude limits corresponding to essentially uninformative color limits.

10.10. *Notes on Individual Objects*

10.10.1. *CWISEP J021243.55+053147.2*

Among our 18 targets phototyped at ≥Y0, 17 have χ^2_{motion} values exceeding our significance threshold for motion confirmation. The remaining candidate with ch1−ch2 color in the Y dwarf regime is CWISEP 0212+0531. For this object, our *Spitzer* astrometric data point clearly shows that despite its extremely red ch1−ch2 color, this object is consistent with being stationary (see Figure 5). We do not count CWISEP 0212+0531 among our list of motion-confirmed Y dwarf candidates.

10.10.2. *CWISEP J022935.43+724616.4*

As noted in §7.2, CWISEP 0229+7246 has two ch2 counterparts but just one blended/elongated ch1 counterpart. We therefore consider it likely that CWISEP 0229+7246 is neither a single moving object nor a pair of closely spaced CPM objects, but rather some form of contaminant. For completeness, we can check the motion obtained by combining the ch2 center of light position with our W2 astrometry, as would be appropriate in the closely spaced CPM scenario. The resulting linear motion is $\mu_\alpha = 9 \pm 27$ mas/yr, $\mu_\delta = -29 \pm 26$ mas/yr. This corresponds to $\chi^2_{motion} = 1.4$, further disfavoring the close CPM system hypothesis.

10.10.3. *CWISEP J144606.62−231717.8*

CWISEP 1446−2317 has the reddest best-fit ch1−ch2 color among our entire sample of brown dwarf candidates, with ch1−ch2 = 3.71 ± 0.44 mag. While this color nominally rivals that of WISE 0855−0714, the reddest known brown dwarf in ch1−ch2 and also the coldest known brown dwarf, we cannot claim that CWISEP 1446−2317 may be similarly cold (see Marocco et al., in prep., for additional follow-up/characterization of this source). Our Gemini J band imaging with FLAMINGOS-2 confirms that CWISEP 1446−2317 is a Y dwarf by establishing a 5σ limit of $J > 22.36$ mag, which corresponds to a 5σ color lower limit of $J-$ch2 > 6.56 mag.

Given our photometric distance constraint of $d < 8.3$ pc (§10.2), we sought to perform a custom WISE+*Spitzer* astrometric analysis capable of enabling a combined parallax and proper motion measurement. Our typical

linear motion fitting approach (§8) relies on extracting W2 detections from coadds spanning multiple WISE sky passes, posing challenges for parallax measurement, which is best suited to fitting WISE astrometry from single exposures or sky passes where the spacecraft position is well-defined. Although CWISEP 1446−2317 is extremely faint at W2 ∼ 16, we nevertheless performed astrometry only on W2 coadds of single WISE sky passes for this target. We also folded in the recently released 2018 NEOWISE W2 imaging for CWISEP 1446−2317 so as to leverage these two additional WISE sky passes. Using the Sanchez et al. (2019) WISE coaddition and source detection methodology, we obtained W2 detections during 11 of the 12 available WISE sky passes throughout the 2010 to 2018 time period. These positional measurements are provided in Table 3. We were unable to extract a CWISEP 1446−2317 W2 detection corresponding to the 2017 February NEOWISE sky pass.

We combined our 11 epochs of WISE astrometry with our *Spitzer* ch2 position from Table 4 to perform a parallax plus proper motion fit accounting for the WISE and *Spitzer* ephemerides. These yielded a motion solution with $\mu_\alpha = -774 \pm 82$ mas/yr, $\mu_\delta = -978 \pm 71$ mas/yr and a parallax of -501 ± 248 mas, with $\chi^2 = 17.4$ for 19 dof. The negative parallax is clearly neither physical nor statistically significant. Consequently, we revert to the simple linear motion fitting used for the rest of our sample (§8.5) when quoting the CWISEP 1446−2317 motion in Table 7. Regardless of the fitting details, the CWISEP 1446−2317 linear motion is detected at very high significance.

We also checked the CatWISE `par_pm` parameter for CWISEP 1446−2317. `par_pm` provides a parallax estimate based only on WISE data spanning 2010-2016 by comparing linear motion fits computed separately for ascending and descending scans, with WISE observing from ∼1 AU on opposite sides of the Sun during opposite scan directions. CWISEP 1446−2317 has CatWISE `par_pm` $= 253 \pm 329$ mas, which is again not statistically significant. More *Spitzer*-precision astrometric follow-up will be needed to obtain a reliable trigonometric parallax for this source (see Marocco et al., in prep., for additional CWISEP 1446−2317 astrometry).

Figure 11 shows WISE, *Spitzer*, Gemini and VISTA image cutouts illustrating the motion and colors of CWISEP 1446−2317. Note that this figure only shows two years out of the six total years worth of W1/W2 imaging available. The three red circles remain fixed in all panels at the 2010 WISE, 2015 WISE and 2019.41 *Spitzer* positions. There is no 2019.41 *Spitzer* counterpart at the 2010 WISE position, nor a WISE counterpart during either 2011 or 2015 at the *Spitzer* 2019.41 position. The 2015 W2 position does not appear perfectly consistent with a linear interpolation between the 2010 W2 and 2019.41 *Spitzer* positions, seemingly dragged slightly southeast by a noise excursion. This underscores the difficulty of performing astrometry for such a faint W2 source so close to the background noise limit. There is no trace of a counterpart in either W1, Gemini J or VISTA K_S. The ch1 counterpart shown is very weak, leading to the large uncertainty on our measured ch1−ch2 color. VISTA provides only a weak K_S−ch2 > 2.06 mag limit.

Lastly, it is interesting to compare the reduced proper motion of CWISEP 1446−2317 ($H_{ch2} = 21.35 \pm 0.12$ mag) to that of the previously known Y dwarf sample. Among all Y dwarfs from the prior literature, only WISE 0855−0714 has a larger H_{ch2} than does CWISEP 1446−2317, as can be seen in Figure 10. However, CWISEP 1446−2317 is a very distant second, with the WISE 0855−0714 H_{ch2} being more than 2 magnitudes larger.

10.10.4. *WISEA J153429.75−104303.3*

WISEA 1534−1043 is the fastest-moving discovery in our sample by multiple metrics: total linear motion ($\mu_{tot} = 2697 \pm 68$ mas/yr), ch2 reduced proper motion ($H_{ch2} = 22.92 \pm 0.06$ mag) and estimated tangential velocity ($V_{tan} = 485^{+73}_{-64}$ km/s). With J−ch2 > 4.79 mag and ch1−ch2 $= 0.93 \pm 0.04$ mag, WISEA 1534−1043 joins a small subpopulation of color outliers within our motion-confirmed sample as illustrated in Figure 7. As discussed in §10.9, we favor an explanation for the unusual properties of WISEA 1534−1043 in which it is a mid-late T subdwarf, based on kinematics and the striking similarity of our color outlier population to the benchmark T8 subdwarf WISE 2005+5424. WISEA 1534−1043 is entirely undetected in our Palomar/WIRC J band follow-up, and deeper J band imaging would be useful toward establishing just how anomalously red this object is in its J−ch2 color. If WISEA 1534−1043 is indeed a subdwarf, that would place it at a closer distance than our current $38.0^{+5.6}_{-4.9}$ pc estimate, and correspondingly reduce its exceptionally large V_{tan} estimate.

Figure 5 includes a scatter plot displaying the measured (RA, Dec) trajectory of WISEA 1534−1043. For WISEA 1534−1043, we attempted the same WISE+*Spitzer* parallax fitting methodology as used in §10.10.3 for CWISEP 1446−2317. In the case of WISEA 1534−1043, the joint parallax plus proper motion fit yields $\mu_\alpha = -1254 \pm 116$ mas/yr, $\mu_\delta = -2406 \pm 84$ mas/yr and parallax of 329 ± 422 mas, with $\chi^2 = 8.5$ for 9 dof. The lower number of dof results from the fact that

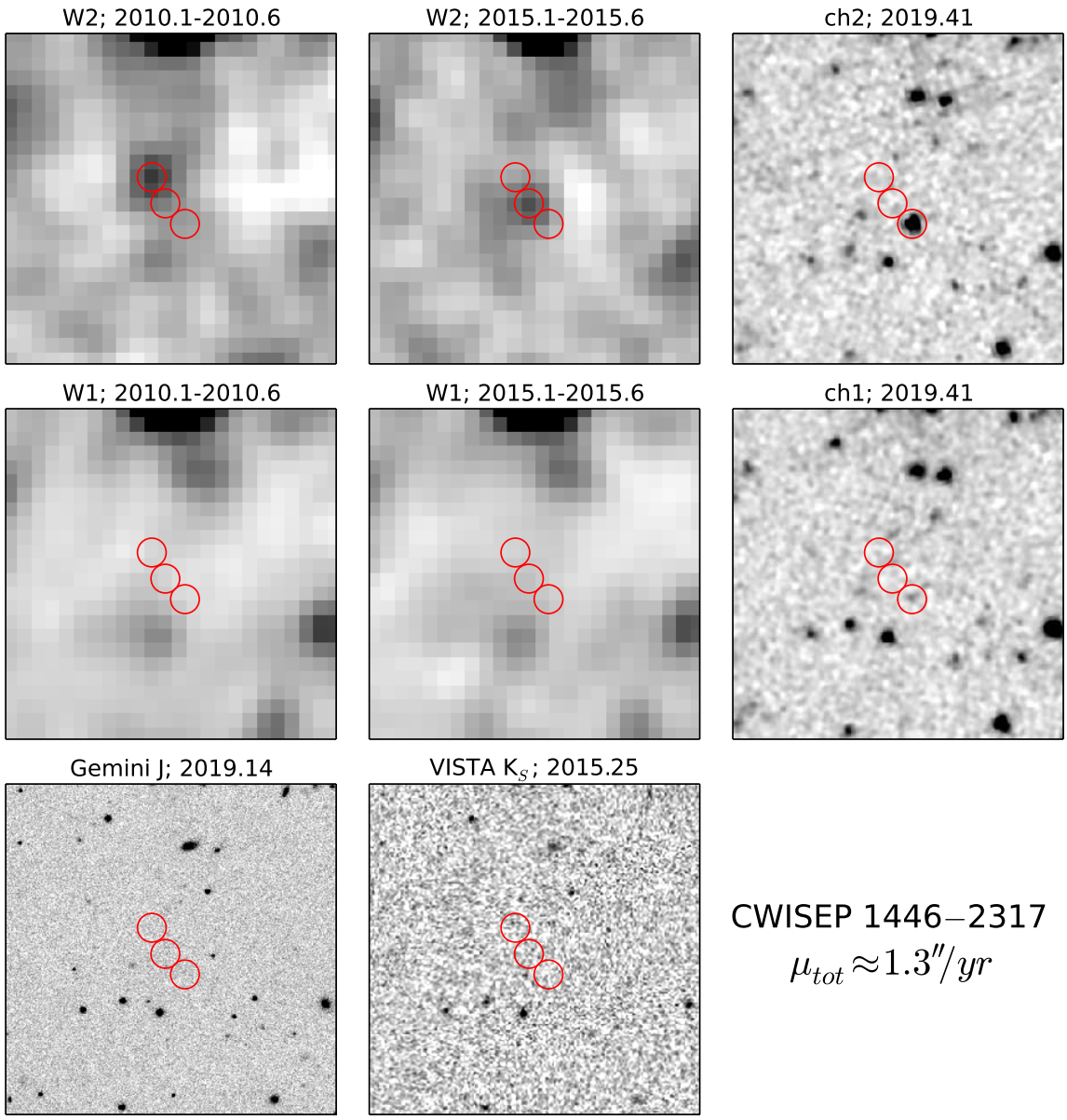

Figure 11. Postage stamps showing available archival and follow-up imaging for CWISEP 1446−2317, our sample's reddest target in terms of best-fit ch1−ch2 color. Each cutout is 1.1′ on a side. East is left and north is up. Within each panel, the red circles indicate the 2010.1-2010.6 WISE position (northeastern circle), the 2015.1-2015.6 WISE position (central circle) and the 2019.41 *Spitzer* position (southwestern circle). CWISEP 1446−2317 appears undetected in W1, Gemini/FLAMINGOS-2 J band follow-up (PI Gelino), and archival VISTA K_S imaging from VHS. *Spitzer* imaging comes from our p14034 campaign. The ch1 detection is very weak, leading to a very large uncertainty on the measured ch1−ch2 color. The WISE images are one-year unWISE meta-coadds, spanning calendar 2010 (2015) in the leftmost (center) column, and have been smoothed by a 6.5″ FWHM Gaussian kernel.

we could only extract single sky pass W2 detections for 7 of 12 WISE sky passes. Our parallax measurement is not at all statistically significant. No CatWISE `par_pm` parallax estimate is available for WISEA 1534−1043, since this target is wholly absent from the CatWISE catalog. More high-precision astrometric follow-up of WISEA 1534−1043 would help pin down its ch2 absolute magnitude and thereby test our subdwarf hypothesis.

Figure 12 shows WISE, *Spitzer*, Palomar, and VISTA image cutouts in the vicinity of WISEA 1534−1043. In this case, we do not smooth the WISE images since the moving target shifts into a position adjacent to much brighter static sources over time. WISEA 1534−1043 has an extremely faint, but nonetheless legitimate, W1 counterpart. WISEA 1534−1043 is quite blue in ch1−ch2 relative to the bulk of our sample, and it is

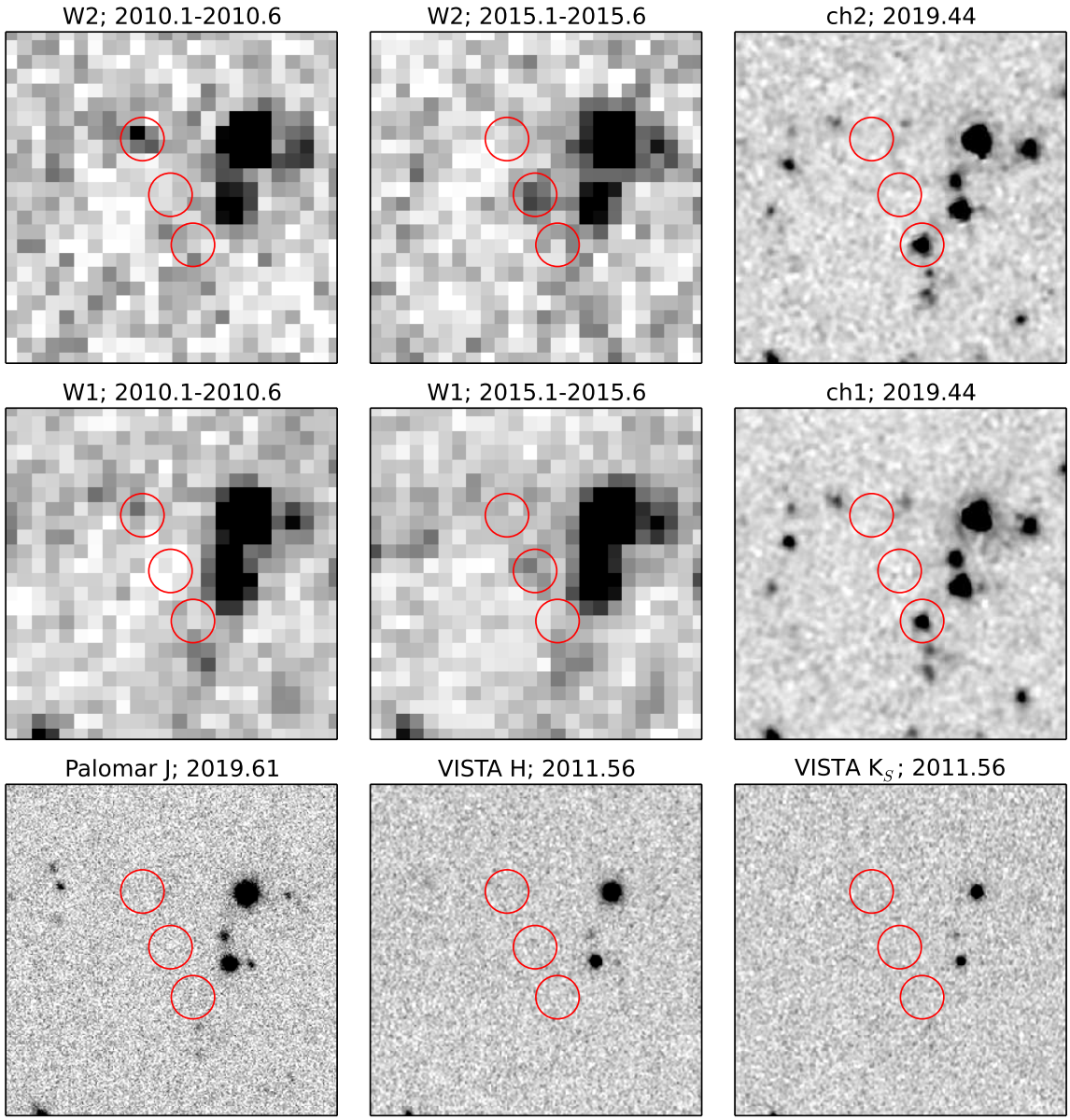

Figure 12. Postage stamps showing available archival and follow-up imaging for WISEA 1534−1043, our sample's highest proper motion target ($\mu_{tot} \approx 2.7''$/yr), which also has the largest ch2 reduced proper motion of any target in our sample ($H_{ch2} \approx 22.9$ mag). Each cutout is $1.1'$ on a side. East is left and north is up. Within each panel, the red circles indicate the 2010.1-2010.6 WISE position (northeastern circle), the 2015.1-2015.6 WISE position (central circle) and the 2019.44 *Spitzer* position (southwestern circle). WISEA 1534−1043 has an extremely faint W1 counterpart. It is undetected in our Palomar/WIRC J band follow-up (PI Marocco) and archival VISTA H, K_S imaging from VHS. *Spitzer* imaging comes from our p14034 campaign. Interestingly, this source has a relatively bright ch1 counterpart, occupying an unusual region of color-color space with ch1−ch2 < 1 and J−ch2 > 4.5. The WISE images are one-year unWISE meta-coadds, spanning calendar 2010 (2015) in the leftmost (center) column. In this case the WISE images are kept unsmoothed for clarity because the target moves into a position adjacent to much brighter static sources over time.

very well detected in both *Spitzer* channels. There is no trace of a counterpart detection in the NIR panels at bottom. As mentioned in §10.9, deeper H band follow-up would be of interest in determining whether WISEA 1534−1043 matches the $J-H>-0.2$ mag trend noted by Mace et al. (2013b) for mid-late T subdwarfs.

10.10.5. *CWISEP J154151.59+523025.0*

This target has two *Spitzer* counterparts with similar magnitudes in both ch1 and ch2. Further complicating matters, the potentially moving W2 source appears contaminated by blending with a much bluer stationary object. Additional follow-up would be needed to conclusively determine whether CWISEP 1541+5230 is a pair of red extragalactic sources or instead two companion brown dwarfs. Both *Spitzer* counterparts, if assumed to be late-type brown dwarfs, have photometric distances consistent with $d\approx 38$ pc and T8 spectral type estimates. The two *Spitzer* sources are separated by 3.65″, which would translate to a projected physical separation of 139 AU using $d=38$ pc. If we assume that CWISEP 1541+5230 is a CPM system, then we obtain a linear motion of $\mu_\alpha=208\pm27$ mas/yr, $\mu_\delta=-209\pm29$ mas/yr by fitting the W2 astrometry in combination with the ch2 center of light position.

10.10.6. *CWISEP J193518.59−154620.3*

Our p14034 photometry of CWISEP 1935−1546 yielded an exceptionally red, though very noisy, *Spitzer* color estimate of 3.24 ± 0.31 mag (Marocco et al. 2019). Because this color interval overlapped with that of the coldest known brown dwarf (WISE 0855−0714; ch1−ch2 $=3.55\pm0.07$), we obtained much deeper ch1 imaging via *Spitzer* DDT program 14279 (p14279; PI Marocco). We also obtained additional ch2 astrometry via observations executed immediately 'back-to-back' with those of p14279, allowing us to measure a much higher S/N color based on nearly simultaneous imaging in both IRAC bands. These additional ch2 astrometric observations were part of DDT program 14224 (p14224; PI Kirkpatrick). Our total p14279 ch1 integration time was 3600 seconds, as compared to just 210 seconds with p14034.

Combining the p14279 and p14224 data acquired on 2019 August 7, we obtain a refined color measurement of ch1−ch2 $=2.984\pm0.034$ mag. So the original CWISEP 1935−1546 color from p14034 appears to have scattered $\sim1\sigma$ red relative to the more accurate value now in hand. In Table 1 we list the newer, higher S/N CWISEP 1935−1546 ch1−ch2 color rather than that from p14034. This color places CWISEP 1935−1546 squarely in the Y1 phototype regime, with a corresponding photometric distance estimate of $9.8^{+1.5}_{-1.3}$ pc. This also corresponds to a $V_{tan}=14^{+4}_{-3}$ km/s estimate significantly refined relative to that initially presented in Marocco et al. (2019). Despite being the third reddest motion-confirmed discovery in our entire sample by central ch1−ch2 color, CWISEP 1935−1546 has the lowest H_{ch2} among our motion-confirmed targets with ≥Y0 phototypes.

11. CONCLUSION

We have undertaken an extensive effort to mine the CatWISE proper motion catalog, and more generally the combined WISE+NEOWISE data set, to discover extremely cold brown dwarfs hitherto overlooked by prior searches. By leveraging the 6.5+ year time baseline afforded by the combination of pre-hibernation and post-reactivation W1/W2 imaging, we are able to perform much deeper motion-based brown dwarf selections than prior all-sky WISE moving object surveys. As a result, we have discovered many faint moving objects with exceptionally red *Spitzer* colors and hence extremely cold temperatures. Based on *Spitzer* ch1−ch2 color measurements and WISE+*Spitzer* motion validation, our sample contains 17 newly discovered motion-confirmed brown dwarfs with best-fit spectral types ≥Y0, 16 of which have J−ch2 detections/limits consistent with being Y dwarfs. Much more follow-up will be required in order to determine which of our Y dwarf candidates listed in Table 12 are indeed Y dwarfs, and ultimately obtain spectral types.

One of our Y dwarf candidates, CWISEP 1446−2317, stands out from the rest with an exceptionally large though very uncertain *Spitzer* color of ch1−ch2 $=3.71\pm0.44$. This source in particular merits additional follow-up to refine its photometry and astrometry (see Marocco et al., in prep., for additional characterization of this source).

Table 12 illustrates that deeper J band follow-up will help push many of our Y dwarf candidates securely into a J−ch2 regime so red as to exclude late T dwarfs. Further astrometric follow-up will be highly valuable on a number of fronts. Trigonometric parallaxes would provide absolute magnitudes which can discriminate between late T and Y spectral types. Trigonometric parallaxes will also be necessary to determine which of our discoveries fall within the 20 pc volume and incorporate these into accurate space density estimates. Deeper H band imaging follow-up would be particularly useful in determining whether our sample of fast-moving color outliers are indeed mid-late T subdwarfs as we have hypothesized.

We anticipate many more very late type CatWISE brown dwarf discoveries in the future. A second and final CatWISE data processing is underway, expected to cat-

alog an additional ∼1 billion WISE-selected objects by virtue of more aggressive source detection/deblending. However, *Spitzer* is a uniquely efficient resource for obtaining spectral type estimates of such discoveries, and upon *Spitzer*'s retirement it will become much more challenging to sift for promising Y dwarf candidates among W2-only moving objects.

The upcoming decade will provide exciting opportunities to discover and characterize the coldest ($T_{eff} \lesssim 300$ K) substellar constituents of the solar neighborhood (e.g., Kirkpatrick et al. 2019b; Leggett et al. 2019). The community will need to select JWST Y dwarf targets of maximum scientific value, to better understand both brown dwarfs themselves and giant exoplanet atmospheres (Leggett et al. 2019). The Near Earth Object Surveyor (formerly NEOCam) will be able to reveal colder, fainter, and more distant Y dwarfs than WISE given resources for coadded processings analogous to those of AllWISE/unWISE/CatWISE (Kirkpatrick et al. 2019b). Determining the low mass cutoff of star formation will require a complete sample out to distances of 20-50 pc (Leggett et al. 2019), far beyond the volume currently mapped (Kirkpatrick et al. 2019a). CatWISE is already making progress on these fronts by mining the WISE/NEOWISE data set for Y dwarf discoveries to its faintest attainable depths.

We wish to thank the anonymous referee. We thank Nicholas Cross for assistance with compiling archival UKIRT/VISTA detections. This research was partially carried out at the Jet Propulsion Laboratory, California Institute of Technology, under a contract with NASA.

CatWISE is funded by NASA under Proposal No. 16-ADAP16-0077 issued through the Astrophysics Data Analysis Program, and uses data from the NASA-funded WISE and NEOWISE projects. AMM acknowledges support from Hubble Fellowship HST-HF2-51415.001-A. FM is supported by an appointment to the NASA Postdoctoral Program at the Jet Propulsion Laboratory, administered by Universities Space Research Association under contract with NASA.

This work is based in part on observations made with the *Spitzer* Space Telescope, which is operated by the Jet Propulsion Laboratory, California Institute of Technology under a contract with NASA.

Based in part on observations obtained at the Gemini Observatory, which is operated by the Association of Universities for Research in Astronomy, Inc., under a cooperative agreement with the NSF on behalf of the Gemini partnership: the National Science Foundation (United States), National Research Council (Canada), CONICYT (Chile), Ministerio de Ciencia, Tecnología e Innovación Productiva (Argentina), Ministério da Ciência, Tecnologia e Inovação (Brazil), and Korea Astronomy and Space Science Institute (Republic of Korea).

Facilities: Spitzer(IRAC), WISE/NEOWISE, Gemini(FLAMINGOS-2), Hale(WIRC), UKIRT(WFCAM), VISTA(VIRCAM), 2MASS

Software: XGBoost (Chen & Guestrin 2016), MOPEX (Makovoz & Khan 2005; Makovoz & Marleau 2005), WiseView (Caselden et al. 2018)

REFERENCES

Abbott, T. M. C., Abdalla, F. B., Allam, S., et al. 2018, ApJS, 239, 18

Beichman, C., Gelino, C. R., Kirkpatrick, J. D., et al. 2013, ApJ, 764, 101

Bertin, E., & Arnouts, S. 1996, A&AS, 117, 393

Burningham, B. 2018, Large-Scale Searches for Brown Dwarfs and Free-Floating Planets, 118

Burrows, A., Sudarsky, D., & Hubeny, I. 2006, ApJ, 640, 1063

Caselden, D., Westin, III, P., Meisner, A., Kuchner, M., & Colin, G. 2018, WiseView: Visualizing motion and variability of faint WISE sources, Astrophysics Source Code Library, , , ascl:1806.004

Chambers, K. C., Magnier, E. A., Metcalfe, N., et al. 2016, arXiv e-prints, arXiv:1612.05560

Chen, T., & Guestrin, C. 2016, in Proceedings of the 22Nd ACM SIGKDD International Conference on Knowledge Discovery and Data Mining, KDD '16 (New York, NY, USA: ACM), 785–794. http://doi.acm.org/10.1145/2939672.2939785

Cushing, M. C., Kirkpatrick, J. D., Gelino, C. R., et al. 2011, ApJ, 743, 50

Cutri, R. M., Wright, E. L., Conrow, T., et al. 2013, Explanatory Supplement to the AllWISE Data Release Products, Tech. rep.

Cutri, R. M., Mainzer, A., Conrow, T., et al. 2015, Explanatory Supplement to the NEOWISE Data Release Products, Tech. rep.

Dey, A., Schlegel, D. J., Lang, D., et al. 2019, AJ, 157, 168

Dupuy, T. J., & Liu, M. C. 2012, ApJS, 201, 19

Dupuy, T. J., Liu, M. C., & Leggett, S. K. 2015, ApJ, 803, 102
Dye, S., Lawrence, A., Read, M. A., et al. 2018, MNRAS, 473, 5113
Edge, A., Sutherland, W., Kuijken, K., et al. 2013, The Messenger, 154, 32
Eikenberry, S., Elston, R., Raines, S. N., et al. 2006, in Society of Photo-Optical Instrumentation Engineers (SPIE) Conference Series, Vol. 6269, Proc. SPIE, 626917
Eisenhardt, P. R. M., Marocco, F., Fowler, J. W., et al. 2019, arXiv e-prints, arXiv:1908.08902
Faherty, J. K., Burgasser, A. J., Cruz, K. L., et al. 2009, AJ, 137, 1
Fazio, G. G., Hora, J. L., Allen, L. E., et al. 2004, ApJS, 154, 10
Gaia Collaboration, Brown, A. G. A., Vallenari, A., et al. 2018, A&A, 616, A1
Gardner, J. P., Mather, J. C., Clampin, M., et al. 2006, SSRv, 123, 485
Griffith, R. L., Kirkpatrick, J. D., Eisenhardt, P. R. M., et al. 2012, AJ, 144, 148
Hodgkin, S. T., Irwin, M. J., Hewett, P. C., & Warren, S. J. 2009, MNRAS, 394, 675
Kirkpatrick, J. D. 2005, ARA&A, 43, 195
Kirkpatrick, J. D., Cushing, M. C., Gelino, C. R., et al. 2011, ApJS, 197, 19
Kirkpatrick, J. D., Gelino, C. R., Cushing, M. C., et al. 2012, ApJ, 753, 156
Kirkpatrick, J. D., Schneider, A., Fajardo-Acosta, S., et al. 2014, ApJ, 783, 122
Kirkpatrick, J. D., Kellogg, K., Schneider, A. C., et al. 2016, ApJS, 224, 36
Kirkpatrick, J. D., Martin, E. C., Smart, R. L., et al. 2019a, ApJS, 240, 19
Kirkpatrick, J. D., Metchev, S. A., Hillenbrand , L. A., et al. 2019b, BAAS, 51, 108
Kuchner, M. J., Faherty, J. K., Schneider, A. C., et al. 2017, ApJL, 841, L19
Lang, D. 2014, AJ, 147, 108
Lawrence, A., Warren, S. J., Almaini, O., et al. 2007, MNRAS, 379, 1599
Leggett, S., Apai, D., Burgasser, A., et al. 2019, BAAS, 51, 95
Leggett, S. K., Morley, C. V., Marley, M. S., et al. 2013, ApJ, 763, 130
Lépine, S., Shara, M. M., & Rich, R. M. 2002, AJ, 124, 1190
Liu, M. C., Dupuy, T. J., Bowler, B. P., Leggett, S. K., & Best, W. M. J. 2012, ApJ, 758, 57
Luhman, K. L. 2013, ApJ, 767, L1
—. 2014a, ApJ, 781, 4
—. 2014b, ApJ, 786, L18
Luhman, K. L., Burgasser, A. J., & Bochanski, J. J. 2011, ApJL, 730, L9
Mace, G. N., Kirkpatrick, J. D., Cushing, M. C., et al. 2013a, ApJS, 205, 6
—. 2013b, ApJ, 777, 36
Mainzer, A., Cushing, M. C., Skrutskie, M., et al. 2011a, ApJ, 726, 30
Mainzer, A., Bauer, J., Grav, T., et al. 2011b, ApJ, 731, 53
Mainzer, A., Bauer, J., Cutri, R., et al. 2014, ApJ, 792, 30
Makovoz, D., & Khan, I. 2005, in Astronomical Society of the Pacific Conference Series, Vol. 347, Astronomical Data Analysis Software and Systems XIV, ed. P. Shopbell, M. Britton, & R. Ebert, 81
Makovoz, D., & Marleau, F. R. 2005, PASP, 117, 1113
Marocco, F., Caselden, D., Meisner, A. M., et al. 2019, ApJ, 881, 17
Martin, E. C., Kirkpatrick, J. D., Beichman, C. A., et al. 2018, ApJ, 867, 109
McMahon, R. G., Banerji, M., Gonzalez, E., et al. 2013, The Messenger, 154, 35
Meisner, A. M., Lang, D., Schlafly, E. F., & Schlegel, D. J. 2019, arXiv e-prints, arXiv:1909.05444
Meisner, A. M., Lang, D., & Schlegel, D. J. 2018a, Research Notes of the American Astronomical Society, 2, 1
—. 2018b, AJ, 156, 69
Meisner, A. M., Lang, D. A., & Schlegel, D. J. 2018c, Research Notes of the American Astronomical Society, 2, 202
Patten, B. M., Stauffer, J. R., Burrows, A., et al. 2006, ApJ, 651, 502
Pinfield, D. J., Gomes, J., Day-Jones, A. C., et al. 2014a, MNRAS, 437, 1009
Pinfield, D. J., Gromadzki, M., Leggett, S. K., et al. 2014b, MNRAS, 444, 1931
Sanchez, J. A., Reddy, V., Thirouin, A., et al. 2019, ApJL, 881, L6
Schlafly, E. F., Meisner, A. M., & Green, G. M. 2019, ApJS, 240, 30
Schneider, A. C., Greco, J., Cushing, M. C., et al. 2016, ApJ, 817, 112
Tinney, C. G., Faherty, J. K., Kirkpatrick, J. D., et al. 2012, ApJ, 759, 60
Tinney, C. G., Kirkpatrick, J. D., Faherty, J. K., et al. 2018, ApJS, 236, 28
Werner, M. W., Roellig, T. L., Low, F. J., et al. 2004, ApJS, 154, 1

Wilson, J. C., Eikenberry, S. S., Henderson, C. P., et al. 2003, in Proc. SPIE, Vol. 4841, Instrument Design and Performance for Optical/Infrared Ground-based Telescopes, ed. M. Iye & A. F. M. Moorwood, 451–458

Wright, E., Eisenhardt, P., Mainzer, A., et al. 2010, AJ, 140, 1868

Wright, E. L., Mainzer, A., Kirkpatrick, J. D., et al. 2014, AJ, 148, 82

Table 1. WISE & *Spitzer* Photometry

Name	motion confirmed	W1 (mag)	W2 (mag)	W1−W2 (mag)	AOR	ch1 (mag)	ch2 (mag)	ch1−ch2 (mag)	search method[c]
CWISEP J000006.01−704851.2	yes	18.390 ± 0.153	15.834 ± 0.051	2.556 ± 0.161	68730112	17.293 ± 0.058	15.836 ± 0.022	1.457 ± 0.062	M2
CWISEP J000110.81−093215.5	yes	18.598 ± 0.259	16.104 ± 0.086	2.494 ± 0.273	68727808	17.573 ± 0.065	15.889 ± 0.021	1.684 ± 0.068	M2
CWISEP J001146.07−471306.8	yes	18.939 ± 0.272	15.986 ± 0.062	2.953 ± 0.279	68486656	17.744 ± 0.090	15.812 ± 0.021	1.931 ± 0.093	M1
CWISEP J003507.77−153233.8	yes	17.351 ± 0.080[a]	15.252 ± 0.039	2.099 ± 0.089	68235776	17.111 ± 0.065	15.228 ± 0.020	1.884 ± 0.068	C6
CWISEP J003915.43+360939.0	no	> 19.043	16.303 ± 0.087	> 2.740	68506112	18.191 ± 0.102	15.982 ± 0.021	2.210 ± 0.104	C8
CWISEP J004158.35+381811.9	yes	18.654 ± 0.248	15.957 ± 0.065	2.697 ± 0.256	68486144	17.817 ± 0.095	16.069 ± 0.024	1.749 ± 0.098	M1
CWISEP J005802.63+723330.3	yes	17.395 ± 0.072	16.109 ± 0.065	1.286 ± 0.097	68731904	17.500 ± 0.062	16.749 ± 0.034	0.751 ± 0.070	C3
CWISEP J010247.48−654226.4	no	19.416 ± 0.512	16.681 ± 0.099	2.735 ± 0.521	68509952	18.787 ± 0.159	16.432 ± 0.023	2.354 ± 0.160	C8
CWISEP J010527.69−783419.3	yes	16.619 ± 0.035[a]	14.996 ± 0.023	1.623 ± 0.042	68237568	17.289 ± 0.071	15.204 ± 0.019	2.085 ± 0.074	C1,C6
CWISEP J010650.61+225159.1	yes	17.524 ± 0.103	15.045 ± 0.036	2.479 ± 0.109	68234752	16.490 ± 0.035	15.135 ± 0.020	1.354 ± 0.040	C1,C2,C6
CWISEP J012735.44−564110.5	no	17.996 ± 0.112	15.757 ± 0.048	2.239 ± 0.122	68495360	17.509 ± 0.072	15.726 ± 0.021	1.782 ± 0.075	M1
CWISEP J012748.35−631056.1	yes	17.128 ± 0.057[a]	15.507 ± 0.039	1.621 ± 0.069	68732672	16.872 ± 0.046	15.578 ± 0.022	1.294 ± 0.051	M1
CWISEP J014607.55−375705.6	yes	18.166 ± 0.149	15.793 ± 0.057	2.373 ± 0.160	68497408	17.396 ± 0.062	15.680 ± 0.021	1.717 ± 0.066	M1
CWISEP J015613.24+325526.6	yes	18.812 ± 0.416	16.063 ± 0.082	2.749 ± 0.424	68164096	17.564 ± 0.087	16.116 ± 0.030	1.448 ± 0.092	C3,C5,C6
CWISEP J020103.10+293801.8	yes	18.049 ± 0.153	15.845 ± 0.067	2.204 ± 0.167	68504320	17.139 ± 0.052	15.963 ± 0.023	1.176 ± 0.057	C3,C6
CWISEP J020938.72+180427.7	yes	18.461 ± 0.331	16.058 ± 0.086	2.403 ± 0.342	68500992	17.925 ± 0.089	16.141 ± 0.024	1.784 ± 0.092	M3
CWISEP J021243.55+053147.2	no	> 19.118	15.931 ± 0.076	> 3.187	68556032	18.931 ± 0.250	16.028 ± 0.024	2.903 ± 0.251	C8
CWISEP J021921.66−265451.8	yes	17.755 ± 0.118	16.162 ± 0.081	1.593 ± 0.143	68730368	17.934 ± 0.093	17.029 ± 0.039	0.906 ± 0.101	C3
CWISEP J022122.41−564125.0	yes	18.375 ± 0.138	15.825 ± 0.045	2.550 ± 0.145	68494848	17.389 ± 0.062	15.649 ± 0.021	1.740 ± 0.065	M1
CWISEP J022513.27+154854.8	no	18.653 ± 0.428	15.646 ± 0.063	3.007 ± 0.433	68725760	17.675 ± 0.099	15.818 ± 0.024	1.857 ± 0.102	M2
CWISEP J022631.82−203439.4	yes	18.478 ± 0.216	16.208 ± 0.086	2.270 ± 0.232	68164352	17.602 ± 0.075	15.962 ± 0.025	1.640 ± 0.079	C3,C6
CWISEP J022935.43+724616.4 N	no	17.401 ± 0.077	15.240 ± 0.035	2.161 ± 0.085	26741760	17.423 ± 0.068	15.982 ± 0.045	1.441 ± 0.081	M2
CWISEP J022935.43+724616.4 S	no	17.401 ± 0.077	15.240 ± 0.035	2.161 ± 0.085	26741760	17.423 ± 0.068	15.819 ± 0.040	1.604 ± 0.078	M2
CWISEP J023842.60−133210.7	yes	> 19.118	16.192 ± 0.088	> 2.926	68728576	19.058 ± 0.219	16.329 ± 0.024	2.729 ± 0.220	M2
CWISEP J024204.91−225604.6	yes	> 19.161	16.473 ± 0.112	> 2.688	68557056	18.403 ± 0.113	16.431 ± 0.024	1.971 ± 0.115	C7
CWISEP J024710.25−145809.9	no	17.532 ± 0.099	16.197 ± 0.089	1.335 ± 0.133	68731392	17.463 ± 0.055	16.641 ± 0.028	0.822 ± 0.062	C3
CWISEP J024810.75−694127.9	no	> 19.135	16.369 ± 0.065	> 2.766	68726784	18.243 ± 0.110	16.352 ± 0.024	1.892 ± 0.113	M2
CWISEP J025747.92−205602.7	no	18.243 ± 0.163	15.625 ± 0.046	2.618 ± 0.169	68497152	16.992 ± 0.052	15.581 ± 0.022	1.411 ± 0.056	M1

Table 1 continued

Table 1 *(continued)*

Name	motion confirmed	W1 (mag)	W2 (mag)	W1−W2 (mag)	AOR	ch1 (mag)	ch2 (mag)	ch1−ch2 (mag)	search method[c]
CWISEP J031130.28+035931.8	yes	18.768 ± 0.305	16.581 ± 0.123	2.187 ± 0.329	68507648	17.816 ± 0.071	17.040 ± 0.036	0.776 ± 0.079	M3
CWISEP J031557.05+203552.4	no	17.146 ± 0.079	15.530 ± 0.057	1.616 ± 0.097	68727296	17.091 ± 0.061	16.006 ± 0.027	1.086 ± 0.066	M2
CWISEP J031908.60+081120.4	no	17.465 ± 0.108	16.058 ± 0.086	1.407 ± 0.138	68498432	17.365 ± 0.064	17.026 ± 0.041	0.339 ± 0.076	M3
CWISEP J031935.50−041231.7	yes	> 18.625	16.420 ± 0.096	> 2.205	68577280	18.844 ± 0.184	16.545 ± 0.026	2.298 ± 0.186	C7
CWISEP J032109.59+693204.5	yes	> 18.488	15.994 ± 0.061	> 2.494	68498688	18.561 ± 0.188	15.928 ± 0.023	2.633 ± 0.190	M3
CWISEP J034336.27+184025.8	no	17.542 ± 0.110	15.984 ± 0.083	1.558 ± 0.138	68733952	17.374 ± 0.057	16.550 ± 0.030	0.824 ± 0.064	C3
CWISEP J034514.82+173528.1	no	18.222 ± 0.209	15.559 ± 0.050	2.663 ± 0.215	68728064	17.424 ± 0.076	15.450 ± 0.021	1.974 ± 0.079	M2
CWISEP J034755.11+123051.9	yes	18.261 ± 0.216	15.273 ± 0.050	2.988 ± 0.222	68164608	16.763 ± 0.045	15.146 ± 0.020	1.617 ± 0.050	C1
CWISEP J034904.05−462827.9	yes	18.929 ± 0.238	16.304 ± 0.070	2.625 ± 0.248	68487424	17.830 ± 0.083	16.305 ± 0.025	1.526 ± 0.086	M1
CWISEP J040106.67+085748.5	yes	> 18.629	15.855 ± 0.074	> 2.774	68500736	17.596 ± 0.078	15.677 ± 0.023	1.918 ± 0.081	M3
CWISEP J040235.55−265145.4	yes	18.030 ± 0.145	15.549 ± 0.047	2.481 ± 0.152	68727552	18.173 ± 0.150	15.453 ± 0.021	2.720 ± 0.152	M2
CWISEP J040324.67+185729.6	no	18.715 ± 0.446	16.150 ± 0.094	2.565 ± 0.456	68505856	17.856 ± 0.086	16.242 ± 0.027	1.615 ± 0.090	C8
CWISEP J040351.00−491605.6	yes	18.001 ± 0.091	16.035 ± 0.050	1.966 ± 0.104	68487680	18.118 ± 0.130	16.127 ± 0.025	1.992 ± 0.132	M1
CWISEP J041025.10+033807.2	no	18.863 ± 0.466	16.264 ± 0.107	2.599 ± 0.478	68729856	17.794 ± 0.071	16.272 ± 0.024	1.522 ± 0.075	M1
CWISEP J042455.68+000221.4	no	> 18.710	15.506 ± 0.050	> 3.204	68728832	17.641 ± 0.090	15.432 ± 0.021	2.208 ± 0.093	C8
CWISEP J042404.54+665011.2	yes	17.820 ± 0.104	15.639 ± 0.053	2.181 ± 0.117	68486912	17.409 ± 0.075	15.661 ± 0.023	1.748 ± 0.078	C6
CWISEP J043034.27+255653.7	yes	17.086 ± 0.080[a]	14.912 ± 0.035	2.174 ± 0.087	68556544	16.035 ± 0.025	14.788 ± 0.018	1.246 ± 0.031	M2
CWISEP J043309.31+100902.9	yes	17.539 ± 0.101	15.094 ± 0.039	2.445 ± 0.108	68236544	16.927 ± 0.050	15.149 ± 0.020	1.778 ± 0.054	C1
CWISEP J044330.73+693828.3	no	17.608 ± 0.088	16.348 ± 0.083	1.260 ± 0.121	68728320	17.271 ± 0.046	16.583 ± 0.027	0.689 ± 0.054	C3
CWISEP J044719.61+202158.1	yes	17.363 ± 0.098	15.519 ± 0.061	1.844 ± 0.115	68726016	17.899 ± 0.122	15.743 ± 0.024	2.156 ± 0.124	C3
CWISEP J050521.29−591311.7	yes	17.636 ± 0.059	16.129 ± 0.053	1.507 ± 0.079	68493056	17.541 ± 0.072	16.160 ± 0.025	1.381 ± 0.076	M1
CWISEP J052346.34−545314.7	yes	19.055 ± 0.267	16.481 ± 0.072	2.574 ± 0.277	68499712	18.557 ± 0.144	16.185 ± 0.023	2.372 ± 0.146	C3,C6
CWISEP J053644.82−305539.3	no	18.926 ± 0.260	15.633 ± 0.046	3.293 ± 0.264	68508416	17.843 ± 0.114	15.518 ± 0.023	2.324 ± 0.116	M1
CWISEP J054233.06+793459.1	no	18.967 ± 0.261	16.119 ± 0.064	2.848 ± 0.269	68732928	17.699 ± 0.073	16.091 ± 0.023	1.608 ± 0.077	M2
CWISEP J055816.68−450233.6	no	18.573 ± 0.157	15.826 ± 0.049	2.747 ± 0.164	68492800	17.631 ± 0.078	15.861 ± 0.023	1.770 ± 0.081	M1
CWISEP J060132.96−592227.3[b]	yes	15.747 ± 0.020[a]	14.468 ± 0.015	1.279 ± 0.025	-	-	-	-	M1
CWISEPR J062436.84−071147.2	yes	17.614 ± 0.120	15.226 ± 0.037	2.388 ± 0.126	68491264	16.902 ± 0.054	15.308 ± 0.021	1.594 ± 0.058	A1,A2
CWISEP J062742.27−215908.1	yes	18.654 ± 0.256	15.947 ± 0.069	2.707 ± 0.265	68504832	17.642 ± 0.087	15.929 ± 0.023	1.713 ± 0.090	C8
CWISEP J063257.49+274629.4	no	> 18.109	15.648 ± 0.070	> 2.461	68499200	17.629 ± 0.080	16.009 ± 0.026	1.620 ± 0.084	M3
CWISEP J063428.10+504925.9	yes	19.068 ± 0.525	15.914 ± 0.069	3.154 ± 0.530	68495104	18.374 ± 0.154	15.955 ± 0.023	2.418 ± 0.155	C3,M1

Table 1 continued

Table 1 *(continued)*

Name	motion confirmed	W1 (mag)	W2 (mag)	W1−W2 (mag)	AOR	ch1 (mag)	ch2 (mag)	ch1−ch2 (mag)	search method[c]
CWISEP J063845.48−615937.2	yes	18.891 ± 0.164	16.745 ± 0.074	2.146 ± 0.180	68488704	18.083 ± 0.094	16.614 ± 0.028	1.469 ± 0.098	M1
CWISEPR J065144.62−115106.1	yes	18.388 ± 0.222	15.592 ± 0.056	2.796 ± 0.229	68493824	16.909 ± 0.049	15.398 ± 0.021	1.511 ± 0.054	M1
CWISEP J070055.19+783834.0	yes	18.998 ± 0.287	16.595 ± 0.104	2.403 ± 0.305	68486400	17.918 ± 0.082	16.712 ± 0.029	1.207 ± 0.086	M1
CWISEP J070214.84−544041.7	yes	19.252 ± 0.372	16.817 ± 0.095	2.435 ± 0.384	68496128	18.189 ± 0.104	16.541 ± 0.027	1.648 ± 0.107	M1
CWISEP J071626.02−371951.1	no	> 18.378	16.176 ± 0.089	> 2.202	68555776	17.360 ± 0.055	15.938 ± 0.022	1.422 ± 0.059	C8
CWISEP J071813.30−061421.1	yes	> 18.114	16.402 ± 0.124	> 1.712	68508160	17.959 ± 0.078	17.077 ± 0.040	0.882 ± 0.087	C8
CWISEP J082400.43+075019.9	no	18.753 ± 0.387	16.380 ± 0.123	2.373 ± 0.406	68509184	18.016 ± 0.089	17.033 ± 0.041	0.983 ± 0.098	C8
CWISEP J084726.55+233558.1	no	17.745 ± 0.115	15.729 ± 0.070	2.016 ± 0.135	68488960	16.965 ± 0.053	15.660 ± 0.025	1.304 ± 0.058	M1
CWISEP J085348.15+112921.5	no	18.093 ± 0.181	15.443 ± 0.047	2.650 ± 0.187	68507904	16.693 ± 0.042	15.448 ± 0.022	1.245 ± 0.047	A1,M1
CWISEP J085820.46+500834.4	no	18.202 ± 0.170	16.084 ± 0.083	2.118 ± 0.189	68501504	17.500 ± 0.070	15.851 ± 0.023	1.649 ± 0.074	M3
CWISEP J085908.26+152527.1	yes	17.692 ± 0.119	15.262 ± 0.042	2.430 ± 0.126	68238080	17.112 ± 0.060	15.229 ± 0.021	1.884 ± 0.063	C1,C6
CWISEP J085938.95+534908.7	yes	> 18.998	15.926 ± 0.069	> 3.072	68556288	18.512 ± 0.171	15.998 ± 0.024	2.514 ± 0.173	C8
CWISEP J090547.50+700239.8	no	18.591 ± 0.226	15.939 ± 0.062	2.652 ± 0.234	68730880	17.848 ± 0.082	15.816 ± 0.021	2.031 ± 0.085	M2
CWISEP J090536.35+740009.1	yes	18.247 ± 0.157	16.455 ± 0.093	1.792 ± 0.182	68489472	17.603 ± 0.061	16.407 ± 0.025	1.196 ± 0.066	M1
CWISEP J091558.51+254713.2	no	18.616 ± 0.347	15.943 ± 0.080	2.673 ± 0.356	68508672	17.684 ± 0.085	16.158 ± 0.028	1.526 ± 0.089	A1
CWISEP J093111.03+232502.1	yes	17.897 ± 0.206	15.726 ± 0.064	2.171 ± 0.216	68492544	17.372 ± 0.076	15.703 ± 0.025	1.670 ± 0.079	C3,C6,M1
CWISEP J093236.66−180029.3	yes	18.315 ± 0.271	15.915 ± 0.071	2.400 ± 0.280	68489216	17.711 ± 0.083	15.704 ± 0.021	2.007 ± 0.085	M1
CWISEP J093852.89+063440.6	yes	17.961 ± 0.143	15.794 ± 0.064	2.167 ± 0.157	68494336	18.442 ± 0.164	15.962 ± 0.025	2.480 ± 0.166	C3,M1
CWISEP J094005.50+523359.2	yes	> 19.207	15.935 ± 0.064	> 3.272	68503296	18.520 ± 0.174	15.754 ± 0.022	2.766 ± 0.175	C7,M3
CWISEP J094615.56+351434.3	yes	18.044 ± 0.151	15.969 ± 0.077	2.075 ± 0.169	68493312	17.178 ± 0.053	16.076 ± 0.026	1.101 ± 0.059	C3,C6,M1
CWISEP J094742.83+384619.3	no	> 18.486	16.217 ± 0.093	> 2.269	68498176	18.191 ± 0.112	16.055 ± 0.025	2.136 ± 0.115	M3
CWISEP J094930.41+663937.2	yes	> 19.197	16.206 ± 0.074	> 2.991	68729600	18.373 ± 0.118	16.097 ± 0.021	2.276 ± 0.120	M2
CWISEP J094957.15−422017.1	no	18.264 ± 0.173	16.302 ± 0.080	1.962 ± 0.191	68733184	18.213 ± 0.111	17.506 ± 0.056	0.707 ± 0.124	C3
CWISEP J095930.71−401046.8	yes	> 18.743	16.834 ± 0.139	> 1.909	68577536	18.235 ± 0.102	17.734 ± 0.059	0.501 ± 0.118	C7
CWISEP J100629.01+105408.5	yes	17.864 ± 0.136	15.487 ± 0.056	2.377 ± 0.147	68495616	17.615 ± 0.090	15.558 ± 0.022	2.057 ± 0.093	M1
CWISEP J100854.84+203136.6	no	> 18.863	15.614 ± 0.060	> 3.249	68732160	17.930 ± 0.126	15.696 ± 0.024	2.234 ± 0.128	M2
CWISEP J101841.86+513108.8	no	17.595 ± 0.091	16.185 ± 0.080	1.410 ± 0.121	68727040	17.234 ± 0.048	16.434 ± 0.027	0.800 ± 0.055	C3
CWISEP J102201.27+145520.2	yes	> 18.541	15.772 ± 0.072	> 2.769	68503552	17.770 ± 0.087	15.831 ± 0.025	1.939 ± 0.090	M3
CWISEP J103453.14+161228.0	yes	17.721 ± 0.126	14.899 ± 0.035	2.822 ± 0.131	68499456	16.589 ± 0.038	14.879 ± 0.019	1.710 ± 0.043	C1,C6
CWISEP J103607.94−304253.1	no	> 18.846	16.279 ± 0.098	> 2.567	68510208	17.674 ± 0.072	16.738 ± 0.034	0.935 ± 0.080	C8

Table 1 continued

Table 1 *(continued)*

Name	motion confirmed	W1 (mag)	W2 (mag)	W1−W2 (mag)	AOR	ch1 (mag)	ch2 (mag)	ch1−ch2 (mag)	search method[c]
CWISEP J104104.20+221613.6	yes	> 18.742	16.249 ± 0.102	> 2.493	68509696	18.924 ± 0.199	16.650 ± 0.029	2.274 ± 0.201	C8
CWISEP J104446.56+001754.9	yes	18.862 ± 0.519	16.160 ± 0.095	2.702 ± 0.528	68502528	18.076 ± 0.106	15.993 ± 0.023	2.083 ± 0.109	C8
CWISEP J104756.81+545741.6	yes	> 19.355	16.339 ± 0.095	> 3.016	68500480	18.731 ± 0.166	16.257 ± 0.024	2.474 ± 0.168	C8
CWISEP J110021.08+094652.9	yes	18.241 ± 0.192	15.514 ± 0.058	2.727 ± 0.201	68493568	17.481 ± 0.082	15.623 ± 0.025	1.858 ± 0.086	C6,M1
CWISEP J111055.12−174738.2	yes	17.270 ± 0.082	15.010 ± 0.035	2.260 ± 0.089	68238592	16.615 ± 0.038	15.038 ± 0.019	1.576 ± 0.042	C1,C6
CWISEP J113010.21+313947.3	yes	17.573 ± 0.092	15.371 ± 0.053	2.202 ± 0.106	68487936	16.556 ± 0.038	15.299 ± 0.020	1.257 ± 0.043	C6
CWISEP J120444.33−235926.8	yes	18.103 ± 0.175	15.273 ± 0.042	2.830 ± 0.180	68236800	16.907 ± 0.050	15.299 ± 0.021	1.608 ± 0.055	C1,C2,C6
CWISEP J121358.13+294237.0	no	18.715 ± 0.247	16.004 ± 0.076	2.711 ± 0.258	68505344	17.855 ± 0.084	16.010 ± 0.023	1.844 ± 0.087	M1
CWISEP J122010.03+281431.3	yes	18.004 ± 0.128	15.767 ± 0.057	2.237 ± 0.140	68494080	17.422 ± 0.067	15.861 ± 0.023	1.561 ± 0.071	C3,M1
CWISEP J124138.41−820051.9	yes	17.385 ± 0.061[a]	15.163 ± 0.026	2.222 ± 0.066	68238848	17.367 ± 0.075	15.337 ± 0.021	2.030 ± 0.077	C1,C6
CWISEP J130255.54+191145.9	yes	18.396 ± 0.188	15.607 ± 0.057	2.789 ± 0.196	68489984	17.381 ± 0.073	15.563 ± 0.023	1.818 ± 0.077	M1
CWISEP J131252.97+341746.5	yes	> 19.202	16.230 ± 0.077	> 2.972	68510464	18.096 ± 0.104	16.392 ± 0.027	1.704 ± 0.108	C8
CWISEP J131208.16−105231.8	no	18.350 ± 0.205	16.071 ± 0.080	2.279 ± 0.220	68492032	18.227 ± 0.135	16.175 ± 0.028	2.052 ± 0.138	C3,M1
CWISEP J131221.97−310845.7	yes	17.801 ± 0.188	15.766 ± 0.058	2.035 ± 0.197	68494592	17.691 ± 0.082	15.809 ± 0.023	1.882 ± 0.086	C3,C6,M1
CWISEP J131350.91−440352.2	yes	18.620 ± 0.223	15.870 ± 0.066	2.750 ± 0.233	68490752	17.243 ± 0.054	15.599 ± 0.021	1.644 ± 0.058	M1
CWISEP J134143.75+574112.9	no	17.954 ± 0.105	15.456 ± 0.039	2.498 ± 0.112	68504576	17.241 ± 0.066	15.522 ± 0.021	1.719 ± 0.069	C4,M3
CWISEP J135336.29−003756.6[b]	yes	18.243 ± 0.174[a]	15.495 ± 0.049	2.748 ± 0.181	-	-	-	-	C6
CWISEP J135937.65−435226.9	yes	> 18.374	16.132 ± 0.083	> 2.242	68509440	18.379 ± 0.135	15.945 ± 0.023	2.434 ± 0.137	C8
CWISEP J140118.30+432554.2	yes	17.614 ± 0.081	15.540 ± 0.041	2.074 ± 0.091	68235008	16.989 ± 0.052	15.641 ± 0.023	1.348 ± 0.057	C1,C2
CWISEP J140247.83+102132.6	yes	15.717 ± 0.027	14.493 ± 0.024	1.224 ± 0.036	68487168	15.214 ± 0.016	14.436 ± 0.018	0.778 ± 0.024	M1
CWISEP J141206.85+234412.4	yes	18.545 ± 0.196	16.239 ± 0.082	2.306 ± 0.212	68491776	17.452 ± 0.060	16.218 ± 0.025	1.234 ± 0.065	M1
CWISEP J141400.68+163153.9	no	17.390 ± 0.080[a]	15.824 ± 0.058	1.566 ± 0.099	68729088	17.431 ± 0.065	16.360 ± 0.030	1.071 ± 0.072	C3
CWISEP J142552.36+485151.3	no	18.013 ± 0.110	16.410 ± 0.078	1.603 ± 0.135	68726528	17.948 ± 0.078	17.055 ± 0.035	0.892 ± 0.085	M2
CWISEP J143439.23−134421.4	yes	> 18.763	16.158 ± 0.101	> 2.605	68500224	18.271 ± 0.130	16.150 ± 0.026	2.121 ± 0.133	M1
CWISEP J144606.62−231717.8	yes	18.281 ± 0.292	15.998 ± 0.094	2.283 ± 0.307	68496896	19.511 ± 0.434	15.802 ± 0.024	3.709 ± 0.435	M1
CWISEP J145837.91+173450.1	yes	16.677 ± 0.045	15.118 ± 0.033	1.559 ± 0.056	68726272	17.114 ± 0.059	15.281 ± 0.021	1.833 ± 0.063	C4
CWISEP J150252.82−304232.8	yes	17.465 ± 0.093	15.071 ± 0.037	2.394 ± 0.100	68237056	16.577 ± 0.038	15.029 ± 0.019	1.548 ± 0.042	C1
CWISEP J151140.51−835918.0	no	19.057 ± 0.383	16.566 ± 0.091	2.491 ± 0.394	68507136	17.662 ± 0.057	16.581 ± 0.026	1.081 ± 0.063	C8
CWISEP J151521.22−215736.9[b]	yes	16.580 ± 0.050[a]	14.951 ± 0.033	1.629 ± 0.060	-	-	-	-	C4,M1
WISEA J153429.75−104303.3	yes	18.264 ± 0.372	16.072 ± 0.202	2.192 ± 0.423	68555520	16.691 ± 0.032	15.766 ± 0.023	0.926 ± 0.039	U1

Table 1 continued

Table 1 *(continued)*

Name	motion confirmed	W1 (mag)	W2 (mag)	W1−W2 (mag)	AOR	ch1 (mag)	ch2 (mag)	ch1−ch2 (mag)	search method[c]
CWISEP J153859.39+482659.1	yes	17.797 ± 0.087	15.770 ± 0.046	2.027 ± 0.098	68238336	18.082 ± 0.140	15.809 ± 0.024	2.272 ± 0.142	C1
CWISEP J154151.59+523025.0 N	no	17.797 ± 0.080[a]	15.703 ± 0.039	2.094 ± 0.089	68497920	18.205 ± 0.142	16.387 ± 0.030	1.818 ± 0.146	M3
CWISEP J154151.59+523025.0 S	no	17.797 ± 0.080[a]	15.703 ± 0.039	2.094 ± 0.089	68497920	18.401 ± 0.154	16.566 ± 0.032	1.836 ± 0.157	M3
CWISEP J160311.60−104620.4	yes	18.293 ± 0.216	15.675 ± 0.066	2.618 ± 0.226	68492288	17.326 ± 0.076	15.575 ± 0.023	1.752 ± 0.079	C3,M1
CWISEP J160835.01−244244.7	yes	17.251 ± 0.096	15.133 ± 0.045	2.118 ± 0.106	68239104	16.621 ± 0.040	15.116 ± 0.019	1.504 ± 0.044	C1
CWISEP J161822.86−062310.2	yes	17.886 ± 0.143	15.824 ± 0.063	2.062 ± 0.156	68499968	17.611 ± 0.079	15.660 ± 0.021	1.951 ± 0.082	M3
CWISEP J162225.92+370118.8	yes	18.896 ± 0.239	16.053 ± 0.057	2.843 ± 0.246	68496384	17.522 ± 0.072	16.214 ± 0.026	1.308 ± 0.076	C3,C6
CWISEP J163200.11+002108.6	no	> 18.625	16.354 ± 0.100	> 2.271	68507392	18.461 ± 0.120	16.870 ± 0.032	1.591 ± 0.124	C8
CWISEP J165215.62+022918.5	yes	17.771 ± 0.123	16.384 ± 0.104	1.387 ± 0.161	68506368	17.677 ± 0.065	16.953 ± 0.035	0.723 ± 0.074	M3
CWISEP J165359.67+214457.2	no	> 18.723	16.256 ± 0.076	> 2.467	68557312	18.047 ± 0.090	16.136 ± 0.023	1.911 ± 0.093	M2
CWISEP J170918.83+000950.5	no	> 18.918	15.846 ± 0.058	> 3.072	68729344	17.523 ± 0.073	15.747 ± 0.023	1.776 ± 0.077	M2
CWISEP J172104.42+595047.7	no	17.808 ± 0.058	16.081 ± 0.049	1.727 ± 0.076	3862272	17.545 ± 0.057	15.535 ± 0.030	2.009 ± 0.065	C6
CWISEP J175746.31+195112.6	no	17.873 ± 0.182	16.260 ± 0.084	1.613 ± 0.200	68502272	18.627 ± 0.149	16.381 ± 0.024	2.246 ± 0.151	C3,C5
CWISEP J182358.73−740246.0	yes	16.722 ± 0.048	15.569 ± 0.051	1.153 ± 0.070	68233216	16.770 ± 0.047	15.566 ± 0.022	1.203 ± 0.052	C2
CWISEP J185658.80+601351.4	yes	17.506 ± 0.059	15.734 ± 0.036	1.772 ± 0.069	68730624	16.814 ± 0.045	15.618 ± 0.022	1.196 ± 0.050	C4
CWISEP J193518.58−154620.3	yes	18.534 ± 0.396	15.852 ± 0.079	2.682 ± 0.404	69998848	18.512 ± 0.030	15.528 ± 0.017	2.984 ± 0.034	M1
WISENF J193656.08+040801.2	yes	> 16.551	14.671 ± 0.222	> 1.880	68576768	17.096 ± 0.061	14.689 ± 0.018	2.407 ± 0.064	U1
CWISEP J194027.48−345650.6	no	18.739 ± 0.432	16.440 ± 0.129	2.299 ± 0.451	68504064	17.347 ± 0.053	16.708 ± 0.030	0.639 ± 0.061	C8
CWISEP J194101.59+542335.9	yes	17.297 ± 0.047	15.417 ± 0.029	1.880 ± 0.055	68498944	17.010 ± 0.054	15.507 ± 0.021	1.504 ± 0.057	C4,M1
CWISEP J194812.42−322334.9	yes	17.669 ± 0.173[a]	15.879 ± 0.082	1.790 ± 0.191	68503808	16.856 ± 0.041	15.827 ± 0.023	1.028 ± 0.046	C6
CWISEP J201146.45−481259.7	yes	17.215 ± 0.081	15.379 ± 0.047	1.836 ± 0.094	68239360	17.814 ± 0.116	15.318 ± 0.021	2.496 ± 0.118	C1,C6
CWISEP J201510.68−675005.6	yes	17.121 ± 0.072	15.014 ± 0.038	2.107 ± 0.081	68501248	15.918 ± 0.023	14.665 ± 0.018	1.254 ± 0.029	C1
CWISEP J203821.53−064930.9	yes	18.804 ± 0.464	16.004 ± 0.080	2.800 ± 0.471	68556800	17.882 ± 0.087	15.619 ± 0.020	2.263 ± 0.089	C8
CWISEP J205019.99−253652.8	yes	17.348 ± 0.103	15.080 ± 0.040	2.268 ± 0.110	68233984	16.622 ± 0.040	15.079 ± 0.019	1.543 ± 0.044	C1,C2,C6
CWISEP J205908.95+024105.6	yes	17.273 ± 0.079[a]	15.620 ± 0.055	1.653 ± 0.096	68731136	17.163 ± 0.062	15.525 ± 0.022	1.638 ± 0.066	U1
CWISEP J210007.87−293139.8	yes	> 18.848	15.960 ± 0.078	> 2.888	68503040	18.351 ± 0.161	15.959 ± 0.023	2.392 ± 0.163	M3
CWISEP J211909.29−192117.4	no	18.279 ± 0.319	15.907 ± 0.078	2.372 ± 0.328	68490240	17.606 ± 0.076	15.771 ± 0.021	1.836 ± 0.079	M1
CWISEP J212828.05+352912.4	yes	18.240 ± 0.157	16.242 ± 0.079	1.998 ± 0.176	68236032	18.111 ± 0.118	17.059 ± 0.043	1.052 ± 0.125	C6
CWISEP J213249.05+690113.7	yes	17.888 ± 0.094	15.179 ± 0.027	2.709 ± 0.098	68234496	17.244 ± 0.069	15.271 ± 0.021	1.974 ± 0.072	C1
CWISEP J213838.74−313808.5	yes	18.000 ± 0.157	15.144 ± 0.042	2.856 ± 0.163	68234240	16.917 ± 0.052	15.136 ± 0.019	1.781 ± 0.055	C1,C2,C6

Table 1 continued

Table 1 *(continued)*

Name	motion confirmed	W1 (mag)	W2 (mag)	W1−W2 (mag)	AOR	ch1 (mag)	ch2 (mag)	ch1−ch2 (mag)	search method[c]
CWISEP J213930.45+042721.6	yes	18.432 ± 0.295	15.804 ± 0.069	2.628 ± 0.303	68497664	17.915 ± 0.101	15.747 ± 0.022	2.168 ± 0.103	M1
CWISEP J215841.50+732842.7	yes	17.007 ± 0.058	14.926 ± 0.029	2.081 ± 0.065	68502016	16.927 ± 0.052	15.160 ± 0.020	1.767 ± 0.055	M3
CWISEP J220452.02+063343.4	no	18.422 ± 0.338	15.976 ± 0.080	2.446 ± 0.347	68731648	17.856 ± 0.094	16.011 ± 0.025	1.845 ± 0.098	M2
CWISEP J221736.94−222647.6	no	17.820 ± 0.120	15.842 ± 0.069	1.978 ± 0.138	68235520	17.741 ± 0.103	15.968 ± 0.026	1.773 ± 0.106	C3,C6
CWISEP J222035.35−810322.6	yes	18.448 ± 0.161	15.953 ± 0.058	2.495 ± 0.171	68233728	17.382 ± 0.075	16.003 ± 0.025	1.378 ± 0.079	C6
CWISEP J223022.60+254907.5	yes	18.344 ± 0.205	16.094 ± 0.076	2.250 ± 0.219	68491008	19.119 ± 0.292	16.290 ± 0.026	2.830 ± 0.293	M1
CWISEP J223138.55−383057.2	yes	> 18.673	16.170 ± 0.087	> 2.503	68506624	18.015 ± 0.095	16.098 ± 0.023	1.917 ± 0.098	C8
CWISEP J224747.42−004103.6	no	17.180 ± 0.079	15.728 ± 0.067	1.452 ± 0.104	46949376	17.010 ± 0.086	15.947 ± 0.036	1.063 ± 0.093	C3
CWISEP J224916.17+371551.4	yes	18.718 ± 0.252	16.481 ± 0.104	2.237 ± 0.273	68505088	18.526 ± 0.138	16.201 ± 0.023	2.324 ± 0.140	C8
CWISEP J225059.28−432057.2	yes	18.651 ± 0.232	16.322 ± 0.089	2.329 ± 0.248	68164864	18.032 ± 0.099	16.145 ± 0.023	1.887 ± 0.102	C6
CWISEP J225156.13+392408.4	yes	18.030 ± 0.131	15.719 ± 0.052	2.311 ± 0.141	68237824	17.291 ± 0.067	15.620 ± 0.023	1.672 ± 0.070	C1
CWISEP J225109.50−074037.7	yes	17.737 ± 0.123	15.202 ± 0.047	2.535 ± 0.132	68233472	16.869 ± 0.053	15.100 ± 0.019	1.769 ± 0.056	C1,C2,C6
CWISEP J225511.56−191516.3	no	18.278 ± 0.199	16.623 ± 0.141	1.655 ± 0.244	68508928	18.933 ± 0.181	18.010 ± 0.073	0.923 ± 0.195	C8
CWISEP J225628.97+400227.3	yes	18.370 ± 0.183	15.928 ± 0.065	2.442 ± 0.194	68489728	18.820 ± 0.226	15.806 ± 0.021	3.014 ± 0.227	C3,M1
CWISEP J230158.30−645858.3	yes	18.401 ± 0.166	15.264 ± 0.034	3.137 ± 0.169	68235264	17.273 ± 0.057	15.364 ± 0.019	1.909 ± 0.060	A2
CWISEP J231047.80+362004.6	no	18.126 ± 0.153	16.237 ± 0.082	1.889 ± 0.174	68732416	17.683 ± 0.066	16.473 ± 0.025	1.209 ± 0.070	M2
CWISEP J231114.50+135148.5	no	18.606 ± 0.343	15.996 ± 0.079	2.610 ± 0.352	68733440	17.382 ± 0.061	15.868 ± 0.023	1.513 ± 0.065	M2
CWISEP J233216.39−290025.0	yes	18.528 ± 0.253	15.921 ± 0.078	2.607 ± 0.265	68496640	16.740 ± 0.036	15.601 ± 0.021	1.140 ± 0.042	M1
CWISEP J235130.42−185800.2	yes	17.410 ± 0.092	15.432 ± 0.048	1.978 ± 0.104	68236288	17.618 ± 0.094	15.590 ± 0.022	2.028 ± 0.097	C1,C6
CWISEP J235547.99+380438.9	yes	> 18.395	15.976 ± 0.067	> 2.419	68163840	18.444 ± 0.259	15.926 ± 0.026	2.518 ± 0.261	C3,C5,C6
CWISEP J235644.78−481456.3	yes	18.910 ± 0.286	16.165 ± 0.078	2.745 ± 0.296	68165120	18.727 ± 0.218	16.040 ± 0.024	2.687 ± 0.220	C3,C6

[a] WISE photometry may be contaminated by blending.

[b] Object is scheduled for p14034 *Spitzer* observations in the near future, but does not yet have *Spitzer* photometry available.

[c] The search method names listed in this column are defined in §4.1-4.3, which also contain explanations of each search's moving object candidate selection procedure.

Table 2. Spurious Candidates

p14034 AOR	CWISEP designation	W2 (mag)
68510720	J075426.59−025947.8	16.36 ± 0.12
68502784	J111337.00+342927.0	16.48 ± 0.13
68505600	J121005.73−150533.3	15.97 ± 0.08
68733696	J132904.57+343524.4	16.31 ± 0.08
68577024	J202736.23−621855.5	16.68 ± 0.14
68506880	J212111.15+005640.0	16.34 ± 0.10

Table 3. WISE W2 Positions used in Joint WISE+*Spitzer* Linear Motion Fits

Name	RA (deg, ICRS)	Dec (deg, ICRS)	σ_{RA} (mas)	σ_{Dec} (mas)	time slice[a]	mean MJD
CWISEP J000006.01−704851.2	0.025954	−70.814036	424	408	pre	55404.23
	0.024768	−70.814293	283	267	post	57330.72
CWISEP J000110.81−093215.5	0.294481	−9.537603	678	691	pre	55431.64
	0.295332	−9.537668	539	540	post	57387.92
CWISEP J001146.07−471306.8	2.941300	−47.218389	620	625	pre	55442.17
	2.942075	−47.218477	364	361	post	57398.73
CWISEP J003507.77−153233.8	8.782612	−15.542104	422	426	pre	55447.53
	8.782597	−15.542193	481	469	post0_1yr	56747.59
	8.782337	−15.542798	396	394	post1_1yr	57115.18
	8.782461	−15.542872	358	357	post2_1yr	57476.03
	8.782416	−15.543088	469	472	post3_1yr	57863.72
CWISEP J003915.43+360939.0	9.814493	36.160926	791	803	pre	55474.81
	9.814085	36.160881	494	496	post	57321.12
CWISEP J004158.35+381811.9	10.492864	38.303419	461	471	pre	55409.12
	10.493334	38.303312	405	402	post	57316.48
CWISEP J005802.63+723330.3	14.514699	72.558011	635	624	pre	55357.74
	14.510806	72.558429	376	353	post	57321.58
CWISEP J010247.48−654226.4	15.698193	−65.707457	789	774	pre	55459.43
	15.697185	−65.707364	817	780	post0_2yr	57032.48
	15.697245	−65.707466	887	831	post2_1yr	57635.12
	15.696512	−65.707690	1086	1028	post3_1yr	57956.83
CWISEP J010527.69−783419.3	16.365313	−78.572101	177	163	pre	55412.76
	16.366899	−78.572277	122	110	post	57478.47
CWISEP J010650.61+225159.1	16.711013	22.866740	328	335	pre	55490.39
	16.710726	22.866440	350	349	post0_1yr	56768.89

Table 3 continued

Table 3 *(continued)*

Name	RA (deg, ICRS)	Dec (deg, ICRS)	σ_{RA} (mas)	σ_{Dec} (mas)	time slice[a]	mean MJD
	16.711028	22.866213	413	417	post1_1yr	57160.75
	16.710850	22.865943	525	535	post2_1yr	57482.24
	16.710533	22.866105	410	414	post3_1yr	57852.42
CWISEP J012735.44−564110.5	21.897551	−56.686198	369	362	pre	55417.12
	21.897902	−56.686289	282	275	post	57454.11
CWISEP J012748.35−631056.1	21.947860	−63.182449	394	377	pre	55422.19
	21.950448	−63.182269	398	378	post0_1yr	56878.40
	21.950847	−63.182216	336	318	post1_1yr	57278.38
	21.951630	−63.182168	377	358	post2_1yr	57620.10
	21.951872	−63.182046	442	415	post3_1yr	57966.68
CWISEP J014607.55−375705.6	26.530931	−37.951706	570	580	pre	55466.49
	26.531826	−37.951327	272	277	post	57376.04
CWISEP J015613.24+325526.6	29.053861	32.924437	844	854	pre	55433.03
	29.055472	32.923613	1071	1066	post0_1yr	56783.84
	29.055614	32.924112	831	826	post1_1yr	57147.85
	29.055405	32.923709	854	866	post2_1yr	57512.37
	29.056087	32.923469	761	782	post3_1yr	57874.19
CWISEP J020103.10+293801.8	30.262257	29.633849	619	642	pre	55451.72
	30.263330	29.633644	461	470	post	57309.39
CWISEP J020938.72+180427.7	32.410829	18.074498	579	591	pre	55416.78
	32.411173	18.074447	798	796	post0_1yr	56781.24
	32.411590	18.074137	908	944	post1_1yr	57144.78
	32.411707	18.074745	957	970	post2_1yr	57528.65
	32.411687	18.074040	906	921	post3_1yr	57844.62
CWISEP J021243.55+053147.2	33.181654	5.529844	631	652	pre	55382.91
	33.181171	5.529847	858	870	post0_1yr	56780.46
	33.181224	5.529676	871	902	post1_1yr	57125.46
	33.181641	5.529932	955	981	post3_1yr	57863.25
CWISEP J021921.66−265451.8	34.839948	−26.915344	730	755	pre	55412.02
	34.840268	−26.914165	507	507	post	57332.52
CWISEP J022122.41−564125.0	35.343121	−56.690469	410	400	pre	55470.52
	35.343625	−56.690221	245	233	post	57406.96
CWISEP J022513.27+154854.8	36.305042	15.815204	512	530	pre	55443.22
	36.305393	15.815025	628	635	post0_1yr	56777.57
	36.305448	15.815299	634	646	post1_1yr	57140.49
	36.305669	15.815005	721	734	post2_1yr	57504.35
	36.305591	15.815198	663	670	post3_1yr	57876.45
CWISEP J022631.82−203439.4	36.632972	−20.577124	573	581	pre	55408.86
	36.632563	−20.577865	875	862	post0_2yr	56944.02
	36.632305	−20.577927	690	689	post2_1yr	57505.37

Table 3 continued

Table 3 *(continued)*

Name	RA (deg, ICRS)	Dec (deg, ICRS)	σ_{RA} (mas)	σ_{Dec} (mas)	time slice[a]	mean MJD
	36.632296	−20.578471	956	964	post3_1yr	57863.40
CWISEP J022935.43+724616.4	37.397684	72.771055	269	275	pre	55343.79
	37.397483	72.771227	240	233	post0_2yr	56977.56
	37.397612	72.771312	233	230	post1_2yr	57695.98
CWISEP J023842.60−133210.7	39.677681	−13.535727	783	807	pre	55395.92
	39.677927	−13.536315	864	870	post0_1yr	56779.26
	39.677567	−13.536849	906	915	post1_1yr	57151.04
	39.677457	−13.537118	1147	1153	post2_1yr	57506.54
CWISEP J024204.91−225604.6	40.519731	−22.934882	715	736	pre	55382.34
	40.521349	−22.934602	755	760	post	57349.82
CWISEP J024710.25−145809.9	41.793254	−14.969759	1016	1040	pre	55365.76
	41.792464	−14.969495	477	482	post	57304.62
CWISEP J024810.75−694127.9	42.044890	−69.690951	577	543	pre	55459.10
	42.045054	−69.691216	357	334	post	57408.94
CWISEP J025747.92−205602.7	44.449439	−20.934140	482	491	pre	55392.80
	44.449770	−20.934010	299	303	post	57325.48
CWISEP J031130.28+035931.8	47.875316	3.991982	930	979	pre	55413.43
	47.876820	3.992834	1017	1043	post	57302.34
CWISEP J031557.05+203552.4	48.987680	20.597619	464	491	pre	55319.37
	48.987737	20.598074	338	349	post	57372.29
CWISEP J031908.60+081120.4	49.785964	8.187889	1026	1066	pre	55314.75
	49.785971	8.189149	607	619	post	57326.47
CWISEP J031935.50−041231.7	49.897193	−4.208561	863	888	pre	55397.05
	49.898204	−4.208902	881	908	post	57338.74
CWISEP J032109.59+693204.5	50.287910	69.534935	648	675	pre	55381.83
	50.290143	69.534583	728	736	post0_1yr	56809.43
	50.290322	69.534803	578	581	post1_1yr	57172.82
	50.290696	69.534371	589	594	post2_1yr	57500.69
	50.292022	69.534303	767	783	post3_1yr	57903.15
CWISEP J034336.27+184025.8	55.900398	18.673614	732	766	pre	55333.00
	55.901389	18.673693	500	524	post	57327.78
CWISEP J034514.82+173528.1	56.311609	17.591319	584	620	pre	55337.41
	56.311848	17.591096	298	304	post	57330.96
CWISEP J034755.11+123051.9	56.979752	12.514043	369	389	pre	55313.34
	56.979780	12.514447	453	471	post0_1yr	56824.30
	56.979549	12.514664	407	420	post1_1yr	57152.63
	56.979560	12.514727	557	578	post2_1yr	57499.94
	56.979646	12.514899	466	482	post3_1yr	57886.87
CWISEP J034904.05−462827.9	57.266547	−46.474724	486	490	pre	55399.40
	57.267109	−46.474275	448	445	post	57288.99

Table 3 continued

Table 3 *(continued)*

Name	RA	Dec	σ_{RA}	σ_{Dec}	time	mean
	(deg, ICRS)	(deg, ICRS)	(mas)	(mas)	slice[a]	MJD
CWISEP J040106.67+085748.5	60.277377	8.963757	597	633	pre	55333.01
	60.277585	8.963423	875	891	post0_1yr	56810.18
	60.277831	8.963312	751	780	post1_1yr	57161.93
	60.277991	8.963312	760	791	post2_1yr	57505.96
	60.278298	8.963284	765	810	post3_1yr	57896.18
CWISEP J040235.55−265145.4	60.647566	−26.862373	330	347	pre	55336.09
	60.648296	−26.862568	353	358	post0_1yr	56766.61
	60.648527	−26.862870	475	483	post1_1yr	57137.41
	60.648792	−26.862727	690	716	post2_1yr	57517.04
CWISEP J040324.67+185729.6	60.852754	18.958556	784	823	pre	55342.23
	60.852886	18.958055	525	542	post	57336.58
CWISEP J040351.00−491605.6	60.961986	−49.268242	406	411	pre	55388.03
	60.962925	−49.268089	335	329	post	57300.89
CWISEP J041025.10+033807.2	62.605065	3.635469	876	917	pre	55335.64
	62.604512	3.635342	575	604	post	57293.23
CWISEP J042455.68+000221.4	66.231943	0.039413	410	435	pre	55325.12
	66.231994	0.039318	521	539	post0_1yr	56795.11
	66.232127	0.039351	490	509	post1_1yr	57154.49
	66.232110	0.039087	572	606	post2_1yr	57522.53
	66.232208	0.039246	610	625	post3_1yr	57893.47
CWISEP J042404.54+665011.2	66.017892	66.836284	360	379	pre	55359.57
	66.019417	66.836467	282	288	post	57357.01
CWISEP J043034.27+255653.7	67.642273	25.948619	281	299	pre	55350.22
	67.643026	25.948268	174	185	post	57365.92
CWISEP J043309.31+100902.9	68.288697	10.151117	339	355	pre	55340.87
	68.288864	10.150832	404	422	post0_1yr	56796.03
	68.288945	10.150761	473	493	post1_1yr	57154.09
	68.288721	10.150549	392	399	post2_1yr	57503.88
	68.288878	10.150517	470	494	post3_1yr	57889.69
CWISEP J044330.73+693828.3	70.877771	69.641984	888	938	pre	55403.29
	70.877930	69.640881	422	437	post	57303.21
CWISEP J044719.61+202158.1	71.831804	20.366738	561	591	pre	55347.05
	71.831636	20.365973	677	700	post0_1yr	56810.35
	71.831473	20.365860	501	522	post1_1yr	57174.72
	71.831633	20.365584	565	591	post2_1yr	57561.85
	71.831551	20.365705	643	664	post3_1yr	57885.79
CWISEP J050521.29−591311.7	76.338345	−59.219309	328	326	pre	55352.35
	76.339348	−59.220517	315	308	post	57292.77
CWISEP J052346.34−545314.7	80.942393	−54.888042	459	486	pre	55337.39
	80.943131	−54.887282	369	380	post	57314.98

Table 3 continued

Table 3 *(continued)*

Name	RA	Dec	σ_{RA}	σ_{Dec}	time	mean
	(deg, ICRS)	(deg, ICRS)	(mas)	(mas)	slice[a]	MJD
CWISEP J053644.82−305539.3	84.186708	−30.927490	474	497	pre	55327.22
	84.186786	−30.927672	232	242	post	57341.79
CWISEP J054233.06+793459.1	85.637735	79.582857	617	658	pre	55381.31
	85.638091	79.583160	320	339	post	57369.25
CWISEP J055816.68−450233.6	89.569714	−45.042731	374	397	pre	55359.93
	89.569492	−45.042565	391	410	post0_1yr	56824.58
	89.569594	−45.042561	479	508	post1_1yr	57183.87
	89.569343	−45.042568	397	422	post2_1yr	57563.99
	89.569340	−45.042506	462	487	post3_1yr	57896.09
CWISEP J060132.96−592227.3	90.387901	−59.374820	94	101	pre	55351.37
	90.387389	−59.374268	116	120	post0_1yr	56820.47
	90.387438	−59.374247	137	142	post1_1yr	57104.39
	90.387261	−59.374196	111	119	post2_1yr	57385.99
	90.387142	−59.374066	108	112	post3_1yr	57735.17
CWISEPR J062436.84−071147.2	96.153655	−7.196548	264	280	pre	55368.03
	96.153514	−7.196523	371	386	post0_1yr	56839.26
	96.153438	−7.196448	365	385	post1_1yr	57204.09
	96.153395	−7.196210	383	407	post2_1yr	57547.81
	96.153457	−7.196134	432	455	post3_1yr	57934.80
CWISEP J062742.27−215908.1	96.926242	−21.985125	579	615	pre	55377.52
	96.926128	−21.985786	358	383	post	57382.88
CWISEP J063257.49+274629.4	98.239021	27.774824	702	744	pre	55377.71
	98.239540	27.774926	353	373	post	57373.94
CWISEP J063428.10+504925.9	98.616383	50.825175	637	672	pre	55355.67
	98.617122	50.823937	696	722	post0_1yr	56833.26
	98.616773	50.823501	892	947	post1_1yr	57197.31
	98.617487	50.823171	530	573	post2_1yr	57550.47
	98.617331	50.823183	684	743	post3_1yr	57935.68
CWISEP J063845.48−615937.2	99.690522	−61.993995	662	685	pre	55422.54
	99.689248	−61.993648	359	379	post	57386.52
CWISEPR J065144.62−115106.1	102.936184	−11.851389	426	449	pre	55387.88
	102.935888	−11.851792	452	472	post0_1yr	56815.32
	102.935895	−11.851773	512	542	post1_1yr	57194.85
	102.935783	−11.851899	586	619	post2_1yr	57586.87
	102.935841	−11.851957	553	585	post3_1yr	57939.80
CWISEP J070055.19+783834.0	105.227081	78.644150	901	963	pre	55368.25
	105.233351	78.642414	708	761	post	57358.29
CWISEP J070214.84−544041.7	105.562164	−54.677699	638	673	pre	55409.70
	105.562108	−54.678520	474	508	post	57349.62
CWISEP J071626.02−371951.1	109.108284	−37.330989	496	526	pre	55399.82

Table 3 continued

Table 3 *(continued)*

Name	RA (deg, ICRS)	Dec (deg, ICRS)	σ_{RA} (mas)	σ_{Dec} (mas)	time slice[a]	mean MJD
	109.108353	−37.330788	409	442	post	57525.85
CWISEP J071813.30−061421.1	109.554815	−6.239489	847	902	pre	55394.54
	109.555580	−6.239248	613	652	post	57457.63
CWISEP J082400.43+075019.9	126.001405	7.838580	1371	1459	pre	55394.92
	126.001796	7.838964	888	959	post0_2yr	57035.01
	126.002119	7.838775	1056	1133	post2_1yr	57593.71
CWISEP J084726.55+233558.1	131.860655	23.599695	804	865	pre	55421.38
	131.860728	23.599402	289	311	post	57394.86
CWISEP J085348.15+112921.5	133.450617	11.489657	468	502	pre	55397.24
	133.450635	11.489145	276	297	post	57438.04
CWISEP J085820.46+500834.4	134.585481	50.142887	592	627	pre	55406.04
	134.585224	50.142841	403	431	post	57498.83
CWISEP J085908.26+152527.1	134.784692	15.424516	404	427	pre	55407.64
	134.784392	15.424041	229	241	post	57416.32
CWISEP J085938.95+534908.7	134.912517	53.819347	512	543	pre	55393.20
	134.912417	53.819028	736	783	post0_1yr	56957.23
	134.912454	53.819176	770	828	post1_1yr	57224.42
	134.912459	53.818956	621	667	post2_1yr	57601.75
	134.911519	53.818787	889	955	post3_1yr	57932.37
CWISEP J090547.50+700239.8	136.447093	70.044693	481	504	pre	55404.69
	136.448460	70.044306	335	360	post	57490.63
CWISEP J090536.35+740009.1	136.399468	74.004338	604	638	pre	55399.63
	136.401687	74.001935	548	584	post	57459.04
CWISEP J091558.51+254713.2	138.993511	25.787110	516	544	pre	55408.04
	138.993849	25.786607	920	971	post0_1yr	56877.66
	138.993798	25.786598	1028	1091	post1_1yr	57233.30
	138.993696	25.786215	819	879	post1_2yr	57759.48
CWISEP J093111.03+232502.1	142.796426	23.417667	742	783	pre	55400.78
	142.795851	23.417006	341	369	post	57443.29
CWISEP J093236.66−180029.3	143.153256	−18.007918	557	596	pre	55424.58
	143.152580	−18.008265	354	376	post	57423.95
CWISEP J093852.89+063440.6	144.720048	6.578744	529	560	pre	55403.99
	144.720639	6.578038	623	662	post0_1yr	56882.20
	144.720718	6.577606	1047	1130	post1_1yr	57240.44
	144.720676	6.577501	615	647	post2_1yr	57592.65
	144.720903	6.577148	912	985	post3_1yr	57956.49
CWISEP J094005.50+523359.2	145.023963	52.566911	787	836	e000	55309.62
	145.023527	52.566610	660	707	e001	55501.02
	145.022808	52.566317	575	618	post0_1yr	56852.10
	145.022714	52.566331	665	706	post1_1yr	57220.52

Table 3 continued

Table 3 *(continued)*

Name	RA (deg, ICRS)	Dec (deg, ICRS)	σ_{RA} (mas)	σ_{Dec} (mas)	time slice[a]	mean MJD
	145.022727	52.566362	600	649	post2_1yr	57563.33
	145.022555	52.566097	687	735	post3_1yr	57947.36
CWISEP J094615.56+351434.3	146.565277	35.243549	559	593	pre	55393.93
	146.564634	35.242460	519	562	post	57439.50
CWISEP J094742.83+384619.3	146.928764	38.772289	676	710	pre	55394.46
	146.928395	38.771896	506	543	post	57388.04
CWISEP J094930.41+663937.2	147.376452	66.660795	555	577	pre	55399.50
	147.376928	66.660186	405	432	post	57500.79
CWISEP J094957.15−422017.1	147.487585	−42.338653	719	750	pre	55446.05
	147.488299	−42.338178	436	464	post	57249.44
CWISEP J095930.71−401046.8	149.878693	−40.178588	977	1027	pre	55450.52
	149.878296	−40.179760	1016	1077	post0_2yr	56928.88
	149.878020	−40.180097	1126	1194	post1_2yr	57625.38
CWISEP J100629.01+105408.5	151.621074	10.902460	503	539	pre	55430.55
	151.621013	10.902348	517	537	post0_1yr	56887.10
	151.620764	10.902281	455	480	post1_1yr	57250.73
	151.620581	10.902379	615	671	post2_1yr	57583.65
	151.620590	10.902253	461	489	post3_1yr	57964.13
CWISEP J100854.84+203136.6	152.228603	20.527057	508	541	pre	55396.49
	152.228470	20.526708	319	343	post	57423.31
CWISEP J101841.86+513108.8	154.674325	51.518481	671	704	pre	55413.97
	154.674470	51.519394	441	473	post	57382.28
CWISEP J102201.27+145520.2	155.505836	14.922535	653	700	pre	55416.00
	155.505129	14.922287	609	645	post0_1yr	56907.25
	155.505111	14.922219	720	757	post1_1yr	57232.42
	155.505019	14.922299	665	705	post2_1yr	57615.87
	155.504660	14.922094	692	757	post3_1yr	57979.69
CWISEP J103453.14+161228.0	158.721696	16.207927	275	292	pre	55430.18
	158.721282	16.207720	178	191	post	57444.17
CWISEP J103607.94−304253.1	159.033472	−30.714505	768	807	pre	55442.56
	159.033147	−30.714718	801	852	post0_2yr	56939.77
	159.032408	−30.715024	866	929	post1_2yr	57631.99
CWISEP J104104.20+221613.6	160.268142	22.270716	1137	1197	pre	55424.70
	160.267286	22.270292	661	715	post	57420.08
CWISEP J104446.56+001754.9	161.194648	0.298747	879	922	pre	55428.76
	161.194027	0.298771	679	720	post0_2yr	57086.35
	161.193376	0.298493	884	956	post1_2yr	57800.07
CWISEP J104756.81+545741.6	161.987505	54.961705	737	774	pre	55409.64
	161.986471	54.961345	822	872	post0_1yr	56861.78
	161.986749	54.961079	1201	1291	post1_1yr	57220.20

Table 3 continued

Table 3 *(continued)*

Name	RA	Dec	σ_{RA}	σ_{Dec}	time	mean
	(deg, ICRS)	(deg, ICRS)	(mas)	(mas)	slice[a]	MJD
	161.985899	54.961833	810	872	post2_1yr	57588.06
	161.985366	54.961315	589	624	post3_1yr	57981.03
CWISEP J110021.08+094652.9	165.088312	9.781192	446	468	pre	55441.46
	165.087419	9.781271	322	343	post	57421.98
CWISEP J111055.12−174738.2	167.729593	−17.793500	252	262	pre	55453.13
	167.729593	−17.794300	179	189	post	57300.30
CWISEP J113010.21+313947.3	172.544572	31.665210	556	584	e000	55343.29
	172.544272	31.664742	457	479	e001	55533.44
	172.542926	31.663485	607	645	e002	56805.43
	172.542803	31.662977	805	843	e003	56995.48
	172.542685	31.663231	463	487	e004	57164.73
	172.542259	31.662989	548	578	e005	57359.00
	172.542084	31.662379	662	703	e006	57525.11
	172.541828	31.662560	626	660	e007	57724.50
	172.541967	31.662391	585	624	e008	57886.59
	172.541482	31.662177	955	1010	e009	58089.13
CWISEP J120444.33−235926.8	181.185037	−23.990345	379	392	pre	55473.19
	181.184678	−23.990982	221	229	post	57312.65
CWISEP J121358.13+294237.0	183.493066	29.709923	764	802	pre	55441.59
	183.492502	29.710262	658	701	post0_1yr	56740.83
	183.492410	29.710162	677	717	post1_1yr	57077.88
	183.491758	29.710256	739	789	post2_1yr	57442.76
	183.491793	29.710207	917	999	post3_1yr	57820.17
CWISEP J122010.03+281431.3	185.042108	28.242307	493	514	pre	55432.30
	185.041655	28.241934	359	382	post	57264.58
CWISEP J124138.41−820051.9	190.407581	−82.014334	218	214	pre	55342.20
	190.409475	−82.014311	215	223	post0_1yr	56838.79
	190.410271	−82.014363	279	284	post1_1yr	57162.32
	190.410421	−82.014397	219	223	post2_1yr	57499.62
	190.411138	−82.014405	259	263	post3_1yr	57896.14
CWISEP J130255.54+191145.9	195.731241	19.196326	424	440	pre	55470.65
	195.731563	19.195908	320	337	post	57310.64
CWISEP J131252.97+341746.5	198.220254	34.296583	756	792	pre	55438.87
	198.220723	34.296156	467	501	post	57302.26
CWISEP J131208.16−105231.8	198.033812	−10.875022	867	905	pre	55405.06
	198.034034	−10.875817	474	506	post	57306.14
CWISEP J131221.97−310845.7	198.091976	−31.145828	494	515	pre	55385.88
	198.091445	−31.146035	708	772	post0_1yr	56765.98
	198.091140	−31.146243	756	809	post1_1yr	57136.72
	198.091119	−31.146337	683	735	post2_1yr	57512.11

Table 3 continued

Table 3 *(continued)*

Name	RA (deg, ICRS)	Dec (deg, ICRS)	σ_{RA} (mas)	σ_{Dec} (mas)	time slice[a]	mean MJD
	198.091248	−31.146460	658	706	post3_1yr	57847.18
CWISEP J131350.91−440352.2	198.462876	−44.064349	486	510	pre	55408.12
	198.461915	−44.064539	310	333	post	57322.26
CWISEP J134143.75+574112.9	205.433107	57.686675	345	356	pre	55427.13
	205.432510	57.686734	191	208	post	57431.42
CWISEP J135336.29−003756.6	208.401890	−0.631791	395	414	pre	55382.92
	208.401411	−0.632207	597	646	post0_1yr	56765.07
	208.400891	−0.632377	499	530	post1_1yr	57146.12
	208.400932	−0.632630	528	573	post2_1yr	57486.32
	208.400645	−0.632560	544	591	post3_1yr	57863.70
CWISEP J135937.65−435226.9	209.907588	−43.873931	949	992	pre	55329.40
	209.906713	−43.874183	513	549	post0_2yr	56940.23
	209.906549	−43.874454	591	629	post1_2yr	57656.65
CWISEP J140118.30+432554.2	210.326650	43.432323	301	312	pre	55476.55
	210.326101	43.431764	425	444	post0_1yr	56755.85
	210.326173	43.431612	419	449	post1_1yr	57115.13
	210.326163	43.431310	403	433	post2_1yr	57486.52
	210.326077	43.431186	462	492	post3_1yr	57836.98
CWISEP J140247.83+102132.6	210.699445	10.359001	152	160	pre	55384.92
	210.699315	10.359152	206	220	post0_1yr	56774.75
	210.699287	10.359113	224	229	post1_1yr	57128.24
	210.699161	10.359192	224	242	post2_1yr	57496.44
	210.699039	10.359171	218	230	post3_1yr	57858.52
CWISEP J141206.85+234412.4	213.029336	23.736429	557	582	pre	55387.60
	213.028016	23.736954	518	552	post	57296.18
CWISEP J141400.68+163153.9	213.502850	16.532132	515	539	pre	55411.15
	213.502888	16.531520	342	367	post	57314.11
CWISEP J142552.36+485151.3	216.468630	48.864368	690	706	pre	55482.54
	216.468002	48.864138	441	466	post	57336.26
CWISEP J143439.23−134421.4	218.663948	−13.739342	715	751	pre	55402.91
	218.663067	−13.739698	648	691	post	57324.21
CWISEP J144606.62−231717.8	221.528336	−23.286992	1000	1000	e000	55231.08
	221.528042	−23.287152	1500	1500	e001	55411.75
	221.527829	−23.287526	1500	1500	e002	56695.72
	221.527829	−23.288360	1000	1000	e003	56876.60
	221.527581	−23.288168	1000	1000	e004	57057.61
	221.527627	−23.288620	1500	1500	e005	57235.43
	221.527138	−23.288836	1500	1500	e006	57424.74
	221.527262	−23.288774	700	700	e007	57594.24
	221.527015	−23.288769	1000	1000	e009	57954.72

Table 3 continued

Table 3 *(continued)*

Name	RA (deg, ICRS)	Dec (deg, ICRS)	σ_{RA} (mas)	σ_{Dec} (mas)	time slice[a]	mean MJD
	221.527057	−23.289164	1000	1000	e010	58153.00
	221.526568	−23.290075	1000	1000	e011	58315.04
CWISEP J145837.91+173450.1	224.658603	17.580152	231	241	pre	55438.81
	224.657754	17.580560	207	229	post	57308.46
CWISEP J150252.82−304232.8	225.720657	−30.709000	306	323	pre	55339.73
	225.719974	−30.709124	192	206	post	57325.26
CWISEP J151140.51−835918.0	227.920439	−83.988064	704	732	pre	55355.13
	227.918951	−83.988214	598	638	post0_2yr	57018.65
	227.917312	−83.988592	723	777	post2_1yr	57547.40
	227.918490	−83.988677	937	1001	post3_1yr	57916.71
CWISEP J151521.22−215736.9	228.838344	−21.959707	326	347	pre	55335.25
	228.838510	−21.960111	375	393	post0_1yr	56816.63
	228.838518	−21.960350	343	365	post1_1yr	57155.42
	228.838750	−21.960402	388	409	post2_1yr	57502.08
	228.839026	−21.960526	430	470	post3_1yr	57889.21
WISEA J153429.75−104303.3	233.624165	−10.717538	700	744	pre	55346.35
	233.623043	−10.720147	947	1012	post0_1yr	56789.25
	233.622179	−10.721101	812	866	post1_1yr	57148.58
	233.621744	−10.721553	921	981	post2_1yr	57514.23
	233.621468	−10.722147	827	880	post3_1yr	57879.12
CWISEP J153859.39+482659.1	234.747532	48.450061	283	294	pre	55399.76
	234.747659	48.449402	236	248	post	57377.87
CWISEP J154151.59+523025.0	235.464346	52.506997	272	280	pre	55387.15
	235.464465	52.506775	382	404	post0_1yr	56772.48
	235.464879	52.506747	427	450	post1_1yr	57129.91
	235.464943	52.506777	333	353	post2_1yr	57470.39
	235.465326	52.506664	360	380	post3_1yr	57852.44
CWISEP J160311.60−104620.4	240.797787	−10.771826	492	522	pre	55332.54
	240.798712	−10.772776	392	417	post	57309.11
CWISEP J160835.01−244244.7	242.145521	−24.712350	377	397	pre	55353.11
	242.145921	−24.712425	421	447	post0_1yr	56814.80
	242.145983	−24.712494	358	384	post1_1yr	57160.85
	242.146048	−24.712298	517	544	post2_1yr	57485.14
	242.146142	−24.712514	477	504	post3_1yr	57902.31
CWISEP J161822.86−062310.2	244.594341	−6.385921	484	512	pre	55348.49
	244.595083	−6.385960	643	686	post0_1yr	56805.98
	244.595314	−6.386234	698	746	post2_1yr	57536.86
	244.595265	−6.386424	595	632	post3_1yr	57895.11
CWISEP J162225.92+370118.8	245.608266	37.022460	444	473	pre	55341.71
	245.607847	37.021996	677	742	post0_1yr	56791.13

Table 3 continued

Table 3 *(continued)*

Name	RA (deg, ICRS)	Dec (deg, ICRS)	σ_{RA} (mas)	σ_{Dec} (mas)	time slice[a]	mean MJD
	245.608103	37.021658	557	595	post1_1yr	57124.51
	245.607792	37.021597	633	685	post2_1yr	57519.97
	245.607388	37.021484	714	765	post3_1yr	57887.24
CWISEP J163200.11+002108.6	248.000646	0.351682	862	908	pre	55333.16
	248.000607	0.352686	629	669	post	57332.42
CWISEP J165215.62+022918.5	253.064696	2.488210	770	818	pre	55356.59
	253.065357	2.488542	593	633	post	57331.79
CWISEP J165359.67+214457.2	253.498709	21.749532	760	793	pre	55353.33
	253.498593	21.749031	429	456	post	57333.13
CWISEP J170918.83+000950.5	257.328642	0.163970	599	628	pre	55342.53
	257.328353	0.164071	368	390	post	57331.94
CWISEP J172104.42+595047.7	260.268458	59.846530	329	340	pre	55349.55
	260.268301	59.846592	190	202	post	57316.10
CWISEP J175746.31+195112.6	269.442696	19.853669	723	767	pre	55366.54
	269.442813	19.853330	401	423	post	57363.13
CWISEP J182358.73−740246.0	275.993117	−74.045640	632	662	pre	55368.60
	275.995594	−74.046179	260	271	post	57351.26
CWISEP J185658.80+601351.4	284.245277	60.231509	272	269	pre	55414.42
	284.244989	60.230588	400	387	post0_1yr	56878.31
	284.244877	60.230468	299	288	post1_1yr	57223.72
	284.245015	60.230138	359	348	post2_1yr	57603.26
	284.244499	60.229938	360	347	post3_1yr	57973.60
CWISEP J193518.58−154620.3	293.826965	−15.772455	568	598	pre	55411.65
	293.827651	−15.772364	393	411	post	57461.94
WISENF J193656.08+040801.2	294.233532	4.134037	313	329	e000	55304.16
CWISEP J194027.48−345650.6	295.114961	−34.947115	1062	1124	pre	55388.49
	295.114101	−34.947386	601	622	post	57470.19
CWISEP J194101.59+542335.9	295.256640	54.393471	208	210	pre	55437.46
	295.256821	54.393300	241	234	post0_1yr	56846.21
	295.256635	54.393158	292	286	post1_1yr	57248.32
	295.256711	54.393083	357	350	post2_1yr	57601.78
	295.256584	54.393009	323	318	post3_1yr	57948.00
CWISEP J194812.42−322334.9	297.052340	−32.392914	636	672	pre	55397.36
	297.051399	−32.393014	409	421	post	57478.16
CWISEP J201146.45−481259.7	302.943546	−48.216132	321	338	pre	55394.56
	302.943752	−48.216594	377	390	post0_2yr	57125.71
	302.943740	−48.216817	263	272	post1_2yr	57779.62
CWISEP J201510.68−675005.6	303.794427	−67.834663	181	190	pre	55441.91
	303.794219	−67.834893	121	123	post	57462.03
CWISEP J203821.53−064930.9	309.589930	−6.824939	681	709	pre	55400.55

Table 3 continued

Table 3 *(continued)*

Name	RA (deg, ICRS)	Dec (deg, ICRS)	σ_{RA} (mas)	σ_{Dec} (mas)	time slice[a]	mean MJD
	309.589601	−6.825352	393	404	post	57400.90
CWISEP J205019.99−253652.8	312.583476	−25.614283	308	326	pre	55399.10
	312.583483	−25.614574	548	541	post0_1yr	56869.63
	312.583263	−25.614627	365	375	post1_1yr	57224.39
	312.583198	−25.614905	467	481	post2_1yr	57578.60
	312.583184	−25.614953	393	410	post3_1yr	57951.57
CWISEP J205908.95+024105.6	314.787091	2.685237	475	488	pre	55419.53
	314.788049	2.684752	295	298	post	57422.98
CWISEP J210007.87−293139.8	315.032452	−29.527616	684	711	pre	55390.76
	315.033169	−29.527730	457	466	post	57415.09
CWISEP J211909.29−192117.4	319.788495	−19.354651	818	844	pre	55416.02
	319.789042	−19.354907	465	475	post	57416.36
CWISEP J212828.05+352912.4	322.117827	35.486833	802	811	pre	55403.68
	322.116742	35.486813	437	433	post	57403.82
CWISEP J213249.05+690113.7	323.203777	69.020385	203	192	pre	55403.78
	323.204682	69.020683	152	137	post	57342.71
CWISEP J213838.74−313808.5	324.660726	−31.635364	321	335	pre	55411.57
	324.661407	−31.635660	503	495	post0_1yr	56865.12
	324.661639	−31.635800	510	508	post1_1yr	57241.27
	324.661744	−31.635867	460	469	post2_1yr	57604.13
	324.661871	−31.635990	423	420	post3_1yr	57957.95
CWISEP J213930.45+042721.6	324.876533	4.456396	664	684	pre	55416.63
	324.876986	4.455841	396	399	post	57422.19
CWISEP J215841.50+732842.7	329.672070	73.478614	164	159	pre	55412.23
	329.672996	73.478464	210	249	post0_1yr	56805.33
	329.673079	73.478576	204	255	post1_1yr	57168.04
	329.673184	73.478353	251	299	post2_1yr	57534.81
	329.673297	73.478452	260	305	post3_1yr	57884.26
CWISEP J220452.02+063343.4	331.216749	6.562685	889	913	pre	55433.32
	331.216747	6.561917	405	410	post	57447.17
CWISEP J221736.94−222647.6	334.403292	−22.446685	1078	1110	pre	55368.64
	334.404060	−22.446670	378	382	post	57414.12
CWISEP J222035.35−810322.6	335.144937	−81.055971	449	440	pre	55378.17
	335.147909	−81.056428	344	328	post	57468.64
CWISEP J223022.60+254907.5	337.594622	25.819101	636	652	pre	55450.21
	337.594031	25.818705	664	661	post0_2yr	57089.81
	337.593434	25.818729	713	713	post1_2yr	57840.47
CWISEP J223138.55−383057.2	337.910262	−38.515555	668	690	pre	55402.23
	337.910850	−38.515984	532	535	post	57408.75
CWISEP J224747.42−004103.6	341.947529	−0.685544	791	808	pre	55463.70

Table 3 continued

Table 3 *(continued)*

Name	RA (deg, ICRS)	Dec (deg, ICRS)	σ_{RA} (mas)	σ_{Dec} (mas)	time slice[a]	mean MJD
	341.947532	−0.684130	373	377	post	57433.76
CWISEP J224916.17+371551.4	342.317666	37.264659	827	837	pre	55453.13
	342.317312	37.263998	531	530	post	57365.43
CWISEP J225059.28−432057.2	342.746780	−43.348677	672	686	pre	55436.33
	342.747277	−43.349520	702	702	post	57355.28
CWISEP J225156.13+392408.4	342.984347	39.402551	448	452	pre	55442.17
	342.983673	39.402297	273	270	post	57347.84
CWISEP J225109.50−074037.7	342.788813	−7.677372	415	422	pre	55430.07
	342.789563	−7.677251	503	502	post0_1yr	56889.04
	342.789917	−7.676962	416	424	post1_1yr	57262.77
	342.790311	−7.676821	450	454	post2_1yr	57642.56
	342.790268	−7.676910	450	453	post3_1yr	57993.93
CWISEP J225511.56−191516.3	343.798027	−19.255979	2005	2048	pre	55415.68
	343.798437	−19.254044	916	929	post	57421.32
CWISEP J225628.97+400227.3	344.119979	40.041065	426	427	pre	55431.64
	344.120817	40.041053	616	602	post0_1yr	56751.66
	344.121262	40.041246	556	547	post1_1yr	57113.87
	344.121314	40.041016	634	627	post2_1yr	57461.25
	344.121608	40.040878	688	675	post3_1yr	57841.78
CWISEP J230158.30−645858.3	345.492877	−64.982623	454	454	e000	55317.99
	345.493031	−64.982648	380	379	e001	55499.64
	345.493205	−64.982776	480	457	e002	56782.42
	345.492711	−64.983019	422	415	e003	56963.24
	345.492532	−64.982969	459	444	e004	57144.69
	345.493035	−64.982862	517	499	e005	57323.52
	345.493108	−64.983012	437	415	e006	57510.24
	345.493213	−64.983034	485	482	e007	57682.52
	345.492994	−64.983492	532	505	e008	57875.46
	345.493167	−64.983291	598	594	e009	58043.03
CWISEP J231047.80+362004.6	347.699458	36.334806	921	941	pre	55456.96
	347.698852	36.334633	468	463	post	57361.89
CWISEP J231114.50+135148.5	347.810799	13.863602	628	638	pre	55443.90
	347.810217	13.863404	374	376	post	57421.80
CWISEP J233216.39−290025.0	353.068163	−29.006548	609	621	pre	55442.42
	353.068217	−29.006870	442	441	post	57435.58
CWISEP J235130.42−185800.2	357.876427	−18.966698	429	443	pre	55438.94
	357.877204	−18.966820	274	273	post	57402.52
CWISEP J235547.99+380438.9	358.949214	38.077449	645	663	pre	55470.37
	358.950054	38.077396	777	754	post0_1yr	56765.38
	358.950182	38.077605	638	640	post1_1yr	57153.43

Table 3 continued

Table 3 *(continued)*

Name	RA (deg, ICRS)	Dec (deg, ICRS)	σ_{RA} (mas)	σ_{Dec} (mas)	time slice[a]	mean MJD
	358.950971	38.077377	589	582	post2_1yr	57487.62
	358.950851	38.077672	573	573	post3_1yr	57835.22
CWISEP J235644.78−481456.3	359.184683	−48.248902	1032	1018	pre	55443.22
	359.186632	−48.249149	497	481	post0_2yr	57143.13
	359.187403	−48.249088	543	538	post1_2yr	57803.90

[a]See §8.3 and Table 5 for discussion and definitions of the WISE time slices used for W2 astrometry.

Table 4. Recalibrated *Spitzer* ch2 Positions

Name	AOR	RA (deg, ICRS)	Dec (deg, ICRS)	σ_{RA} (mas)	σ_{Dec} (mas)	MJD	method number[a]	N_{calib}
CWISEP J000006.01−704851.2	68730112	0.02385537	−70.81443752	42	36	58711.09	2	13
CWISEP J000110.81−093215.5	68727808	0.29543643	−9.53797990	25	27	58559.84	3	8
CWISEP J001146.07−471306.8	68486656	2.94245662	−47.21861888	47	59	58531.38	3	9
CWISEP J003507.77−153233.8	68235776	8.78254804	−15.54325614	25	32	58427.81	3	6
CWISEP J003915.43+360939.0	68506112	9.81402661	36.16052959	26	23	58583.45	1	12
CWISEP J004158.35+381811.9	68486144	10.49371897	38.30336814	35	42	58468.55	1	10
CWISEP J005802.63+723330.3	68731904	14.51001015	72.55856213	65	54	58594.58	1	35
CWISEP J010247.48−654226.4	68509952	15.69697472	−65.70750484	62	40	58473.60	6	12
CWISEP J010527.69−783419.3	68237568	16.36883289	−78.57247246	52	24	58433.05	1	14
CWISEP J010650.61+225159.1	68234752	16.71061275	22.86605883	21	35	58422.33	3	9
CWISEP J012735.44−564110.5	68495360	21.89769161	−56.68621504	27	57	58499.03	3	7
CWISEP J012748.35−631056.1	68732672	21.95195768	−63.18183282	49	43	58551.68	3	16
CWISEP J014607.55−375705.6	68497408	26.53242038	−37.95091598	21	20	58552.20	3	7
CWISEP J015613.24+325526.6	68164096	29.05688486	32.92350544	46	46	58440.24	2	16
CWISEP J020103.10+293801.8	68504320	30.26370010	29.63336271	33	30	58470.04	3	11
CWISEP J020938.72+180427.7	68500992	32.41199524	18.07415696	32	45	58471.93	3	8
CWISEP J021243.55+053147.2	68556032	33.18130221	5.52993419	29	30	58599.83	3	6
CWISEP J021921.66−265451.8	68730368	34.84078553	−26.91396331	75	74	58574.21	3	5
CWISEP J022122.41−564125.0	68494848	35.34405691	−56.69029231	23	21	58472.54	2	10
CWISEP J022513.27+154854.8	68725760	36.30567186	15.81531619	145	83	58602.87	9	11
CWISEP J022631.82−203439.4	68164352	36.63215752	−20.57838279	71	73	58431.15	6	10
CWISEP J022935.43+724616.4 N	26741760	37.39850608	72.77155816	93	83	54906.77	1	40
CWISEP J022935.43+724616.4 S	26741760	37.39665397	72.77113514	86	75	54906.77	1	40
CWISEP J023842.60−133210.7	68728576	39.67740350	−13.53752892	62	54	58603.20	3	7
CWISEP J024204.91−225604.6	68557056	40.52249074	−22.93446201	29	31	58593.64	3	6

Table 4 continued

Table 4 *(continued)*

Name	AOR	RA	Dec	σ_{RA}	σ_{Dec}	MJD	method	N_{calib}
		(deg, ICRS)	(deg, ICRS)	(mas)	(mas)		number[a]	
CWISEP J024710.25−145809.9	68731392	41.79265236	−14.96945429	67	42	58593.43	9	7
CWISEP J024810.75−694127.9	68726784	42.04500470	−69.69113100	50	33	58552.21	1	12
CWISEP J025747.92−205602.7	68497152	44.44969657	−20.93370573	22	34	58470.58	3	8
CWISEP J031130.28+035931.8	68507648	47.87685640	3.99246667	61	64	58467.98	2	10
CWISEP J031557.05+203552.4	68727296	48.98782628	20.59796257	42	38	58617.90	1	11
CWISEP J031908.60+081120.4	68498432	49.78556821	8.18886652	75	74	58467.53	3	5
CWISEP J031935.50−041231.7	68577280	49.89853078	−4.20885654	37	40	58609.04	3	9
CWISEP J032109.59+693204.5	68498688	50.29368774	69.53427617	37	39	58469.54	1	46
CWISEP J034336.27+184025.8	68733952	55.90073168	18.67369501	48	48	58624.93	3	13
CWISEP J034514.82+173528.1	68728064	56.31200628	17.59095052	28	28	58624.94	3	11
CWISEP J034755.11+123051.9	68164608	56.97973852	12.51497456	31	25	58468.24	2	11
CWISEP J034904.05−462827.9	68487424	57.26737072	−46.47365188	32	35	58473.58	3	10
CWISEP J040106.67+085748.5	68500736	60.27822056	8.96294780	28	37	58468.53	3	14
CWISEP J040235.55−265145.4	68727552	60.64958777	−26.86361399	63	54	58603.19	3	10
CWISEP J040324.67+185729.6	68505856	60.85263479	18.95816852	56	40	58471.91	2	11
CWISEP J040351.00−491605.6	68487680	60.96303694	−49.26790141	38	41	58471.68	3	10
CWISEP J041025.10+033807.2	68729856	62.60462293	3.63527815	33	30	58635.20	2	11
CWISEP J042455.68+000221.4	68728832	66.23229318	0.03921896	43	30	58633.86	2	12
CWISEP J042404.54+665011.2	68486912	66.02027373	66.83636451	34	48	58479.14	1	27
CWISEP J043034.27+255653.7	68556544	67.64342191	25.94810246	31	32	58635.21	1	18
CWISEP J043309.31+100902.9	68236544	68.28907254	10.15026354	27	37	58471.05	2	15
CWISEP J044330.73+693828.3	68728320	70.87836222	69.64102641	50	46	58648.83	1	22
CWISEP J044719.61+202158.1	68726016	71.83173489	20.36516650	32	28	58640.93	1	16
CWISEP J050521.29−591311.7	68493056	76.34040148	−59.22162499	33	33	58493.60	2	17
CWISEP J052346.34−545314.7	68499712	80.94401093	−54.88680636	42	37	58490.76	3	10
CWISEP J053644.82−305539.3	68508416	84.18683452	−30.92759191	32	23	58481.51	1	10
CWISEP J054233.06+793459.1	68732928	85.63799445	79.58314781	36	29	58559.34	1	12
CWISEP J055816.68−450233.6	68492800	89.56940192	−45.04252697	87	44	58481.69	2	17
CWISEPR J062436.84−071147.2	68491264	96.15341104	−7.19629315	40	26	58516.85	1	41
CWISEP J062742.27−215908.1	68504832	96.92623170	−21.98606594	30	31	58518.01	1	18
CWISEP J063257.49+274629.4	68499200	98.23934757	27.77502111	40	39	58503.44	1	33
CWISEP J063428.10+504925.9	68495104	98.61732182	50.82257394	38	33	58507.81	1	17
CWISEP J063845.48−615937.2	68488704	99.68882416	−61.99337025	71	46	58490.24	1	20
CWISEPR J065144.62−115106.1	68493824	102.93589409	−11.85194477	27	26	58535.78	1	38
CWISEP J070055.19+783834.0	68486400	105.23691074	78.64175314	46	46	58494.47	1	10
CWISEP J070214.84−544041.7	68496128	105.56188808	−54.67901657	45	47	58516.88	1	20
CWISEP J071626.02−371951.1	68555776	109.10839230	−37.33077950	39	33	58535.13	1	32
CWISEP J071813.30−061421.1	68508160	109.55593921	−6.23914659	69	68	58516.86	1	57
CWISEP J082400.43+075019.9	68509184	126.00164205	7.83894211	75	72	58535.12	2	17
CWISEP J084726.55+233558.1	68488960	131.86076818	23.59920333	37	36	58539.98	3	7

Table 4 continued

Table 4 *(continued)*

Name	AOR	RA	Dec	σ_{RA}	σ_{Dec}	MJD	method	N_{calib}
		(deg, ICRS)	(deg, ICRS)	(mas)	(mas)		number[a]	
CWISEP J085348.15+112921.5	68507904	133.45069449	11.48919129	33	47	58539.96	2	11
CWISEP J085820.46+500834.4	68501504	134.58499868	50.14282167	54	33	58524.29	2	12
CWISEP J085908.26+152527.1	68238080	134.78440239	15.42385142	29	47	58539.97	3	10
CWISEP J085938.95+534908.7	68556288	134.91174975	53.81867728	34	44	58540.02	3	9
CWISEP J090547.50+700239.8	68730880	136.44865859	70.04452095	26	21	58559.33	3	7
CWISEP J090536.35+740009.1	68489472	136.40333548	74.00079349	31	48	58509.74	3	9
CWISEP J091558.51+254713.2	68508672	138.99385676	25.78653366	39	44	58543.08	3	10
CWISEP J093111.03+232502.1	68492544	142.79561049	23.41658011	32	33	58544.06	3	5
CWISEP J093236.66−180029.3	68489216	143.15217919	−18.00838695	34	31	58567.17	1	20
CWISEP J093852.89+063440.6	68494336	144.72114196	6.57700050	46	50	58555.38	4	10
CWISEP J094005.50+523359.2	68503296	145.02227353	52.56601748	46	24	58542.98	3	11
CWISEP J094615.56+351434.3	68493312	146.56454664	35.24200351	58	51	58542.05	2	11
CWISEP J094742.83+384619.3	68498176	146.92830968	38.77175299	91	49	58542.04	6	11
CWISEP J094930.41+663937.2	68729600	147.37660966	66.66003119	54	45	58553.28	3	10
CWISEP J094957.15−422017.1	68733184	147.48854442	−42.33802594	109	108	58574.40	1	70
CWISEP J095930.71−401046.8	68577536	149.87817796	−40.18036991	112	111	58577.93	1	45
CWISEP J100629.01+105408.5	68495616	151.62049970	10.90239112	35	29	58577.18	2	10
CWISEP J100854.84+203136.6	68732160	152.22829729	20.52654386	37	58	58558.69	6	5
CWISEP J101841.86+513108.8	68727040	154.67452734	51.51934616	40	44	58553.29	3	9
CWISEP J102201.27+145520.2	68503552	155.50450138	14.92207108	33	41	58559.99	3	6
CWISEP J103453.14+161228.0	68499456	158.72109612	16.20759141	34	65	58559.98	3	5
CWISEP J103607.94−304253.1	68510208	159.03281467	−30.71484791	54	54	58587.81	1	17
CWISEP J104104.20+221613.6	68509696	160.26712707	22.26973552	47	41	58594.51	3	6
CWISEP J104446.56+001754.9	68502528	161.19281382	0.29845508	32	33	58581.39	3	9
CWISEP J104756.81+545741.6	68500480	161.98547964	54.96133792	37	38	58542.02	3	9
CWISEP J110021.08+094652.9	68493568	165.08682533	9.78115233	40	39	58572.32	9	8
CWISEP J111055.12−174738.2	68238592	167.72963950	−17.79455020	70	40	58602.18	3	13
CWISEP J113010.21+313947.3	68487936	172.54105818	31.66144612	42	64	58600.82	9	5
CWISEP J120444.33−235926.8	68236800	181.18437510	−23.99145802	31	31	58602.17	1	14
CWISEP J121358.13+294237.0	68505344	183.49219972	29.71013447	40	39	58574.96	3	9
CWISEP J122010.03+281431.3	68494080	185.04120626	28.24171721	32	31	58598.77	3	7
CWISEP J124138.41−820051.9	68238848	190.41152361	−82.01423050	57	50	58425.32	1	33
CWISEP J130255.54+191145.9	68489984	195.73155415	19.19573617	53	83	58602.15	3	7
CWISEP J131252.97+341746.5	68510464	198.22107861	34.29598342	55	49	58591.64	3	8
CWISEP J131208.16−105231.8	68492032	198.03385882	−10.87573942	41	52	58613.40	3	13
CWISEP J131221.97−310845.7	68494592	198.09075160	−31.14658275	31	30	58624.55	1	10
CWISEP J131350.91−440352.2	68490752	198.46126925	−44.06479216	38	32	58622.95	1	31
CWISEP J134143.75+574112.9	68504576	205.43234762	57.68666593	29	78	58573.15	3	6
CWISEP J135937.65−435226.9	68509440	209.90630307	−43.87448090	35	41	58633.49	1	37
CWISEP J140118.30+432554.2	68235008	210.32602811	43.43087557	43	30	58419.34	3	8

Table 4 continued

Table 4 *(continued)*

Name	AOR	RA	Dec	σ_{RA}	σ_{Dec}	MJD	method	N_{calib}
		(deg, ICRS)	(deg, ICRS)	(mas)	(mas)		number[a]	
CWISEP J140247.83+102132.6	68487168	210.69909427	10.35917083	49	42	58613.41	9	7
CWISEP J141206.85+234412.4	68491776	213.02755699	23.73700131	48	34	58613.43	3	8
CWISEP J141400.68+163153.9	68729088	213.50312991	16.53217610	61	69	58613.42	3	8
CWISEP J142552.36+485151.3	68726528	216.46796266	48.86471825	58	61	58588.79	3	9
CWISEP J143439.23−134421.4	68500224	218.66269634	−13.73975795	53	46	58633.47	2	13
CWISEP J144606.62−231717.8	68496896	221.52628287	−23.28947384	33	37	58633.48	2	18
CWISEP J145837.91+173450.1	68726272	224.65736126	17.58070375	32	27	58626.15	2	10
CWISEP J150252.82−304232.8	68237056	225.71946267	−30.70927564	25	33	58427.80	1	13
CWISEP J151140.51−835918.0	68507136	227.91888011	−83.98841937	42	40	58490.23	1	19
WISEA J153429.75−104303.3	68555520	233.62091671	−10.72358186	27	28	58644.32	1	20
CWISEP J153859.39+482659.1	68238336	234.74784024	48.44903282	45	54	58418.52	3	7
CWISEP J154151.59+523025.0 N	68497920	235.46579224	52.50681563	57	91	58598.11	3	9
CWISEP J154151.59+523025.0 S	68497920	235.46449495	52.50617877	61	93	58598.11	3	9
CWISEP J160311.60−104620.4	68492288	240.79914670	−10.77353243	30	26	58469.19	1	11
CWISEP J160835.01−244244.7	68239104	242.14628653	−24.71251400	33	25	58442.21	1	36
CWISEP J161822.86−062310.2	68499968	244.59521009	−6.38637035	26	31	58469.19	1	13
CWISEP J162225.92+370118.8	68496384	245.60729535	37.02130786	38	46	58469.15	2	10
CWISEP J163200.11+002108.6	68507392	248.00057619	0.35253114	46	46	58469.17	1	11
CWISEP J165215.62+022918.5	68506368	253.06567761	2.48859715	58	57	58469.16	1	21
CWISEP J165359.67+214457.2	68557312	253.49875382	21.74888542	40	33	58657.06	2	17
CWISEP J170918.83+000950.5	68729344	257.32831459	0.16432932	26	27	58669.54	1	26
CWISEP J172104.42+595047.7	3862272	260.26838196	59.84667974	61	40	52975.74	1	16
CWISEP J175746.31+195112.6	68502272	269.44282233	19.85352764	32	32	58471.97	1	31
CWISEP J182358.73−740246.0	68233216	275.99657525	−74.04641231	56	52	58448.99	1	23
CWISEP J185658.80+601351.4	68730624	284.24430005	60.22964024	30	36	58559.33	1	12
CWISEP J193518.58−154620.3	68488448	293.82778626	−15.77235013	29	25	58493.51	1	52
WISENF J193656.08+040801.2	68576768	294.23235507	4.13120728	31	20	58525.50	1	92
CWISEP J194027.48−345650.6	68504064	295.11449035	−34.94751455	48	47	58493.51	1	23
CWISEP J194101.59+542335.9	68498944	295.25670541	54.39298422	31	34	58471.96	1	34
CWISEP J194812.42−322334.9	68503808	297.05120413	−32.39295664	42	27	58494.13	1	21
CWISEP J201146.45−481259.7	68239360	302.94397653	−48.21692427	43	33	58503.06	1	14
CWISEP J201510.68−675005.6	68501248	303.79406769	−67.83508286	31	37	58472.53	2	12
CWISEP J203821.53−064930.9	68556800	309.58944064	−6.82578390	36	25	58510.33	1	17
CWISEP J205019.99−253652.8	68233984	312.58304287	−25.61494640	26	37	58508.48	2	13
CWISEP J205908.95+024105.6	68731136	314.78863725	2.68416011	30	30	58551.33	1	17
CWISEP J210007.87−293139.8	68503040	315.03349264	−29.52788224	37	38	58509.48	2	17
CWISEP J211909.29−192117.4	68490240	319.78904654	−19.35486447	31	26	58517.11	2	15
CWISEP J212828.05+352912.4	68236032	322.11672271	35.48637727	75	75	58432.61	1	51
CWISEP J213249.05+690113.7	68234496	323.20530812	69.02077519	55	44	58425.07	1	24
CWISEP J213838.74−313808.5	68234240	324.66221995	−31.63611554	22	35	58515.05	1	13

Table 4 continued

Table 4 *(continued)*

Name	AOR	RA (deg, ICRS)	Dec (deg, ICRS)	σ_{RA} (mas)	σ_{Dec} (mas)	MJD	method number[a]	N_{calib}
CWISEP J213930.45+042721.6	68497664	324.87702071	4.45537284	25	22	58531.97	1	16
CWISEP J215841.50+732842.7	68502016	329.67344392	73.47850960	114	29	58467.44	1	23
CWISEP J220452.02+063343.4	68731648	331.21632223	6.56188601	64	43	58551.77	6	16
CWISEP J221736.94−222647.6	68235520	334.40396987	−22.44652307	49	38	58529.15	2	12
CWISEP J222035.35−810322.6	68233728	335.14895865	−81.05653137	51	43	58435.14	1	10
CWISEP J223022.60+254907.5	68491008	337.59325011	25.81806309	47	38	58548.77	1	19
CWISEP J223138.55−383057.2	68506624	337.91150228	−38.51649715	35	27	58523.83	3	9
CWISEP J224747.42−004103.6	46949376	341.94749199	−0.68427358	58	65	56312.31	1	12
CWISEP J224916.17+371551.4	68505088	342.31707292	37.26374196	32	31	58554.12	1	19
CWISEP J225059.28−432057.2	68164864	342.74751734	−43.34975131	38	73	58523.86	3	11
CWISEP J225156.13+392408.4	68237824	342.98339318	39.40224969	24	29	58420.28	1	21
CWISEP J225109.50−074037.7	68233472	342.79053727	−7.67692220	40	36	58548.47	2	11
CWISEP J225511.56−191516.3	68508928	343.79803367	−19.25520324	131	131	58541.14	2	10
CWISEP J225628.97+400227.3	68489728	344.12214325	40.04078021	29	29	58562.32	1	24
CWISEP J230158.30−645858.3	68235264	345.49336781	−64.98352893	34	21	58490.77	3	10
CWISEP J231047.80+362004.6	68732416	347.69962913	36.33475502	37	33	58574.50	1	18
CWISEP J231114.50+135148.5	68733440	347.81001500	13.86352942	32	48	58559.36	3	9
CWISEP J233216.39−290025.0	68496640	353.06832785	−29.00730341	28	21	58540.94	3	10
CWISEP J235130.42−185800.2	68236288	357.87760747	−18.96682764	40	27	58425.09	6	9
CWISEP J235547.99+380438.9	68163840	358.95117559	38.07755247	38	41	58422.31	1	21
CWISEP J235644.78−481456.3	68165120	359.18817070	−48.24923064	29	29	58412.37	3	5

NOTE—N_{calib} is the number of *Gaia* DR2 calibrators used for *Spitzer* ch2 astrometric recalibration of each AOR, as discussed in §8.4.1.

[a]The astrometric calibrator selection 'method number' here refers to the method number listed in Table 6 and explained in §8.4.1.

Table 5. unWISE Meta-coadd Time Slices

Time Slice Name	approx. time period (calendar years)
pre	2010.0-2011.1
post	2014 & 2015 & 2016 & 2017
post0_1yr	2014
post1_1yr	2015
post2_1yr	2016
post3_1yr	2017
post0_2yr	2014 & 2015
post1_2yr	2016 & 2017

Table 6. Cuts Defining *Spitzer-Gaia* Astrometric Calibrator Samples

method number	min. ch2 SNR	min. BCD cov. frac.	*Gaia* PM required	$N_{calib,min}$	number of AORs
1	100	1.0	yes	10	67
2	50	1.0	yes	10	28
3	30	1.0	yes	5	57
4	100	1.0	no	10	1
5	50	1.0	no	10	0
6	30	1.0	no	5	6
7	100	0.5	yes	10	0
8	50	0.5	yes	10	0
9	30	0.5	yes	5	5

Table 7. WISE+*Spitzer* Linear Motion Fitting Results

Name	α_0	δ_0	σ_{α_0}	σ_{δ_0}	MJD_0	μ_α	μ_δ	μ_{tot}	χ^2_{motion}	χ^2	# dof	χ^2_ν
	(deg, ICRS)	(deg, ICRS)	(mas)	(mas)		mas/yr	mas/yr	mas/yr				
CWISEP J000006.01−704851.2	0.0238910	−70.8144313	42	36	58656.07	-277 ± 40	-153 ± 38	317 ± 40	63.3	0.08	2	0.04
CWISEP J000110.81−093215.5	0.2954347	−9.5379786	26	27	58552.36	345 ± 72	-194 ± 73	396 ± 72	30.2	3.34	2	1.67
CWISEP J001146.07−471306.8	2.9424406	−47.2186142	47	58	58486.49	325 ± 63	-117 ± 63	346 ± 63	30.2	0.29	2	0.15
CWISEP J003507.77−153233.8	8.7825466	−15.5432421	25	32	58394.44	20 ± 41	-553 ± 41	553 ± 41	181.8	14.45	8	1.81
CWISEP J003915.43+360939.0	9.8140272	36.1605309	27	23	58577.21	-127 ± 78	-227 ± 79	260 ± 79	10.9	1.75	2	0.87
CWISEP J004158.35+381811.9	10.4937097	38.3033679	35	42	58437.39	297 ± 51	-8 ± 52	297 ± 51	34.1	0.54	2	0.27
CWISEP J005802.63+723330.3	14.5100692	72.5585540	64	54	58534.48	-474 ± 61	196 ± 59	513 ± 60	72.1	6.72	2	3.36
CWISEP J010247.48−654226.4	15.6969790	−65.7075044	62	41	58453.38	-186 ± 85	-35 ± 82	189 ± 85	5.0	1.88	6	0.31
CWISEP J010527.69−783419.3	16.3685566	−78.5724495	48	23	58280.05	333 ± 21	-180 ± 18	378 ± 21	340.3	22.84	2	11.42
CWISEP J010650.61+225159.1	16.7106177	22.8660649	22	35	58385.82	-167 ± 34	-278 ± 35	324 ± 35	87.6	13.37	8	1.67
CWISEP J012735.44−564110.5	21.8976927	−56.6862172	27	57	58455.16	4 ± 40	8 ± 40	9 ± 40	0.1	3.59	2	1.80
CWISEP J012748.35−631056.1	21.9518596	−63.1818606	47	42	58445.67	660 ± 37	307 ± 35	728 ± 37	392.2	27.96	8	3.49
CWISEP J014607.55−375705.6	26.5324150	−37.9509194	21	21	58541.43	510 ± 53	384 ± 54	638 ± 53	143.4	1.29	2	0.65
CWISEP J015613.24+325526.6	29.0568626	32.9235107	46	46	58419.89	1138 ± 84	-373 ± 84	1197 ± 84	204.0	8.55	8	1.07
CWISEP J020103.10+293801.8	30.2636947	29.6333653	34	31	58456.75	508 ± 67	-235 ± 69	560 ± 67	69.4	1.65	2	0.82
CWISEP J020938.72+180427.7	32.4119873	18.0741597	32	45	58451.63	487 ± 61	-161 ± 63	513 ± 61	70.0	5.14	8	0.64
CWISEP J021243.55+053147.2	33.1813030	5.5299336	29	30	58588.49	-102 ± 63	56 ± 65	116 ± 63	3.4	4.05	6	0.67
CWISEP J021921.66−265451.8	34.8407666	−26.9139810	74	73	58517.37	353 ± 74	484 ± 76	599 ± 76	62.8	5.39	2	2.70
CWISEP J022122.41−564125.0	35.3440503	−56.6902923	24	21	58454.17	243 ± 43	33 ± 42	245 ± 43	32.3	3.58	2	1.79
CWISEP J022513.27+154854.8	36.3056408	15.8152988	132	81	58384.82	229 ± 54	85 ± 52	245 ± 54	20.7	4.24	8	0.53
CWISEP J022631.82−203439.4	36.6321750	−20.5783558	70	73	58362.17	-325 ± 65	-538 ± 65	628 ± 65	92.7	1.99	6	0.33
CWISEP J022935.43+724616.4 N	37.3982422	72.7714650	78	72	55436.54	-144 ± 28	-145 ± 27	204 ± 28	54.0	43.37	4	10.84
CWISEP J022935.43+724616.4 S	37.3968899	72.7711547	74	67	55368.95	139 ± 28	75 ± 27	158 ± 28	32.7	13.11	4	3.28
CWISEP J023842.60−133210.7	39.6774081	−13.5375104	61	54	58569.96	-158 ± 74	-742 ± 76	758 ± 76	100.6	3.11	6	0.52
CWISEP J024204.91−225604.6	40.5224841	−22.9344630	29	31	58586.09	1049 ± 77	169 ± 79	1062 ± 77	192.6	0.10	2	0.05
CWISEP J024710.25−145809.9	41.7926505	−14.9694556	67	43	58571.14	-62 ± 88	89 ± 90	108 ± 89	1.5	5.86	2	2.93
CWISEP J024810.75−694127.9	42.0450051	−69.6911310	50	34	58522.07	7 ± 59	-31 ± 55	32 ± 56	0.3	2.03	2	1.01
CWISEP J025747.92−205602.7	44.4496962	−20.9337098	23	35	58452.11	55 ± 49	229 ± 50	235 ± 50	21.9	4.74	2	2.37

Table 7 continued

Table 7 *(continued)*

Name	α_0	δ_0	σ_{α_0}	σ_{δ_0}	MJD_0	μ_α	μ_δ	μ_{tot}	χ^2_{motion}	χ^2	# dof	χ^2_ν
	(deg, ICRS)	(deg, ICRS)	(mas)	(mas)		mas/yr	mas/yr	mas/yr				
CWISEP J031130.28+035931.8	47.8768496	3.9924660	61	64	58450.57	595 ± 105	138 ± 111	611 ± 106	33.4	6.58	2	3.29
CWISEP J031557.05+203552.4	48.9878240	20.5979615	42	39	58577.83	62 ± 46	82 ± 48	102 ± 48	4.6	4.88	2	2.44
CWISEP J031908.60+081120.4	49.7855761	8.1888656	75	73	58434.99	-243 ± 102	205 ± 106	318 ± 104	9.4	11.45	2	5.73
CWISEP J031935.50−041231.7	49.8985275	−4.2088561	37	41	58600.25	519 ± 92	-99 ± 94	528 ± 92	33.2	0.95	2	0.48
CWISEP J032109.59+693204.5	50.2936284	69.5342819	37	40	58443.81	972 ± 61	-297 ± 63	1016 ± 61	275.2	11.62	8	1.45
CWISEP J034336.27+184025.8	55.9007363	18.6736946	48	49	58599.52	-61 ± 71	25 ± 74	66 ± 71	0.9	21.63	2	10.82
CWISEP J034514.82+173528.1	56.3120041	17.5909526	28	28	58606.63	152 ± 52	-148 ± 54	212 ± 53	16.1	0.00	2	0.00
CWISEP J034755.11+123051.9	56.9797369	12.5149653	31	26	58435.00	20 ± 37	380 ± 38	380 ± 38	98.3	5.27	8	0.66
CWISEP J034904.05−462827.9	57.2673653	−46.4736606	32	35	58452.20	236 ± 54	494 ± 54	548 ± 54	103.3	2.51	2	1.26
CWISEP J040106.67+085748.5	60.2782164	8.9629526	29	38	58452.79	357 ± 61	-359 ± 64	507 ± 62	65.9	2.71	8	0.34
CWISEP J040235.55−265145.4	60.6494799	−26.8635386	60	53	58440.51	755 ± 32	-571 ± 33	947 ± 33	832.5	16.93	6	2.82
CWISEP J040324.67+185729.6	60.8526375	18.9581692	56	41	58452.93	-98 ± 81	-95 ± 84	137 ± 83	2.7	3.57	2	1.79
CWISEP J040351.00−491605.6	60.9630254	−49.2679072	38	41	58426.72	256 ± 44	157 ± 45	300 ± 44	46.2	3.65	2	1.82
CWISEP J041025.10+033807.2	62.6046231	3.6352786	33	31	58627.10	-97 ± 83	-72 ± 87	121 ± 84	2.1	2.39	2	1.19
CWISEP J042455.68+000221.4	66.2322875	0.0392211	43	31	58589.11	153 ± 39	-70 ± 40	169 ± 39	18.8	2.01	8	0.25
CWISEP J042404.54+665011.2	66.0202303	66.8363662	34	48	58422.26	395 ± 39	7 ± 41	395 ± 39	104.2	2.19	2	1.10
CWISEP J043034.27+255653.7	67.6433968	25.9481134	31	32	58559.18	401 ± 27	-197 ± 29	447 ± 27	267.5	0.87	2	0.44
CWISEP J043309.31+100902.9	68.2890654	10.1502782	27	36	58424.36	174 ± 34	-384 ± 36	422 ± 35	141.9	6.99	8	0.87
CWISEP J044330.73+693828.3	70.8783551	69.6410275	50	46	58623.07	111 ± 76	-156 ± 79	191 ± 78	6.0	11.28	2	5.64
CWISEP J044719.61+202158.1	71.8317332	20.3651770	32	29	58618.86	41 ± 49	-620 ± 52	621 ± 52	144.6	5.47	8	0.68
CWISEP J050521.29−591311.7	76.3403687	−59.2215888	33	33	58448.04	461 ± 36	-1003 ± 35	1104 ± 36	964.6	7.88	2	3.94
CWISEP J052346.34−545314.7	80.9439898	−54.8868202	42	37	58455.92	419 ± 49	518 ± 51	667 ± 50	176.7	1.98	2	0.99
CWISEP J053644.82−305539.3	84.1868335	−30.9275925	32	24	58457.06	46 ± 45	5 ± 46	47 ± 45	1.1	1.93	2	0.97
CWISEP J054233.06+793459.1	85.6379950	79.5831471	36	29	58540.27	6 ± 58	75 ± 61	75 ± 61	1.5	1.18	2	0.59
CWISEP J055816.68−450233.6	89.5694062	−45.0425330	81	44	58352.04	-81 ± 39	69 ± 39	106 ± 39	7.4	2.02	8	0.25
CWISEP J060132.96−592227.3	90.3874560	−59.3743566	50	52	56767.53	-209 ± 20	414 ± 21	464 ± 21	497.4	8.30	6	1.38
CWISEPR J062436.84−071147.2	96.1534148	−7.1962981	39	27	58446.95	-90 ± 28	106 ± 29	139 ± 28	24.2	6.76	8	0.84
CWISEP J062742.27−215908.1	96.9262310	−21.9860615	30	32	58501.69	25 ± 58	-376 ± 62	377 ± 62	36.8	0.99	2	0.49
CWISEP J063257.49+274629.4	98.2393490	27.7750194	41	40	58480.14	14 ± 67	92 ± 71	93 ± 71	1.7	5.16	2	2.58
CWISEP J063428.10+504925.9	98.6173188	50.8225904	38	33	58487.08	190 ± 61	-1057 ± 64	1074 ± 64	280.6	6.35	8	0.79

Table 7 continued

Table 7 *(continued)*

Name	α_0 (deg, ICRS)	δ_0 (deg, ICRS)	σ_{α_0} (mas)	σ_{δ_0} (mas)	MJD$_0$	μ_α mas/yr	μ_δ mas/yr	μ_{tot} mas/yr	χ^2_{motion}	χ^2	# dof	χ^2_ν
CWISEP J063845.48−615937.2	99.6888430	−61.9933801	70	46	58446.38	-311 ± 67	286 ± 69	423 ± 68	38.8	0.71	2	0.35
CWISEPR J065144.62−115106.1	102.9358948	−11.8519416	27	27	58511.18	-74 ± 41	-196 ± 43	210 ± 43	23.8	4.86	8	0.61
CWISEP J070055.19+783834.0	105.2368732	78.6417616	46	46	58482.39	814 ± 96	-966 ± 103	1263 ± 100	160.8	0.81	2	0.41
CWISEP J070214.84−544041.7	105.5618914	−54.6790057	45	47	58491.25	-83 ± 67	-558 ± 71	564 ± 71	62.8	0.21	2	0.10
CWISEP J071626.02−371951.1	109.1083915	−37.3307807	39	34	58512.21	37 ± 54	78 ± 58	86 ± 57	2.3	0.20	2	0.10
CWISEP J071813.30−061421.1	109.5559281	−6.2391499	69	68	58485.30	466 ± 90	141 ± 96	487 ± 91	28.7	0.02	2	0.01
CWISEP J082400.43+075019.9	126.0016447	7.8389405	75	72	58512.95	-43 ± 123	105 ± 132	113 ± 131	0.8	3.66	4	0.92
CWISEP J084726.55+233558.1	131.8607674	23.5992073	37	36	58516.78	43 ± 66	-218 ± 71	222 ± 71	9.7	0.02	2	0.01
CWISEP J085348.15+112921.5	133.4506930	11.4891927	33	46	58500.74	42 ± 47	-131 ± 51	138 ± 51	7.4	4.84	2	2.42
CWISEP J085820.46+500834.4	134.5850031	50.1428221	54	33	58501.60	-141 ± 63	-27 ± 67	143 ± 63	5.1	0.12	2	0.06
CWISEP J085908.26+152527.1	134.7844045	15.4238600	29	47	58492.65	-81 ± 40	-263 ± 43	275 ± 43	41.6	2.52	2	1.26
CWISEP J085938.95+534908.7	134.9117592	53.8186842	35	44	58511.53	-230 ± 53	-298 ± 56	377 ± 55	46.7	5.67	8	0.71
CWISEP J090547.50+700239.8	136.4486544	70.0445205	27	21	58547.11	196 ± 50	-10 ± 53	197 ± 50	15.3	7.26	2	3.63
CWISEP J090536.35+740009.1	136.4033148	74.0008111	31	48	58494.02	465 ± 67	-1490 ± 71	1561 ± 70	493.5	0.44	2	0.22
CWISEP J091558.51+254713.2	138.9938542	25.7865366	39	44	58517.10	120 ± 56	-206 ± 59	238 ± 59	16.6	4.79	6	0.80
CWISEP J093111.03+232502.1	142.7956140	23.4165857	32	33	58528.96	-295 ± 69	-474 ± 73	558 ± 72	60.0	0.24	2	0.12
CWISEP J093236.66−180029.3	143.1521859	−18.0083844	35	31	58547.74	-431 ± 56	-182 ± 60	468 ± 57	67.3	0.17	2	0.08
CWISEP J093852.89+063440.6	144.7211265	6.5770243	46	50	58511.93	453 ± 54	-731 ± 57	860 ± 56	236.1	1.81	8	0.23
CWISEP J094005.50+523359.2	145.0222817	52.5660222	46	24	58522.22	-343 ± 50	-299 ± 53	455 ± 52	78.1	2.95	10	0.29
CWISEP J094615.56+351434.3	146.5645538	35.2420221	58	51	58502.54	-229 ± 61	-634 ± 65	674 ± 65	108.9	1.06	2	0.53
CWISEP J094742.83+384619.3	146.9283136	38.7717593	90	50	58501.73	-135 ± 72	-212 ± 75	251 ± 74	11.6	0.26	2	0.13
CWISEP J094930.41+663937.2	147.3766137	66.6600392	54	45	58515.07	-5 ± 59	-298 ± 62	298 ± 62	23.5	1.98	2	0.99
CWISEP J094957.15−422017.1	147.4885119	−42.3380471	105	104	58439.05	261 ± 71	229 ± 74	347 ± 73	22.9	1.16	2	0.58
CWISEP J095930.71−401046.8	149.8781840	−40.1803387	111	110	58512.73	-131 ± 101	-681 ± 106	693 ± 106	43.2	2.06	4	0.51
CWISEP J100629.01+105408.5	151.6205056	10.9023902	35	30	58547.59	-259 ± 47	12 ± 49	259 ± 47	30.8	4.05	8	0.51
CWISEP J100854.84+203136.6	152.2283025	20.5265504	37	58	58515.53	-136 ± 51	-208 ± 55	248 ± 54	21.1	0.37	2	0.18
CWISEP J101841.86+513108.8	154.6745261	51.5193433	41	44	58531.16	50 ± 68	265 ± 72	270 ± 72	14.1	6.07	2	3.03
CWISEP J102201.27+145520.2	155.5045106	14.9220742	33	41	58538.06	-537 ± 61	-189 ± 65	569 ± 61	86.8	1.16	8	0.14
CWISEP J103453.14+161228.0	158.7211188	16.2076055	34	62	58435.26	-235 ± 29	-143 ± 32	275 ± 30	87.2	0.25	2	0.12
CWISEP J103607.94−304253.1	159.0328176	−30.7148463	54	54	58562.14	-196 ± 78	-116 ± 82	228 ± 79	8.3	5.52	4	1.38

Table 7 continued

Table 7 *(continued)*

Name	α_0	δ_0	σ_{α_0}	σ_{δ_0}	MJD_0	μ_α	μ_δ	μ_{tot}	χ^2_{motion}	χ^2	# dof	χ^2_ν
	(deg, ICRS)	(deg, ICRS)	(mas)	(mas)		mas/yr	mas/yr	mas/yr				
CWISEP J104104.20+221613.6	160.2671291	22.2697391	47	42	58585.15	-325 ± 111	-467 ± 118	569 ± 115	24.4	1.53	2	0.76
CWISEP J104446.56+001754.9	161.1928198	0.2984562	33	34	58572.66	-852 ± 85	-160 ± 90	866 ± 85	103.1	3.08	4	0.77
CWISEP J104756.81+545741.6	161.9854882	54.9613395	38	38	58525.41	-462 ± 72	-132 ± 76	480 ± 73	43.8	8.08	8	1.01
CWISEP J110021.08+094652.9	165.0868452	9.7811543	40	39	58531.96	-626 ± 47	-40 ± 49	627 ± 47	179.4	1.16	2	0.58
CWISEP J111055.12−174738.2	167.7296340	−17.7944962	64	40	58410.16	24 ± 28	-395 ± 27	396 ± 27	212.6	9.24	2	4.62
CWISEP J113010.21+313947.3	172.5411784	31.6615769	42	62	58486.91	-1185 ± 35	-1476 ± 38	1893 ± 37	2684.6	11.72	18	0.65
CWISEP J120444.33−235926.8	181.1843852	−23.9914417	31	31	58557.19	-263 ± 37	-473 ± 38	542 ± 38	208.2	0.18	2	0.09
CWISEP J121358.13+294237.0	183.4922016	29.7101348	40	39	58551.73	-189 ± 64	9 ± 68	189 ± 64	8.6	14.08	8	1.76
CWISEP J122010.03+281431.3	185.0412133	28.2417212	32	32	58576.01	-345 ± 50	-237 ± 52	419 ± 50	69.4	0.34	2	0.17
CWISEP J124138.41−820051.9	190.4111402	−82.0142553	50	45	58106.00	230 ± 23	65 ± 23	239 ± 23	105.1	9.52	8	1.19
CWISEP J130255.54+191145.9	195.7315475	19.1957537	53	80	58491.72	95 ± 44	-232 ± 47	251 ± 47	29.0	2.10	2	1.05
CWISEP J131252.97+341746.5	198.2210708	34.2959882	55	49	58562.62	289 ± 74	-228 ± 78	368 ± 75	24.0	0.20	2	0.10
CWISEP J131208.16−105231.8	198.0338602	−10.8757384	41	52	58593.28	-49 ± 80	-166 ± 84	173 ± 83	4.3	5.83	2	2.92
CWISEP J131221.97−310845.7	198.0907598	−31.1465777	31	31	58602.89	-421 ± 48	-312 ± 51	524 ± 49	113.6	1.81	8	0.23
CWISEP J131350.91−440352.2	198.4612845	−44.0647872	38	32	58592.27	-471 ± 47	-202 ± 50	513 ± 48	116.5	0.45	2	0.23
CWISEP J134143.75+574112.9	205.4323635	57.6866713	30	74	58492.38	-149 ± 34	-22 ± 38	151 ± 34	19.6	1.75	2	0.87
CWISEP J135336.29−003756.6	208.4012529	−0.6322388	223	238	56701.39	-653 ± 84	-448 ± 90	792 ± 86	84.6	3.53	6	0.59
CWISEP J135937.65−435226.9	209.9063082	−43.8744784	36	42	58615.69	-296 ± 72	-205 ± 77	360 ± 74	23.9	1.48	4	0.37
CWISEP J140118.30+432554.2	210.3260378	43.4309089	42	30	58353.31	-172 ± 33	-659 ± 34	682 ± 34	400.7	3.83	8	0.48
CWISEP J140247.83+102132.6	210.6991320	10.3591566	44	39	58216.97	-140 ± 17	57 ± 17	151 ± 17	83.5	8.51	8	1.06
CWISEP J141206.85+234412.4	213.0275676	23.7369981	48	34	58590.72	-625 ± 58	204 ± 61	657 ± 58	126.7	3.67	2	1.84
CWISEP J141400.68+163153.9	213.5031181	16.5321538	60	68	58524.98	143 ± 51	181 ± 54	231 ± 53	19.2	29.84	2	14.92
CWISEP J142552.36+485151.3	216.4679680	48.8647060	58	60	58545.20	-141 ± 69	272 ± 72	306 ± 71	18.5	9.42	2	4.71
CWISEP J143439.23−134421.4	218.6627039	−13.7397557	53	46	58611.75	-473 ± 74	-152 ± 78	497 ± 75	44.4	0.72	2	0.36
CWISEP J144606.62−231717.8	221.5262966	−23.2894624	34	37	58616.31	-860 ± 69	-954 ± 69	1285 ± 69	342.6	21.41	20	1.07
CWISEP J145837.91+173450.1	224.6573867	17.5806926	32	27	58554.34	-469 ± 25	215 ± 26	516 ± 25	436.3	4.76	2	2.38
CWISEP J150252.82−304232.8	225.7194826	−30.7092702	25	33	58380.33	-458 ± 32	-132 ± 34	477 ± 32	222.3	2.05	2	1.02
CWISEP J151140.51−835918.0	227.9188793	−83.9884181	43	40	58469.21	-35 ± 69	-125 ± 73	130 ± 73	3.2	4.08	6	0.68
CWISEP J151521.22−215736.9	228.8385873	−21.9601747	165	175	56794.73	255 ± 66	-429 ± 70	499 ± 69	52.3	6.33	6	1.05
WISEA J153429.75−104303.3	233.6209262	−10.7235637	27	29	58634.28	-1254 ± 65	-2387 ± 69	2697 ± 68	1565.8	5.08	8	0.63

Table 7 continued

Table 7 *(continued)*

Name	α_0 (deg, ICRS)	δ_0 (deg, ICRS)	σ_{α_0} (mas)	σ_{δ_0} (mas)	MJD_0	μ_α mas/yr	μ_δ mas/yr	μ_{tot} mas/yr	χ^2_{motion}	χ^2	# dof	χ^2_ν
CWISEP J153859.39+482659.1	234.7478251	48.4490749	44	52	58296.88	98 ± 32	-450 ± 34	461 ± 34	184.2	0.52	2	0.26
CWISEP J154151.59+523025.0 N	235.4656234	52.5068123	55	80	58291.34	409 ± 28	-48 ± 31	412 ± 28	216.9	17.12	8	2.14
CWISEP J154151.59+523025.0 S	235.4645297	52.5062999	57	82	58266.45	-14 ± 28	-374 ± 31	374 ± 31	148.2	54.35	8	6.79
CWISEP J160311.60−104620.4	240.7991406	−10.7735237	30	26	58454.23	547 ± 52	-740 ± 55	920 ± 54	288.2	1.27	2	0.63
CWISEP J160835.01−244244.7	242.1462779	−24.7125120	33	26	58406.40	290 ± 37	-71 ± 39	299 ± 37	64.6	1.52	8	0.19
CWISEP J161822.86−062310.2	244.5952072	−6.3863681	26	31	58453.28	303 ± 51	-201 ± 54	364 ± 52	48.5	8.53	6	1.42
CWISEP J162225.92+370118.8	245.6073116	37.0213231	38	46	58425.10	-361 ± 46	-473 ± 49	595 ± 48	154.2	5.38	8	0.67
CWISEP J163200.11+002108.6	248.0005765	0.3525295	47	46	58454.71	-31 ± 90	252 ± 95	254 ± 95	7.1	4.97	2	2.49
CWISEP J165215.62+022918.5	253.0656696	2.4885946	58	57	58442.79	406 ± 82	145 ± 87	432 ± 83	27.2	0.24	2	0.12
CWISEP J165359.67+214457.2	253.4987525	21.7488879	40	33	58640.88	60 ± 69	-221 ± 72	229 ± 72	10.1	1.35	2	0.68
CWISEP J170918.83+000950.5	257.3283154	0.1643273	27	27	58656.23	-102 ± 55	175 ± 58	202 ± 57	12.5	1.37	2	0.68
CWISEP J172104.42+595047.7	260.2683795	59.8466722	58	40	53261.59	-10 ± 16	-32 ± 17	33 ± 17	4.0	1.43	2	0.72
CWISEP J175746.31+195112.6	269.4428220	19.8535267	33	32	58459.19	39 ± 72	27 ± 76	47 ± 73	0.4	3.20	2	1.60
CWISEP J182358.73−740246.0	275.9965126	−74.0463976	55	52	58383.86	371 ± 58	-309 ± 60	483 ± 59	67.3	0.69	2	0.34
CWISEP J185658.80+601351.4	284.2443326	60.2296897	30	35	58474.24	-228 ± 28	-776 ± 27	809 ± 27	872.4	5.98	8	0.75
CWISEP J193518.58−154620.3	293.8277840	−15.7723504	29	25	58482.28	305 ± 61	40 ± 64	308 ± 61	25.5	1.25	2	0.63
WISENF J193656.08+040801.2	294.2323616	4.1312231	31	20	58507.54	-479 ± 36	-1155 ± 37	1250 ± 37	1130.2	-	0	-
CWISEP J194027.48−345650.6	295.1144888	−34.9475130	48	47	58481.29	-19 ± 108	-168 ± 114	169 ± 114	2.2	5.31	2	2.66
CWISEP J194101.59+542335.9	295.2567040	54.3930038	30	33	58348.47	8 ± 22	-214 ± 22	215 ± 22	92.0	3.58	8	0.45
CWISEP J194812.42−322334.9	297.0512077	−32.3929568	42	27	58480.41	-368 ± 67	2 ± 70	368 ± 67	29.9	1.67	2	0.84
CWISEP J201146.45−481259.7	302.9439641	−48.2169094	42	33	58439.13	134 ± 35	-324 ± 36	350 ± 36	94.6	2.37	4	0.59
CWISEP J201510.68−675005.6	303.7940891	−67.8350564	30	35	58309.55	-62 ± 20	-194 ± 21	204 ± 21	91.7	1.73	2	0.86
CWISEP J203821.53−064930.9	309.5894424	−6.8257801	37	25	58498.59	-201 ± 68	-401 ± 71	448 ± 70	40.6	0.97	2	0.49
CWISEP J205019.99−253652.8	312.5830506	−25.6149376	26	36	58461.39	-182 ± 32	-276 ± 34	330 ± 34	96.5	4.49	8	0.56
CWISEP J205908.95+024105.6	314.7886251	2.6841705	30	30	58527.32	658 ± 48	-513 ± 49	834 ± 49	294.0	4.55	2	2.28
CWISEP J210007.87−293139.8	315.0334875	−29.5278805	37	38	58493.21	372 ± 71	-128 ± 74	394 ± 72	30.3	0.23	2	0.11
CWISEP J211909.29−192117.4	319.7890460	−19.3548643	31	26	58509.55	160 ± 82	-50 ± 84	168 ± 82	4.2	1.98	2	0.99
CWISEP J212828.05+352912.4	322.1167327	35.4863939	74	74	58377.15	-290 ± 83	-299 ± 84	416 ± 84	24.8	7.89	2	3.95
CWISEP J213249.05+690113.7	323.2051650	69.0207454	50	42	58158.47	244 ± 24	159 ± 22	291 ± 23	157.2	1.56	2	0.78
CWISEP J213838.74−313808.5	324.6622036	−31.6361072	22	35	58481.77	542 ± 34	-325 ± 35	632 ± 34	336.9	0.63	8	0.08

Table 7 continued

Table 7 *(continued)*

Name	α_0	δ_0	σ_{α_0}	σ_{δ_0}	MJD_0	μ_α	μ_δ	μ_{tot}	χ^2_{motion}	χ^2	# dof	χ^2_ν
	(deg, ICRS)	(deg, ICRS)	(mas)	(mas)		mas/yr	mas/yr	mas/yr				
CWISEP J213930.45+042721.6	324.8770200	4.4553757	25	22	58524.32	162 ± 67	-465 ± 69	493 ± 68	51.8	1.79	2	0.90
CWISEP J215841.50+732842.7	329.6733966	73.4785142	89	29	58200.99	162 ± 23	-32 ± 18	165 ± 23	52.0	10.01	8	1.25
CWISEP J220452.02+063343.4	331.2163311	6.5618894	63	44	58524.83	-299 ± 83	-223 ± 85	373 ± 84	19.8	6.60	2	3.30
CWISEP J221736.94−222647.6	334.4039704	−22.4465251	49	38	58510.64	82 ± 89	121 ± 90	146 ± 90	2.7	4.50	2	2.25
CWISEP J222035.35−810322.6	335.1488953	−81.0565232	51	43	58383.55	262 ± 50	-226 ± 49	346 ± 50	48.5	0.67	2	0.33
CWISEP J223022.60+254907.5	337.5932596	25.8180721	47	38	58527.52	-535 ± 68	-491 ± 69	726 ± 68	113.4	5.55	4	1.39
CWISEP J223138.55−383057.2	337.9114974	−38.5164936	35	28	58513.68	441 ± 72	-433 ± 74	618 ± 73	72.6	2.18	2	1.09
CWISEP J224747.42−004103.6	341.9474932	−0.6842782	57	64	56336.39	34 ± 116	378 ± 117	380 ± 117	10.5	23.44	2	11.72
CWISEP J224916.17+371551.4	342.3170746	37.2637442	32	31	58545.41	-203 ± 84	-361 ± 85	414 ± 84	24.0	0.31	2	0.16
CWISEP J225059.28−432057.2	342.7475126	−43.3497456	38	73	58503.31	225 ± 75	-434 ± 77	489 ± 76	40.9	0.73	2	0.36
CWISEP J225156.13+392408.4	342.9833992	39.4022511	25	29	58399.63	-310 ± 48	-113 ± 48	330 ± 48	48.0	0.79	2	0.40
CWISEP J225109.50−074037.7	342.7905094	−7.6769274	40	36	58493.01	696 ± 41	163 ± 41	715 ± 41	305.7	10.48	8	1.31
CWISEP J225511.56−191516.3	343.7980417	−19.2551834	130	130	58505.94	-166 ± 186	-314 ± 190	355 ± 189	3.5	20.39	2	10.19
CWISEP J225628.97+400227.3	344.1221247	40.0407842	29	29	58535.53	696 ± 43	-165 ± 43	716 ± 43	278.4	5.26	8	0.66
CWISEP J230158.30−645858.3	345.4933541	−64.9835116	34	21	58442.51	107 ± 30	-441 ± 29	453 ± 29	246.9	24.25	18	1.35
CWISEP J231047.80+362004.6	347.6996243	36.3347544	37	34	58563.06	286 ± 86	37 ± 87	288 ± 86	11.2	12.91	2	6.45
CWISEP J231114.50+135148.5	347.8100199	13.8635280	32	48	58536.94	-295 ± 63	17 ± 64	296 ± 63	22.1	1.97	2	0.98
CWISEP J233216.39−290025.0	353.0683272	−29.0073009	29	22	58532.57	72 ± 65	-360 ± 66	367 ± 66	31.3	1.53	2	0.76
CWISEP J235130.42−185800.2	357.8775955	−18.9668268	40	28	58394.73	492 ± 47	-46 ± 48	494 ± 47	111.2	0.17	2	0.09
CWISEP J235547.99+380438.9	358.9511591	38.0775517	38	41	58395.29	666 ± 64	51 ± 65	668 ± 64	108.7	6.49	8	0.81
CWISEP J235644.78−481456.3	359.1881598	−48.2492296	30	30	58403.37	1048 ± 91	-133 ± 90	1056 ± 91	133.4	0.49	4	0.12

NOTE—χ^2_ν is the reduced χ^2 of the linear motion fit, defined as $\chi^2_\nu = \chi^2/(\#\ \text{dof})$.

Table 8. 2MASS Counterparts

Name	2MASS desig.	J_{2MASS}	H_{2MASS}	$K_{S,2MASS}$
CWISEP J140247.83+102132.6	2MASS J14024796+1021318	16.443 ± 0.139	>15.692	>16.369
CWISEP J201510.68−675005.6	2MASS J20151069−6750029	17.027 ± 0.181	>16.731	>16.374

Table 9. NIR photometry from Gemini, Palomar, UKIRT and VISTA for motion-confirmed targets

Name	J_{MKO} (mag)	origin of J_{MKO}	H_{MKO} (mag)	origin of H_{MKO}	K_{MKO} (mag)	origin of K_{MKO}	K_S (mag)	origin of K_S
CWISEP J000006.01−704851.2	18.28 ± 0.05	VIRCAM	-	-	-	-	18.99 ± 0.27	VIRCAM
CWISEP J001146.07−471306.8	19.22 ± 0.11	VIRCAM	19.79 ± 0.34	VIRCAM	-	-	> 18.35	VIRCAM
CWISEP J003507.77−153233.8	19.13 ± 0.03	WIRC	-	-	-	-	-	-
CWISEP J004158.35+381811.9	19.26 ± 0.07	WIRC	19.54 ± 0.22	WFCAM	-	-	-	-
CWISEP J010650.61+225159.1	17.41 ± 0.03	WFCAM	-	-	-	-	-	-
CWISEP J012748.35−631056.1	17.82 ± 0.03	VIRCAM	-	-	-	-	18.10 ± 0.19	VIRCAM
CWISEP J015613.24+325526.6	21.46 ± 0.30	WIRC	-	-	-	-	-	-
CWISEP J020103.10+293801.8	17.91 ± 0.03	WFCAM	18.19 ± 0.06	WFCAM	18.24 ± 0.12	WFCAM	-	-
CWISEP J020938.72+180427.7	> 19.50	WFCAM	-	-	-	-	-	-
CWISEP J022122.41−564125.0	18.78 ± 0.05	VIRCAM	-	-	-	-	> 18.30	VIRCAM
CWISEP J023842.60−133210.7	> 21.46	WIRC	-	-	-	-	> 18.32	VIRCAM
CWISEP J024204.91−225604.6	> 20.56	VIRCAM	-	-	-	-	> 18.41	VIRCAM
CWISEP J031130.28+035931.8	> 19.74	WFCAM	> 18.86	WFCAM	> 18.27	WFCAM	-	-
CWISEP J031935.50−041231.7	20.54 ± 0.19	WIRC	-	-	-	-	-	-
CWISEP J032109.59+693204.5	> 21.16	WIRC	-	-	-	-	-	-
CWISEP J034755.11+123051.9	17.96 ± 0.05	WFCAM	-	-	-	-	-	-
CWISEP J034904.05−462827.9	18.77 ± 0.09	VIRCAM	> 18.86	VIRCAM	-	-	18.61 ± 0.31	VIRCAM
CWISEP J040106.67+085748.5	19.47 ± 0.19	WFCAM	-	-	> 18.73	WFCAM	-	-
CWISEP J040235.55−265145.4	> 20.34	VIRCAM	-	-	-	-	> 18.41	VIRCAM
CWISEP J040351.00−491605.6	20.19 ± 0.26	VIRCAM	> 19.14	VIRCAM	-	-	> 18.30	VIRCAM
CWISEP J042404.54+665011.2	19.45 ± 0.08	WIRC	-	-	-	-	-	-
CWISEP J043034.27+255653.7	17.30 ± 0.02	WFCAM	-	-	17.92 ± 0.16	WFCAM	-	-
CWISEP J043309.31+100902.9	17.94 ± 0.04	WFCAM	-	-	> 18.03	WFCAM	-	-
CWISEP J044719.61+202158.1	> 19.82	WFCAM	-	-	> 18.20	WFCAM	-	-
CWISEP J050521.29−591311.7	20.93 ± 0.29	VIRCAM	-	-	-	-	> 18.38	VIRCAM
CWISEP J052346.34−545314.7	> 20.01	VIRCAM	> 19.08	VIRCAM	-	-	> 18.43	VIRCAM
CWISEPR J062436.84−071147.2	18.61 ± 0.05	WIRC	-	-	-	-	> 17.58	VIRCAM
CWISEP J063428.10+504925.9	> 19.52	WFCAM	-	-	-	-	-	-

Table 9 continued

Table 9 *(continued)*

Name	J_{MKO} (mag)	origin of J_{MKO}	H_{MKO} (mag)	origin of H_{MKO}	K_{MKO} (mag)	origin of K_{MKO}	K_S (mag)	origin of K_S
CWISEP J063845.48−615937.2	19.30 ± 0.05	FLAMINGOS-2	-	-	-	-	> 17.85	VIRCAM
CWISEPR J065144.62−115106.1	18.20 ± 0.02	WIRC	-	-	-	-	> 17.56	VIRCAM
CWISEP J070055.19+783834.0	> 20.36	WIRC	-	-	-	-	-	-
CWISEP J070214.84−544041.7	19.54 ± 0.05	FLAMINGOS-2	-	-	-	-	-	-
CWISEP J085908.26+152527.1	19.20 ± 0.14	WFCAM	-	-	-	-	-	-
CWISEP J085938.95+534908.7	> 19.70	WFCAM	-	-	-	-	-	-
CWISEP J090536.35+740009.1	20.45 ± 0.14	WIRC	-	-	-	-	-	-
CWISEP J093111.03+232502.1	18.53 ± 0.10	WFCAM	-	-	-	-	-	-
CWISEP J093236.66−180029.3	20.04 ± 0.07	FLAMINGOS-2	-	-	-	-	> 17.98	VIRCAM
CWISEP J093852.89+063440.6	21.03 ± 0.12[a]	FLAMINGOS-2	> 19.69	WFCAM	> 18.79	WFCAM	-	-
CWISEP J094005.50+523359.2	> 21.26	WIRC	-	-	-	-	-	-
CWISEP J094615.56+351434.3	18.45 ± 0.07	WFCAM	-	-	-	-	-	-
CWISEP J095930.71−401046.8	> 19.49	VIRCAM	-	-	-	-	> 17.87	VIRCAM
CWISEP J100629.01+105408.5	19.80 ± 0.06	FLAMINGOS-2	> 19.02	WFCAM	> 18.64	WFCAM	-	-
CWISEP J102201.27+145520.2	> 19.76	WFCAM	-	-	-	-	-	-
CWISEP J103453.14+161228.0	17.68 ± 0.03	WFCAM	-	-	-	-	-	-
CWISEP J104104.20+221613.6	> 19.58	WFCAM	-	-	-	-	-	-
CWISEP J104446.56+001754.9	20.34 ± 0.21	VIRCAM	> 19.65	VIRCAM	-	-	> 18.97	VIRCAM
CWISEP J104756.81+545741.6	> 19.83	WFCAM	-	-	-	-	-	-
CWISEP J110021.08+094652.9	-	-	> 18.91	WFCAM	> 18.34	WFCAM	-	-
CWISEP J111055.12−174738.2	17.75 ± 0.02	WIRC	-	-	-	-	17.72 ± 0.17	VIRCAM
CWISEP J120444.33−235926.8	17.90 ± 0.03	VIRCAM	-	-	-	-	-	-
CWISEP J122010.03+281431.3	18.50 ± 0.03	WIRC	19.09 ± 0.23	WFCAM	> 18.51	WFCAM	-	-
CWISEP J124138.41−820051.9	20.44 ± 0.12	FLAMINGOS-2	-	-	-	-	-	-
CWISEP J131252.97+341746.5	19.09 ± 0.17	WFCAM	> 18.95	WFCAM	> 18.27	WFCAM	-	-
CWISEP J131221.97−310845.7	18.70 ± 0.12	VIRCAM	-	-	-	-	> 17.88	VIRCAM
CWISEP J131350.91−440352.2	18.27 ± 0.04	VIRCAM	-	-	-	-	18.68 ± 0.29	VIRCAM
CWISEP J135336.29−003756.6	19.97 ± 0.06	FLAMINGOS-2	> 19.45	WFCAM	-	-	> 18.94	VIRCAM
CWISEP J135937.65−435226.9	> 19.31	VIRCAM	-	-	-	-	> 17.91	VIRCAM
CWISEP J140118.30+432554.2	18.40 ± 0.08	WFCAM	-	-	-	-	-	-

Table 9 continued

Table 9 *(continued)*

Name	J_{MKO} (mag)	origin of J_{MKO}	H_{MKO} (mag)	origin of H_{MKO}	K_{MKO} (mag)	origin of K_{MKO}	K_S (mag)	origin of K_S
CWISEP J143439.23−134421.4	> 19.54	VIRCAM	> 18.81	VIRCAM	-	-	> 18.01	VIRCAM
CWISEP J144606.62−231717.8	> 22.36	FLAMINGOS-2	-	-	-	-	> 17.86	VIRCAM
CWISEP J145837.91+173450.1	18.39 ± 0.07	WFCAM	-	-	-	-	-	-
CWISEP J150252.82−304232.8	17.62 ± 0.03	VIRCAM	-	-	-	-	> 17.71	VIRCAM
CWISEP J151521.22−215736.9	17.48 ± 0.03	VIRCAM	-	-	-	-	18.52 ± 0.38	VIRCAM
WISEA J153429.75−104303.3	> 20.56	WIRC	> 18.58	VIRCAM	-	-	> 17.85	VIRCAM
CWISEP J153859.39+482659.1	20.26 ± 0.10	WIRC	-	-	-	-	-	-
CWISEP J160311.60−104620.4	19.13 ± 0.21	VIRCAM	-	-	-	-	> 17.97	VIRCAM
CWISEP J160835.01−244244.7	17.66 ± 0.04	WFCAM	> 18.81	WFCAM	18.46 ± 0.18	WFCAM	-	-
CWISEP J161822.86−062310.2	20.42 ± 0.24	WIRC	-	-	-	-	-	-
CWISEP J165215.62+022918.5	> 19.48	WFCAM	-	-	-	-	-	-
CWISEP J182358.73−740246.0	17.84 ± 0.06	VIRCAM	-	-	-	-	> 17.85	VIRCAM
CWISEP J193518.58−154620.3	> 21.70	FLAMINGOS-2	-	-	-	-	> 18.00	VIRCAM
WISENF J193656.08+040801.2	> 19.57	WFCAM	-	-	-	-	-	-
CWISEP J194101.59+542335.9	17.72 ± 0.04	WFCAM	-	-	-	-	-	-
CWISEP J194812.42−322334.9	-	-	-	-	-	-	17.98 ± 0.25	VIRCAM
CWISEP J201146.45−481259.7	> 20.08	VIRCAM	> 19.05	VIRCAM	-	-	> 18.46	VIRCAM
CWISEP J201510.68−675005.6	16.90 ± 0.02	VIRCAM	-	-	-	-	-	-
CWISEP J203821.53−064930.9	19.56 ± 0.20	VIRCAM	-	-	-	-	> 18.10	VIRCAM
CWISEP J205019.99−253652.8	17.57 ± 0.01	WIRC	-	-	-	-	> 17.39	VIRCAM
CWISEP J210007.87−293139.8	> 19.96	WIRC	-	-	-	-	> 17.91	VIRCAM
CWISEP J212828.05+352912.4	> 19.68	WFCAM	-	-	-	-	-	-
CWISEP J213249.05+690113.7	19.45 ± 0.04	WIRC	-	-	-	-	-	-
CWISEP J213838.74−313808.5	18.59 ± 0.07	VIRCAM	-	-	-	-	> 17.43	VIRCAM
CWISEP J213930.45+042721.6	20.44 ± 0.10	FLAMINGOS-2	-	-	-	-	-	-
CWISEP J215841.50+732842.7	19.13 ± 0.60	WIRC	-	-	-	-	-	-
CWISEP J222035.35−810322.6	18.46 ± 0.03	FLAMINGOS-2	-	-	-	-	> 17.50	VIRCAM
CWISEP J223022.60+254907.5	> 21.16	WIRC	-	-	-	-	-	-
CWISEP J223138.55−383057.2	19.69 ± 0.13	VIRCAM	-	-	-	-	> 18.38	VIRCAM
CWISEP J224916.17+371551.4	> 19.53	WFCAM	-	-	-	-	-	-

Table 9 continued

Table 9 *(continued)*

Name	J_{MKO} (mag)	origin of J_{MKO}	H_{MKO} (mag)	origin of H_{MKO}	K_{MKO} (mag)	origin of K_{MKO}	K_S (mag)	origin of K_S
CWISEP J225059.28−432057.2	19.90 ± 0.16	VIRCAM	-	-	-	-	> 18.47	VIRCAM
CWISEP J225109.50−074037.7	18.09 ± 0.03	FLAMINGOS-2	-	-	-	-	> 17.92	VIRCAM
CWISEP J225628.97+400227.3	21.70 ± 0.41	WIRC	-	-	-	-	-	-
CWISEP J230158.30−645858.3	20.46 ± 0.28	VIRCAM	-	-	-	-	> 18.19	VIRCAM
CWISEP J233216.39−290025.0	17.95 ± 0.03	FLAMINGOS-2	18.01 ± 0.03	VIRCAM	-	-	17.86 ± 0.07	VIRCAM
CWISEP J235130.42−185800.2	19.38 ± 0.04	WIRC	-	-	-	-	-	-
CWISEP J235547.99+380438.9	20.28 ± 0.10	WIRC	-	-	-	-	-	-
CWISEP J235644.78−481456.3	21.77 ± 0.28	FLAMINGOS-2	> 19.14	VIRCAM	-	-	> 18.30	VIRCAM

[a] CWISEP 0938+0634 appears to be in a sky region with nebulosity based on our Gemini J band image. While this may be contaminating its J band photometry, CWISEP 0938+0634 is nevertheless a real compact source with unambiguously confirmed motion (see Figure 5).

Table 10. J band follow-up for candidates not motion confirmed.

CWISEP designation	J_{MKO} (mag)	origin
J021243.55+053147.2	22.75 ± 0.78	WIRC
J042455.68+000221.4	19.66 ± 0.07	WIRC
J100854.84+203136.6	20.73 ± 0.39	WIRC
J121358.13+294237.0	18.97 ± 0.05	WIRC
J131208.16−105231.8	20.60 ± 0.09	FLAMINGOS-2
J172104.42+595047.7	20.42 ± 0.13	WIRC
J175746.31+195112.6	> 21.36[a]	WIRC
J221736.94−222647.6	> 21.56[a,b]	FLAMINGOS-2

[a] Quoted limits are 5σ.

[b] A smudge appears at the location of CWISEP 2217−2226, for which we quote a J magnitude lower limit.

Table 11. Derived Properties for Motion-confirmed Targets with *Spitzer* Imaging Available

Name	SpT (phototype)	M_{ch2} (mag)	distance (pc)	T_{eff} (K)	H_{ch2} (mag)	V_{tan} (km/s)
CWISEP J000006.01−704851.2	7.0	$13.21^{+0.31}_{-0.30}$	$33.5^{+5.1}_{-4.4}$	813^{+85}_{-85}	$18.34^{+0.29}_{-0.26}$	50^{+10}_{-9}
CWISEP J000110.81−093215.5	7.5	$13.43^{+0.31}_{-0.31}$	$31.0^{+4.7}_{-4.1}$	720^{+85}_{-85}	$18.88^{+0.44}_{-0.36}$	58^{+14}_{-13}
CWISEP J001146.07−471306.8	8.5	$13.73^{+0.33}_{-0.32}$	$26.1^{+4.2}_{-3.6}$	628^{+88}_{-87}	$18.50^{+0.44}_{-0.36}$	43^{+10}_{-10}
CWISEP J003507.77−153233.8	8.0	$13.67^{+0.31}_{-0.31}$	$20.5^{+3.2}_{-2.8}$	646^{+85}_{-85}	$18.94^{+0.17}_{-0.16}$	54^{+9}_{-8}
CWISEP J004158.35+381811.9	8.0	$13.51^{+0.32}_{-0.32}$	$32.5^{+5.2}_{-4.5}$	695^{+89}_{-89}	$18.43^{+0.41}_{-0.34}$	46^{+11}_{-10}
CWISEP J005802.63+723330.3	4.5	$12.43^{+0.24}_{-0.24}$	$73.2^{+8.6}_{-7.8}$	-	$20.30^{+0.27}_{-0.24}$	178^{+30}_{-28}
CWISEP J010527.69−783419.3	9.0	$13.94^{+0.32}_{-0.32}$	$17.9^{+2.8}_{-2.4}$	576^{+85}_{-84}	$18.09^{+0.12}_{-0.12}$	32^{+5}_{-5}
CWISEP J010650.61+225159.1	6.5	$13.12^{+0.30}_{-0.30}$	$25.3^{+3.8}_{-3.3}$	858^{+83}_{-83}	$17.69^{+0.25}_{-0.22}$	39^{+7}_{-7}
CWISEP J012748.35−631056.1	6.5	$13.07^{+0.30}_{-0.30}$	$31.7^{+4.7}_{-4.1}$	885^{+84}_{-84}	$19.89^{+0.11}_{-0.11}$	109^{+17}_{-15}
CWISEP J014607.55−375705.6	7.5	$13.47^{+0.31}_{-0.31}$	$27.7^{+4.2}_{-3.7}$	707^{+85}_{-85}	$19.70^{+0.19}_{-0.18}$	84^{+15}_{-13}
CWISEP J015613.24+325526.6	7.0	$13.20^{+0.31}_{-0.31}$	$38.3^{+5.9}_{-5.1}$	817^{+90}_{-90}	$21.51^{+0.16}_{-0.15}$	217^{+37}_{-33}
CWISEP J020103.10+293801.8	6.0	$12.99^{+0.30}_{-0.30}$	$39.2^{+5.9}_{-5.1}$	939^{+85}_{-85}	$19.70^{+0.28}_{-0.25}$	104^{+20}_{-18}
CWISEP J020938.72+180427.7	8.0	$13.55^{+0.32}_{-0.32}$	$33.0^{+5.2}_{-4.5}$	682^{+88}_{-88}	$19.69^{+0.28}_{-0.25}$	80^{+16}_{-15}
CWISEP J021921.66−265451.8	5.0	$12.86^{+0.30}_{-0.30}$	$68.2^{+10.2}_{-8.9}$	1073^{+97}_{-96}	$20.92^{+0.30}_{-0.26}$	193^{+38}_{-35}
CWISEP J022122.41−564125.0	8.0	$13.50^{+0.31}_{-0.31}$	$26.9^{+4.1}_{-3.6}$	698^{+85}_{-85}	$17.59^{+0.42}_{-0.35}$	31^{+7}_{-7}
CWISEP J022631.82−203439.4	7.5	$13.39^{+0.31}_{-0.31}$	$32.8^{+5.1}_{-4.4}$	738^{+87}_{-87}	$19.95^{+0.24}_{-0.22}$	98^{+18}_{-17}
CWISEP J023842.60−133210.7	≥ 11.0	$15.05^{+0.54}_{-0.51}$	$18.0^{+4.8}_{-4.0}$	399^{+97}_{-93}	$20.73^{+0.23}_{-0.21}$	65^{+18}_{-16}
CWISEP J024204.91−225604.6	8.5	$13.78^{+0.34}_{-0.34}$	$33.8^{+5.7}_{-4.9}$	615^{+91}_{-90}	$21.56^{+0.16}_{-0.15}$	170^{+31}_{-28}
CWISEP J031130.28+035931.8	5.0	$12.53^{+0.25}_{-0.24}$	$79.9^{+9.5}_{-8.7}$	-	$20.97^{+0.41}_{-0.35}$	231^{+49}_{-47}

Table 11 continued

Table 11 *(continued)*

Name	SpT (phototype)	M_{ch2} (mag)	distance (pc)	T_{eff} (K)	H_{ch2} (mag)	V_{tan} (km/s)
CWISEP J031935.50−041231.7	9.5	$14.27^{+0.44}_{-0.42}$	$28.5^{+6.0}_{-5.2}$	510^{+99}_{-96}	$20.16^{+0.41}_{-0.35}$	71^{+20}_{-18}
CWISEP J032109.59+693204.5	10.5	$14.86^{+0.48}_{-0.46}$	$16.3^{+3.8}_{-3.2}$	421^{+94}_{-92}	$20.96^{+0.14}_{-0.13}$	79^{+19}_{-16}
CWISEP J034755.11+123051.9	7.5	$13.36^{+0.30}_{-0.30}$	$22.8^{+3.4}_{-3.0}$	747^{+83}_{-83}	$18.05^{+0.23}_{-0.21}$	41^{+7}_{-7}
CWISEP J034904.05−462827.9	7.0	$13.27^{+0.31}_{-0.31}$	$40.4^{+6.2}_{-5.4}$	784^{+89}_{-88}	$20.00^{+0.23}_{-0.21}$	105^{+19}_{-17}
CWISEP J040106.67+085748.5	8.5	$13.71^{+0.32}_{-0.32}$	$24.7^{+3.9}_{-3.4}$	633^{+86}_{-86}	$19.20^{+0.29}_{-0.25}$	59^{+12}_{-11}
CWISEP J040235.55−265145.4	≥ 11.0	$15.03^{+0.43}_{-0.42}$	$12.2^{+2.6}_{-2.2}$	401^{+89}_{-87}	$20.33^{+0.08}_{-0.08}$	55^{+12}_{-10}
CWISEP J040351.00−491605.6	8.5	$13.81^{+0.35}_{-0.35}$	$29.0^{+5.0}_{-4.4}$	608^{+93}_{-92}	$18.52^{+0.35}_{-0.30}$	41^{+9}_{-9}
CWISEP J042404.54+665011.2	8.0	$13.50^{+0.31}_{-0.31}$	$27.0^{+4.2}_{-3.6}$	696^{+86}_{-86}	$18.64^{+0.23}_{-0.20}$	51^{+9}_{-8}
CWISEP J043034.27+255653.7	6.0	$13.04^{+0.30}_{-0.30}$	$22.4^{+3.3}_{-2.9}$	907^{+82}_{-82}	$18.04^{+0.14}_{-0.13}$	47^{+8}_{-7}
CWISEP J043309.31+100902.9	8.0	$13.54^{+0.31}_{-0.31}$	$21.0^{+3.2}_{-2.8}$	684^{+84}_{-83}	$18.27^{+0.19}_{-0.18}$	42^{+7}_{-7}
CWISEP J044719.61+202158.1	9.0	$14.05^{+0.36}_{-0.35}$	$21.8^{+3.8}_{-3.3}$	553^{+90}_{-89}	$19.71^{+0.19}_{-0.18}$	64^{+12}_{-11}
CWISEP J050521.29−591311.7	6.5	$13.14^{+0.31}_{-0.31}$	$40.2^{+6.1}_{-5.3}$	846^{+88}_{-87}	$21.37^{+0.08}_{-0.07}$	210^{+33}_{-29}
CWISEP J052346.34−545314.7	9.5	$14.39^{+0.39}_{-0.38}$	$22.8^{+4.4}_{-3.8}$	489^{+92}_{-90}	$20.30^{+0.17}_{-0.16}$	72^{+15}_{-13}
CWISEPR J062436.84−071147.2	7.5	$13.34^{+0.31}_{-0.31}$	$24.8^{+3.8}_{-3.3}$	756^{+84}_{-84}	$16.03^{+0.49}_{-0.40}$	16^{+4}_{-4}
CWISEP J062742.27−215908.1	7.5	$13.47^{+0.32}_{-0.32}$	$31.1^{+4.9}_{-4.2}$	709^{+88}_{-88}	$18.81^{+0.39}_{-0.33}$	56^{+13}_{-12}
CWISEP J063428.10+504925.9	10.0	$14.47^{+0.41}_{-0.40}$	$19.8^{+4.0}_{-3.4}$	476^{+92}_{-91}	$21.11^{+0.14}_{-0.13}$	101^{+21}_{-18}
CWISEP J063845.48−615937.2	7.0	$13.22^{+0.31}_{-0.31}$	$47.8^{+7.4}_{-6.5}$	808^{+91}_{-91}	$19.74^{+0.38}_{-0.32}$	96^{+21}_{-20}
CWISEPR J065144.62−115106.1	7.0	$13.26^{+0.30}_{-0.30}$	$26.8^{+4.0}_{-3.5}$	790^{+84}_{-84}	$17.01^{+0.50}_{-0.41}$	27^{+7}_{-6}
CWISEP J070055.19+783834.0	6.0	$13.01^{+0.31}_{-0.30}$	$54.9^{+8.3}_{-7.2}$	925^{+91}_{-90}	$22.22^{+0.18}_{-0.17}$	329^{+56}_{-51}
CWISEP J070214.84−544041.7	7.5	$13.39^{+0.32}_{-0.32}$	$42.6^{+6.8}_{-5.9}$	734^{+92}_{-91}	$20.30^{+0.29}_{-0.26}$	114^{+23}_{-21}
CWISEP J071813.30−061421.1	5.0	$12.53^{+0.25}_{-0.24}$	$81.3^{+9.7}_{-8.8}$	-	$20.51^{+0.45}_{-0.37}$	188^{+42}_{-41}
CWISEP J085908.26+152527.1	8.0	$13.67^{+0.31}_{-0.31}$	$20.5^{+3.2}_{-2.7}$	645^{+84}_{-84}	$17.43^{+0.37}_{-0.31}$	27^{+6}_{-5}
CWISEP J085938.95+534908.7	10.0	$14.64^{+0.44}_{-0.42}$	$18.7^{+4.0}_{-3.4}$	451^{+94}_{-91}	$18.88^{+0.34}_{-0.30}$	33^{+9}_{-8}
CWISEP J090536.35+740009.1	6.0	$13.01^{+0.30}_{-0.30}$	$47.9^{+7.2}_{-6.3}$	930^{+87}_{-87}	$22.37^{+0.10}_{-0.10}$	354^{+56}_{-49}
CWISEP J093111.03+232502.1	7.5	$13.42^{+0.31}_{-0.31}$	$28.6^{+4.4}_{-3.9}$	726^{+87}_{-87}	$19.44^{+0.30}_{-0.27}$	76^{+15}_{-14}
CWISEP J093236.66−180029.3	8.5	$13.83^{+0.32}_{-0.32}$	$23.7^{+3.8}_{-3.3}$	602^{+86}_{-86}	$19.05^{+0.28}_{-0.25}$	52^{+11}_{-10}
CWISEP J093852.89+063440.6	10.0	$14.58^{+0.43}_{-0.41}$	$18.9^{+4.0}_{-3.4}$	460^{+93}_{-91}	$20.63^{+0.15}_{-0.14}$	77^{+17}_{-15}
CWISEP J094005.50+523359.2	≥ 11.0	$15.12^{+0.47}_{-0.45}$	$13.4^{+3.1}_{-2.6}$	391^{+91}_{-89}	$19.04^{+0.26}_{-0.23}$	29^{+7}_{-7}
CWISEP J094615.56+351434.3	5.5	$12.95^{+0.30}_{-0.30}$	$42.2^{+6.3}_{-5.5}$	975^{+86}_{-86}	$20.22^{+0.22}_{-0.20}$	135^{+24}_{-22}
CWISEP J094930.41+663937.2	9.5	$14.24^{+0.36}_{-0.35}$	$23.6^{+4.2}_{-3.6}$	517^{+89}_{-88}	$18.47^{+0.50}_{-0.41}$	33^{+9}_{-9}
CWISEP J095930.71−401046.8	3.5	$12.25^{+0.23}_{-0.23}$	$124.8^{+14.6}_{-13.2}$	-	$21.94^{+0.36}_{-0.31}$	410^{+79}_{-76}
CWISEP J100629.01+105408.5	8.5	$13.90^{+0.33}_{-0.33}$	$21.4^{+3.5}_{-3.0}$	585^{+87}_{-86}	$17.62^{+0.43}_{-0.36}$	26^{+6}_{-6}
CWISEP J102201.27+145520.2	8.5	$13.74^{+0.32}_{-0.32}$	$26.2^{+4.2}_{-3.6}$	626^{+87}_{-87}	$19.61^{+0.25}_{-0.22}$	71^{+14}_{-12}
CWISEP J103453.14+161228.0	7.5	$13.46^{+0.30}_{-0.30}$	$19.2^{+2.9}_{-2.5}$	710^{+83}_{-83}	$17.08^{+0.25}_{-0.22}$	25^{+5}_{-4}
CWISEP J104104.20+221613.6	9.5	$14.23^{+0.45}_{-0.43}$	$30.4^{+6.7}_{-5.7}$	517^{+103}_{-99}	$20.43^{+0.49}_{-0.40}$	82^{+24}_{-23}
CWISEP J104446.56+001754.9	9.0	$13.94^{+0.34}_{-0.34}$	$25.7^{+4.3}_{-3.8}$	577^{+89}_{-88}	$20.68^{+0.23}_{-0.21}$	106^{+21}_{-19}
CWISEP J104756.81+545741.6	10.0	$14.57^{+0.43}_{-0.41}$	$21.7^{+4.6}_{-3.9}$	461^{+94}_{-91}	$19.66^{+0.36}_{-0.31}$	50^{+13}_{-12}
CWISEP J110021.08+094652.9	8.0	$13.64^{+0.32}_{-0.32}$	$25.0^{+3.9}_{-3.4}$	655^{+87}_{-87}	$19.61^{+0.17}_{-0.16}$	74^{+13}_{-12}
CWISEP J111055.12−174738.2	7.5	$13.32^{+0.30}_{-0.30}$	$22.1^{+3.3}_{-2.9}$	763^{+83}_{-83}	$18.03^{+0.16}_{-0.15}$	41^{+7}_{-6}
CWISEP J113010.21+313947.3	6.0	$13.05^{+0.30}_{-0.30}$	$28.2^{+4.2}_{-3.7}$	901^{+83}_{-83}	$21.68^{+0.05}_{-0.05}$	253^{+38}_{-33}

Table 11 continued

Table 11 *(continued)*

Name	SpT (phototype)	M_{ch2} (mag)	distance (pc)	T_{eff} (K)	H_{ch2} (mag)	V_{tan} (km/s)
CWISEP J120444.33−235926.8	7.5	$13.35^{+0.31}_{-0.30}$	$24.5^{+3.7}_{-3.2}$	751^{+84}_{-84}	$18.97^{+0.16}_{-0.15}$	63^{+10}_{-9}
CWISEP J122010.03+281431.3	7.0	$13.30^{+0.31}_{-0.31}$	$32.5^{+5.0}_{-4.3}$	770^{+86}_{-86}	$18.97^{+0.28}_{-0.25}$	64^{+13}_{-12}
CWISEP J124138.41−820051.9	8.5	$13.87^{+0.32}_{-0.32}$	$19.7^{+3.1}_{-2.7}$	595^{+85}_{-85}	$17.23^{+0.22}_{-0.20}$	22^{+4}_{-4}
CWISEP J130255.54+191145.9	8.0	$13.59^{+0.32}_{-0.31}$	$24.8^{+3.9}_{-3.4}$	670^{+86}_{-86}	$17.56^{+0.45}_{-0.37}$	30^{+7}_{-7}
CWISEP J131252.97+341746.5	7.5	$13.46^{+0.33}_{-0.32}$	$38.7^{+6.2}_{-5.4}$	713^{+92}_{-91}	$19.22^{+0.50}_{-0.40}$	67^{+18}_{-17}
CWISEP J131221.97−310845.7	8.0	$13.67^{+0.32}_{-0.32}$	$26.8^{+4.2}_{-3.7}$	646^{+87}_{-86}	$19.40^{+0.22}_{-0.20}$	67^{+12}_{-11}
CWISEP J131350.91−440352.2	7.5	$13.39^{+0.31}_{-0.31}$	$27.7^{+4.2}_{-3.6}$	736^{+84}_{-84}	$19.15^{+0.21}_{-0.19}$	67^{+12}_{-11}
CWISEP J135937.65−435226.9	10.0	$14.50^{+0.39}_{-0.38}$	$19.5^{+3.7}_{-3.2}$	472^{+90}_{-89}	$18.73^{+0.50}_{-0.40}$	33^{+9}_{-9}
CWISEP J140118.30+432554.2	6.5	$13.12^{+0.30}_{-0.30}$	$32.0^{+4.8}_{-4.2}$	861^{+85}_{-85}	$19.81^{+0.11}_{-0.11}$	103^{+16}_{-14}
CWISEP J140247.83+102132.6	5.0	$12.53^{+0.25}_{-0.24}$	$24.1^{+2.8}_{-2.6}$	-	$15.33^{+0.25}_{-0.23}$	17^{+3}_{-3}
CWISEP J141206.85+234412.4	6.0	$13.03^{+0.30}_{-0.30}$	$43.4^{+6.5}_{-5.7}$	912^{+86}_{-86}	$20.31^{+0.20}_{-0.19}$	135^{+24}_{-21}
CWISEP J143439.23−134421.4	9.0	$14.00^{+0.36}_{-0.35}$	$27.0^{+4.8}_{-4.2}$	565^{+92}_{-91}	$19.63^{+0.35}_{-0.30}$	63^{+15}_{-14}
CWISEP J144606.62−231717.8	≥ 11.0	> 16.23	< 8.3	< 381	$21.35^{+0.12}_{-0.12}$	< 53
CWISEP J145837.91+173450.1	8.0	$13.61^{+0.31}_{-0.31}$	$21.6^{+3.3}_{-2.9}$	664^{+84}_{-84}	$18.84^{+0.11}_{-0.10}$	53^{+9}_{-7}
CWISEP J150252.82−304232.8	7.0	$13.29^{+0.30}_{-0.30}$	$22.3^{+3.3}_{-2.9}$	775^{+83}_{-83}	$18.42^{+0.15}_{-0.14}$	50^{+8}_{-7}
WISEA J153429.75−104303.3	5.0	$12.87^{+0.30}_{-0.30}$	$38.0^{+5.6}_{-4.9}$	1062^{+83}_{-83}	$22.92^{+0.06}_{-0.06}$	485^{+73}_{-64}
CWISEP J153859.39+482659.1	9.5	$14.23^{+0.38}_{-0.37}$	$20.7^{+3.9}_{-3.3}$	518^{+92}_{-91}	$19.13^{+0.17}_{-0.16}$	45^{+9}_{-8}
CWISEP J160311.60−104620.4	8.0	$13.51^{+0.31}_{-0.31}$	$25.9^{+4.0}_{-3.5}$	694^{+87}_{-86}	$20.39^{+0.13}_{-0.13}$	113^{+19}_{-17}
CWISEP J160835.01−244244.7	7.0	$13.25^{+0.30}_{-0.30}$	$23.6^{+3.5}_{-3.1}$	793^{+83}_{-83}	$17.49^{+0.29}_{-0.26}$	33^{+7}_{-6}
CWISEP J161822.86−062310.2	8.5	$13.76^{+0.32}_{-0.32}$	$24.0^{+3.8}_{-3.3}$	621^{+86}_{-86}	$18.46^{+0.34}_{-0.29}$	41^{+9}_{-8}
CWISEP J162225.92+370118.8	6.5	$13.09^{+0.31}_{-0.30}$	$42.2^{+6.4}_{-5.6}$	878^{+88}_{-88}	$20.09^{+0.18}_{-0.17}$	119^{+20}_{-18}
CWISEP J165215.62+022918.5	4.5	$12.43^{+0.24}_{-0.24}$	$80.4^{+9.4}_{-8.6}$	-	$20.13^{+0.46}_{-0.38}$	165^{+37}_{-36}
CWISEP J182358.73−740246.0	6.0	$13.01^{+0.30}_{-0.30}$	$32.4^{+4.8}_{-4.2}$	927^{+85}_{-84}	$18.98^{+0.28}_{-0.25}$	74^{+14}_{-13}
CWISEP J185658.80+601351.4	6.0	$13.01^{+0.30}_{-0.30}$	$33.3^{+5.0}_{-4.3}$	930^{+84}_{-84}	$20.16^{+0.08}_{-0.08}$	128^{+20}_{-17}
CWISEP J193518.58−154620.3	≥ 11.0	$15.57^{+0.31}_{-0.31}$	$9.8^{+1.5}_{-1.3}$	347^{+81}_{-81}	$17.97^{+0.48}_{-0.39}$	14^{+4}_{-3}
WISENF J193656.08+040801.2	10.0	$14.45^{+0.32}_{-0.32}$	$11.1^{+1.8}_{-1.5}$	479^{+83}_{-83}	$20.17^{+0.07}_{-0.07}$	66^{+11}_{-9}
CWISEP J194101.59+542335.9	7.0	$13.25^{+0.31}_{-0.30}$	$28.3^{+4.3}_{-3.7}$	793^{+85}_{-84}	$17.16^{+0.24}_{-0.22}$	29^{+5}_{-5}
CWISEP J194812.42−322334.9	5.5	$12.91^{+0.30}_{-0.30}$	$38.3^{+5.7}_{-5.0}$	1011^{+84}_{-84}	$18.65^{+0.44}_{-0.37}$	67^{+16}_{-15}
CWISEP J201146.45−481259.7	10.0	$14.61^{+0.37}_{-0.36}$	$13.9^{+2.5}_{-2.2}$	455^{+87}_{-86}	$18.04^{+0.24}_{-0.21}$	23^{+5}_{-4}
CWISEP J201510.68−675005.6	6.0	$13.05^{+0.30}_{-0.30}$	$21.1^{+3.1}_{-2.7}$	903^{+82}_{-82}	$16.21^{+0.24}_{-0.22}$	20^{+4}_{-3}
CWISEP J203821.53−064930.9	9.5	$14.21^{+0.33}_{-0.33}$	$19.1^{+3.1}_{-2.7}$	521^{+85}_{-85}	$18.88^{+0.37}_{-0.32}$	41^{+9}_{-9}
CWISEP J205019.99−253652.8	7.0	$13.29^{+0.30}_{-0.30}$	$22.8^{+3.4}_{-3.0}$	777^{+83}_{-83}	$17.67^{+0.23}_{-0.21}$	36^{+6}_{-6}
CWISEP J205908.95+024105.6	7.5	$13.38^{+0.31}_{-0.31}$	$26.8^{+4.1}_{-3.6}$	738^{+85}_{-85}	$20.13^{+0.13}_{-0.13}$	106^{+17}_{-15}
CWISEP J210007.87−293139.8	9.5	$14.43^{+0.42}_{-0.40}$	$20.2^{+4.1}_{-3.5}$	484^{+94}_{-92}	$18.93^{+0.44}_{-0.36}$	38^{+10}_{-10}
CWISEP J212828.05+352912.4	5.5	$12.92^{+0.31}_{-0.31}$	$67.1^{+10.2}_{-9.0}$	999^{+102}_{-101}	$20.16^{+0.49}_{-0.40}$	132^{+33}_{-32}
CWISEP J213249.05+690113.7	8.5	$13.79^{+0.32}_{-0.31}$	$19.8^{+3.1}_{-2.7}$	614^{+85}_{-85}	$17.59^{+0.18}_{-0.17}$	27^{+5}_{-4}
CWISEP J213838.74−313808.5	8.0	$13.54^{+0.31}_{-0.31}$	$20.8^{+3.2}_{-2.8}$	683^{+84}_{-84}	$19.14^{+0.12}_{-0.12}$	62^{+10}_{-9}
CWISEP J213930.45+042721.6	9.0	$14.07^{+0.34}_{-0.34}$	$21.7^{+3.6}_{-3.1}$	550^{+88}_{-87}	$19.21^{+0.33}_{-0.28}$	51^{+11}_{-10}
CWISEP J215841.50+732842.7	8.0	$13.53^{+0.31}_{-0.31}$	$21.2^{+3.2}_{-2.8}$	688^{+84}_{-84}	$16.25^{+0.33}_{-0.28}$	17^{+3}_{-3}
CWISEP J222035.35−810322.6	6.5	$13.14^{+0.31}_{-0.31}$	$37.4^{+5.7}_{-5.0}$	847^{+88}_{-88}	$18.70^{+0.34}_{-0.29}$	61^{+13}_{-12}

Table 11 continued

Table 11 *(continued)*

Name	SpT (phototype)	M_{ch2} (mag)	distance (pc)	T_{eff} (K)	H_{ch2} (mag)	V_{tan} (km/s)
CWISEP J223022.60+254907.5	≥ 11.0	$15.25^{+0.70}_{-0.64}$	$16.1^{+5.6}_{-4.4}$	377^{+106}_{-98}	$20.59^{+0.22}_{-0.20}$	56^{+20}_{-16}
CWISEP J223138.55−383057.2	8.5	$13.71^{+0.33}_{-0.32}$	$30.0^{+4.9}_{-4.2}$	634^{+88}_{-88}	$20.05^{+0.27}_{-0.24}$	88^{+18}_{-16}
CWISEP J224916.17+371551.4	9.5	$14.31^{+0.38}_{-0.37}$	$23.9^{+4.5}_{-3.9}$	503^{+91}_{-90}	$19.28^{+0.50}_{-0.40}$	47^{+13}_{-12}
CWISEP J225059.28−432057.2	8.0	$13.67^{+0.33}_{-0.33}$	$31.2^{+5.1}_{-4.4}$	644^{+89}_{-88}	$19.59^{+0.37}_{-0.32}$	72^{+16}_{-15}
CWISEP J225156.13+392408.4	7.5	$13.42^{+0.31}_{-0.31}$	$27.5^{+4.2}_{-3.7}$	725^{+86}_{-85}	$18.21^{+0.34}_{-0.29}$	43^{+9}_{-8}
CWISEP J225109.50−074037.7	8.0	$13.53^{+0.31}_{-0.31}$	$20.6^{+3.1}_{-2.7}$	687^{+84}_{-84}	$19.37^{+0.13}_{-0.12}$	70^{+11}_{-10}
CWISEP J225628.97+400227.3	≥ 11.0	$15.64^{+0.60}_{-0.56}$	$10.8^{+3.2}_{-2.6}$	341^{+93}_{-89}	$20.08^{+0.14}_{-0.13}$	37^{+11}_{-9}
CWISEP J230158.30−645858.3	8.5	$13.70^{+0.31}_{-0.31}$	$21.5^{+3.3}_{-2.9}$	636^{+84}_{-84}	$18.65^{+0.14}_{-0.14}$	46^{+8}_{-7}
CWISEP J233216.39−290025.0	6.0	$12.97^{+0.30}_{-0.30}$	$33.5^{+5.0}_{-4.4}$	957^{+83}_{-83}	$18.42^{+0.43}_{-0.36}$	58^{+14}_{-13}
CWISEP J235130.42−185800.2	8.5	$13.86^{+0.33}_{-0.33}$	$22.2^{+3.6}_{-3.1}$	595^{+88}_{-87}	$19.06^{+0.22}_{-0.20}$	52^{+10}_{-9}
CWISEP J235547.99+380438.9	10.0	$14.65^{+0.58}_{-0.54}$	$18.0^{+5.0}_{-4.2}$	450^{+109}_{-102}	$20.05^{+0.22}_{-0.20}$	57^{+17}_{-14}
CWISEP J235644.78−481456.3	10.5	$14.97^{+0.54}_{-0.51}$	$16.4^{+4.3}_{-3.6}$	408^{+98}_{-94}	$21.16^{+0.20}_{-0.18}$	82^{+23}_{-19}

NOTE—Photometric spectral type values are defined such that SpT = 6 for T6, SpT = 7 for T7,... SpT = 11 for Y1.

Table 12. Summary of Motion-confirmed Discoveries Meriting Further Follow-up to Better Assess Y dwarf Candidacy

Name	SpT (phototype)	ch1−ch2 (mag)	$[(ch1-ch2)-2.4]/\sigma_{ch1-ch2}$ (dimensionless)	J−ch2 (mag)
CWISEP J144606.62−231717.8	≥ 11.0	3.709 ± 0.435	3.01	> 6.56
CWISEP J225628.97+400227.3	≥ 11.0	3.014 ± 0.227	2.71	5.90 ± 0.41
CWISEP J193518.58−154620.3	≥ 11.0	2.984 ± 0.034	17.15	> 6.17
CWISEP J223022.60+254907.5	≥ 11.0	2.830 ± 0.293	1.47	> 4.87
CWISEP J094005.50+523359.2	≥ 11.0	2.766 ± 0.175	2.09	> 5.50
CWISEP J023842.60−133210.7	≥ 11.0	2.729 ± 0.220	1.50	> 5.13
CWISEP J040235.55−265145.4	≥ 11.0	2.720 ± 0.152	2.10	> 4.89
CWISEP J235644.78−481456.3	10.5	2.687 ± 0.220	1.31	5.73 ± 0.28
CWISEP J032109.59+693204.5	10.5	2.633 ± 0.190	1.23	> 5.23
CWISEP J235547.99+380438.9	10.0	2.518 ± 0.261	0.45	4.35 ± 0.10[a]
CWISEP J085938.95+534908.7	10.0	2.514 ± 0.173	0.66	> 3.70
CWISEP J201146.45−481259.7	10.0	2.496 ± 0.118	0.82	> 4.76
CWISEP J093852.89+063440.6	10.0	2.480 ± 0.166	0.48	5.07 ± 0.12
CWISEP J104756.81+545741.6	10.0	2.474 ± 0.168	0.44	> 3.57
CWISEP J135937.65−435226.9	10.0	2.434 ± 0.137	0.25	> 3.36
CWISEP J063428.10+504925.9	10.0	2.418 ± 0.155	0.12	> 3.57
WISENF J193656.08+040801.2	10.0	2.407 ± 0.064	0.10	> 4.88
phototype < 10, no $J <$ (ch2 + 5) detection, within 1σ of ch1−ch2 = 2.4				
CWISEP J210007.87−293139.8	9.5	2.392 ± 0.163	−0.05	> 4.00
CWISEP J052346.34−545314.7	9.5	2.372 ± 0.146	−0.19	> 3.83
CWISEP J224916.17+371551.4	9.5	2.324 ± 0.140	−0.54	> 3.33
CWISEP J104104.20+221613.6	9.5	2.274 ± 0.201	−0.62	> 2.93
phototype < 10, ch1−ch2 > 2.11 mag, no $J <$ (ch2 + 5) detection, not within 1σ of ch1−ch2 = 2.4				
CWISEP J094930.41+663937.2	9.5	2.276 ± 0.120	−1.03	-
CWISEP J044719.61+202158.1	9.0	2.156 ± 0.124	−1.97	> 4.08
CWISEP J143439.23−134421.4	9.0	2.121 ± 0.133	−2.10	> 3.39

[a]The relatively blue J−ch2 color of CWISEP 2355+3804 suggests that it is a late T dwarf despite its *Spitzer*-based phototype of Y0.

NOTE—Photometric spectral type values are defined such that SpT = 6 for T6, SpT = 7 for T7,... SpT = 11 for Y1.